N° d'ordre : ANNÉE 2013

THÈSE / UNIVERSITÉ DE RENNES 1
sous le sceau de l'Université Européenne de Bretagne

pour le grade de

DOCTEUR DE L'UNIVERSITÉ DE RENNES 1

Mention : Traitement du Signal et Télécommunications

École doctorale MATISSE

présentée par

Trong Nhan LE

préparée à l'unité de recherche UMR6074 IRISA
Institut de recherche en informatique et systèmes aléatoires - CAIRN
École Nationale Supérieure des Sciences Appliquées et de Technologie

---

Global Power Manager System for Self-Powered Autonomous Wireless Sensor Node

devant le jury composé de :

DIOURIS Jean-Francois
Professeur à l'Université de Nantes / rapporteur

PHAM Cong Duc
Professeur à l'Université de Pau / rapporteur

BERNIER Carolyn
Ingénieur-chercheur à CEA-LETI Grenoble / examinateur

DIGUET Jean-Philippe
Professeur à l'Université de Bretagne / examinateur

MAGNO Michele
Chercheur à ETH Zurich / examinateur

SENTIEYS Olivier
Professeur à l'Université de Rennes 1 / directeur de these

BERDER Olivier
Maître de Conférences à l'Université de Rennes 1/ co-directeur de these

PEGATOQUET Alain
Maître de Conférences à l'Université de Nice/ co-directeur de these

"Computers are incredibly fast, accurate and stupid; humans are incredibly slow, inaccurate and brilliant; together they are powerful beyond imagination."

— Albert Einstein

Acknowledgements

More than three years working in this thesis is the most memorical period in my life. It is really a miracle that I can work on my dream when I was a child, an autonomous system. It is also an honor for me to work and study in two dynamic laboratories, CAIRN in Lannion and LEAT in Nice.

Firstly, I grateful thank my supervisor Oliver Sentieys, the head of CAIRN, and co-supervisor Olivier Berder in Lannion for their patience and positive comments to improve my works when I met troubles. I will always remember the first review of my paper from Olivier Sentieys. All of his feedbacks have significantly changed my minds in writing scientific papers. Moreover, I would like to thank Samuel Mouget and Romain Fontaine for their designs and supports in PowWow platforms.

Secondly, I faithfully thank my supervisor Alain Pegatoquet for his encouragements when I was in LEAT, Nice. He spent a lot of his time for many discussions of the works in this thesis that I really appreciate. Moreover, he gave me a lot of ideas to improve my works. I also would like to thank Trinh Le Huy who helped me in hardwares of PowWow platforms.

Finally, I sincerely thank my parents, my younger sister and my girlfriend for their endless loves and supports throughout all these years of my education.

The work presented in this thesis is supported by the French National Research Agency (ANR) project GRECO bearing reference ANR-2010-SEGI-004-04.

Contents

Abbreviations

WSN	Wireless sensor network
EH-WSN	Energy harvesting WSN
PM	Power manager
EM	Energy monitor
AF-EP	Adaptive filter-based energy predictor
PID-PM	Power manager using PID controller
EM-PM	Power manager using EM
PE-PM	Positive energy power manager
NE-PM	Negative energy power manager
PEO-PM	Periodic power manager
WVR-PM	Wake-up variation reduction power manager
KAN-PM	Kansal power manager
CL-PM	Close-loop power manager
OL-PM	Open-loop power manager
OutCap	Output capacitor (primary storage)
StoreCap	Stored capacitor (secondary storage)
T_C	Cycle of periodic energy source
T_{EI}	Harvesting energy interval of T_C
T_{NEI}	Non-harvesting energy interval of T_C
$T_S(n)$	Duration of slot n
$T_{WI}(n)$	Wake-up interval during slot n
$V_S(n)$	Voltage of StoreCap at the end of slot n
$\tilde{e}_S(n)$	Energy in StoreCap at the end of slot n
$\tilde{e}_H(n)$	Harvested energy during slot n
$\tilde{e}_C(n)$	Consumed energy during slot n
$\tilde{P}_H(n)$	Harvested power during slot n
$\hat{e}_H(n)$	Predicted harvested energy for slot n
$\hat{e}_C(n)$	Predicted consumed energy for slot n
$\hat{P}_H(n)$	Predicted harvested power during slot n
P_{Sleep}	Power of the WSN node in sleeping mode

P_{Leak}	Leakage power of the whole system
CCA	Clear channel assessment
CBT	Calculation before transmission
SEN	Sensing
WUB	Wake-up beacon
ACK	Acknowledgment
DT	Data transmission
DR	Data reception

List of Figures

List of Tables

Chapter 1

Introduction

1.1 Internet of Things and Wireless Sensor Networks

Developments of wireless objects in our living spaces such as mobile phones, RFID tags, home appliances or monitoring cameras have openned a future internet, which is refferred as Internet of Things (IoT) [7]. Identified by a unique address, any wireless object is able to join the network and communicate with others as traditional computers through internet, based on standard communication protocols [8]. IoT is opening a novel opportunity for proliferation of Wireless Sensor Networks (WSNs), which can provide a wide range of monitoring applications such as monitoring spaces (environment, agriculture) or monitoring objects (human healthcare, smart buildings)[9].

A wireless sensor node, the basic object of WSNs, is usually comprised of a low-power sensing device, an embedded microcontroller, and a wireless transceiver [10]. The embedded microcontroller is generally used for collecting and processing the signal data taken from the sensors. Sensor elements produce a measurable response to a change in the physical world such as temperature, humidity, pressure and moisture. The wireless transceiver provides a medium to transfer information extracted from the sensors to a base station or through inter-communications among many nodes. Recent advancements in micro-electro-mechanical-systems (MEMS) technology, radi transceivers for wireless communications, and digital electronics have facilitated the development of low-cost, low power, multi-functional sensor nodes that are small in size and more and more efficient for processing and wireless communications [11]. Due to the short distance of the radio

frequency (RF) transceiver (e.g. 30m with CC2420, the transceiver from Texas Instruments), monitoring applications on remote places or large areas require a large number of randomly deployed wireless sensor nodes that constructs a WSN [12]. Many types of sensors such as seismic, magnetic, thermal, visual, infrared, and acoustic provide various WSN applications ranging from home automation [13], parking guidance [14], patient healthcare [15], to military surveillance [16].

In the last decade, many platforms of wireless sensor nodes from academia to industry are proposed such as Crossbow Mica2 [17], BTnode [18] or Intel Imote [19]. All of these platforms are low cost, small size and have especially, high energy efficency since energy consumption is the main constraint in WSNs. However, energy optimization of these platforms is performed mainly on hardware components. Therefore, the PowWow platform proposed in [20], which benefits from both hardware, software and protocol optimizations, is used in this thesis. PowWow is based on a low-power microcontroller MSP430 and RF transceiver CC2420. The design of PowWow is flexible and can easily intergrate a harvesting circuit for additional energy. Moreover, the protocol based on RICER (Receiver Initiated CyclEd Receiver) for communications among wireless nodes has been optimized. The consumed energy of protocol stacks has also been characterized in terms of energy and execution time [6]. The memory footprint is only 6 kbytes for the stack layers and less than 11 kbytes including an application of temperature sensing and mobile node tracking [20]. These advantages make PowWow a suitable choice for validating our works in this thesis.

1.2 Energy Harvesting Wireless Sensor Networks

Although WSNs can be easily used for monitoring applications in some places where cables are difficult and costly to draw, battery maintainance becomes a burden if widely used (e.g. large factories, dangerous places). This issue opens two different approaches in extending the system lifetime of WSNs. In the first one, a variety of methods and techniques to reduce power consumption, and therefore increase the system lifetime, has been proposed. Reducing RF energy consumption of the devices significantly reduces the power consumption so there are a number of novel hardware (e.g. wake-up radio

TABLE 1.1: Power density of popular harvesting technologies [5].

Harvesting device	Power density
PV-direct sun	15mW/cm^2
PV-cloudy day	0.15 mW/cm^2
PV-indoor	6 μW/cm^2
PV-desk lamp	0.57 mW/cm^2
Piezoelectric-shoe	330 μW/cm^2
Thermoelectric-100C gradient	40 μW/cm^2
Wind generator-15km/h [25]	7.93mW

receivers [21]), software (e.g. MAC and routing algorithm [22]) and duty cycle optimization approaches in this field [23][24]. Although system lifetime is improved, it is still crippled by the limited energy in the batteries, which are used for the energy storage.

In a second approach, alternative energy sources have been integrated to supplement, or even replace batteries. Thanks to advancements in harvesting energy techniques, everlasting environmental energy can be extracted and brings a breakthrough to design completely autonomous Energy Harvesting (EH) WSNs. A wide range of harvesting devices, which are cheap, tiny, and high power density have been proposed and can be applied to EH-WSNs such as photovoltaics (PVs) for solar energy [26], themoelectric for thermal energy [27] or wind generator for air-flow energy [25]. Table 1.1 summarizes their potential power density. It can be observed that solar energy extracted by PVs provides the highest power density. Moreover, PVs are small in size, inexpensive and easy to deploy compared to other harvesters. Therefore, PVs are the most widely used in EH-WSN platforms [28].

Although environmental energy can be scavenged for as long as desired, the amount of harvested energy has temporal variations due to the change of environmental conditions. Moreover, different energy sources usually have different behaviors. While solar energy in outdoor and light energy in indoor are periodic and can be predicted in a short future, thermal and wind energy are more arbitrary and unpredictable. The EH-WSN node cannot work at a fix performance as it can be underflowed (the node is shut down) when harvested energy is reduced and overflowed (harvested energy is wasted) when harvested energy is increased. Therefore, a Power Manager (PM) is often embedded in the EH-WSN node to adapt its computation load according to the harvested energy. Instead of minimizing the consumed energy [29] [30] or maximizing the system lifetime [31] [32] as in battery-powered WSN, the PM makes the harvesting node converge to Energy

Neutral Operation (ENO) [33], which means that consumed energy is equal to harvested energy for a long period. This strategy can provide a theoretically infinite lifetime (until its hardware is outdated). The next section will present an overview of current PM techniques in EH-WSN.

1.3 Power Manager in Energy Harvesting WSNs

Power manager techniques which are applied in EH-WSNs are classified into three categories: dynamic power manager, dynamic voltage and frequency scaling, and duty cycle power manager. Among these techniques, duty cycle power manager is the most popular approach. Their basic principles are described in the following subsections.

1.3.1 Dynamic power manager

Dynamic Power Manager (DPM) techniques are well studied and practiced in embedded systems. A fundamental principle of DPM techniques is that, all components composed a system are not required to work at their full performance [34]. Because most systems are designed to perform multiple functions (e.g. sensing, processing, and communicating in WSNs), many components are not required to be activated at a given time. As a consequence, these components can be turn into low-power states such as idle or sleep by the DPM [35][36] for energy saving. DPM does not have a fixed shape and can be implemented in either software or hardware [37]. In software, DPM can be implemented on the Operating System (OS) or directly at the application level. In hardware, DPM can be applied to a circuit module or a chip [34]. However, the main drawback of DPM techniques is that once in a low-power state, bringing a component back to the active state requires additional energy and especially, the latency to serve incoming tasks.

In addition, simply shutting off components as soon as they are not used might waste energy. It is due to the fact that it takes time to recover system states and sometimes the saved energy is less than the consumed energy during state transitions [34]. The concept of break-even time (T_{be}), which means the minimum length of idle time to achieve energy saving, is proposed to reduce this problem [38]. The system should only be shutdown when idle time is greater than T_{be} [37] because of the consumed energy to wake-up. This concept is illustrated in Fig. 1.1.

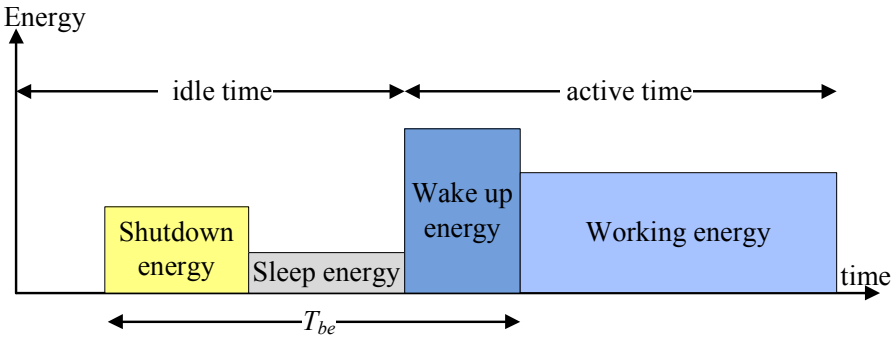

FIGURE 1.1: Break-even time based dynamic power manager. If the idle time is less than T_{be}, the system is not required to shutdown as additional energy to wake-up will be greater than running energy during this period.

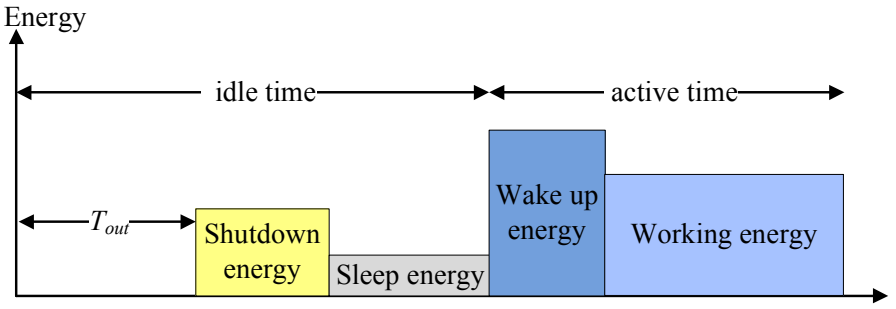

FIGURE 1.2: Timeout strategy in dynamic power manager.

Authors in [39] introduce a simple DPM strategy that uses a timeout value T_{out} and assumes the system will continue to be idle for at least T_{be} as shown in Fig. 1.2. The timeout strategy can be classified to adaptive or non-adaptive. In the non-adaptive technique, a fixed timeout strategy is proposed as T_{out} is a predefined value. In adaptive approach, T_{out} can be updated from recent historical values. However, timeout techniques have two main disadvantages. First, the prediction must be accurate or the system will lose rather than save power. Second, there is still some energy dissipated during the waiting period. This method can be useful for systems such as WSNs in which, the idle time is long in average.

In two different surveys of DPM techniques presented in [37] [40], authors classify DPM into two categories: predictive schemes and stochastic schemes. Instead of waiting for a fixed time period as in timeout schemes, predictive schemes attempt to predict the timing of future input events of the system and schedule shutdown (usually to a single power efficient state) based on these predictions. However, predictive approaches suffer wrong predictions as shown in Fig. 1.3. The system can be turned into low-power state too late or wake-up too early, that causes the waste of energy. Therefore, it is necessary to

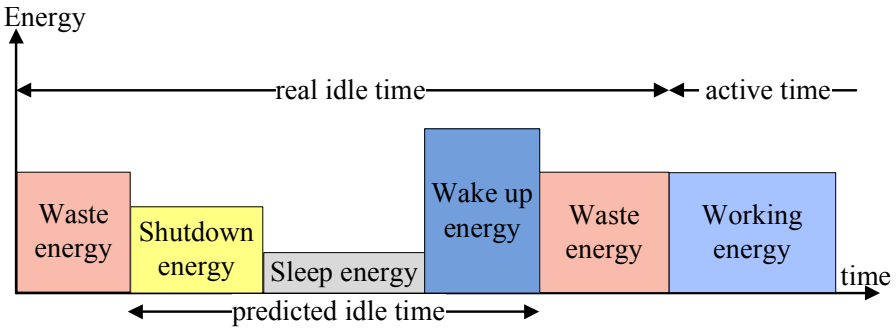

FIGURE 1.3: Predictive scheme in dynamic power manager. Waste energy occurs when the system turns to idle too late or wakes-up too soon.

improve the average error of prediction methods and reduce the delay overhead [35][41] in predictive schemes.

On the other hand, stochastic schemes, rather than eliminating uncertainty of predictions, model the system and the workload as Markov chains [42][40]. In these approaches, the energy consumption and transition times between many states (e.g. active, idle, sleep) of the system and other complex components (e.g. buffers, queues) are modeled as an optimization problem. Then, a trade-off between energy consumption and performance of the system is determined [40]. Stochastic schemes are well-researched category of DPM techniques [43][44][45] due to their several advantages compared to predictive schemes. The most advantage is that, they present global optimizations as different states and resources of a system are considered in Markov models. In addition, they provide a solution (in polynomial time) for the performance-constrained energy optimization problem. Finally, the strength and optimality of randomized policies can be exploited in stochastic schemes [40][46]. However, the limitation of stochastic techniques is an assumption of the priori knowledge of the system and its workload. In reality, workloads are often non-stationary and depend on real-time activities of a system.

1.3.2 Dynamic Voltage and Frequency Scaling (DVFS)

Dynamic Voltage and Frequency Scaling (DVFS) technique is another technique which is aimed at changing the system energy consumption profile. This technique exploits the variations in the workload for dynamically adjusting the voltage and frequency of processors in order to reduce power and energy consumption. These techniques have a potential for reducing the energy consumption. The challenge, however, is to preserve the feasibility of schedule and provide deadline guarantees. These techniques are of particular

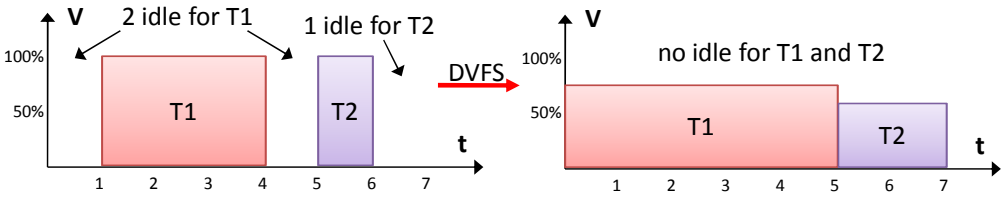

FIGURE 1.4: Two tasks are scaled by using DVFS technique.

effectiveness and interest because energy consumption of the processor is quadratically related to the supply voltage [47] [48]. Another advantage of these techniques is that, when the energy availability is low, they allow the system to keep running at a low speed with reduced energy consumption, without compromising the execution of important tasks.

DVFS techniques save energy consumption by using idle time of sensor nodes. Fig. 1.4 illustrates a simple example of how a DVFS technique saves energy consumption under the control of a scheduler. There are two tasks T1 and T2 where deadlines are 5 and 7, respectively. Taking into account the idle time for each task, DVFS schemes might reduce the system voltage, and therefore, prolong the system lifetime. They have been demonstrated to obtain significant energy savings for time-constrained systems [47] [49] [50]. However these algorithms do not perform well without considering the WSN workloads. Researches in [51] proposed a task-driven feedback algorithm according to the workloads of a sensor node and fix the errors through the PID control model. The improved algorithm could save 30% energy consumption compared to previous DVFS techniques.

In [52], authors apply a cooperative technique using DVFS and Dynamic Modulation Scaling (DMS) to sensor nodes for minimizing energy consumption. DMS saves energy by varying the constellation size (the number of bits per symbol) in transmission [53]. Similar to DVFS, DMS reduces energy consumption in exchange of the communication speed. Employing both DVFS and DMS can bring even more reserved energy compared to independently used. This cooperative architecture is based on the predicted workload of the processor and the transceiver. Prediction algorithm focuses on the periodic operations of sensor nodes such as acquiring temperature and humidity every minute. Therefore, the behavior of threads and communications on the sensor nodes also has periodic characteristics. The system predicts the workload of the processor and transceiver based on the stored log data. After that, it determines the appropriate processor voltage

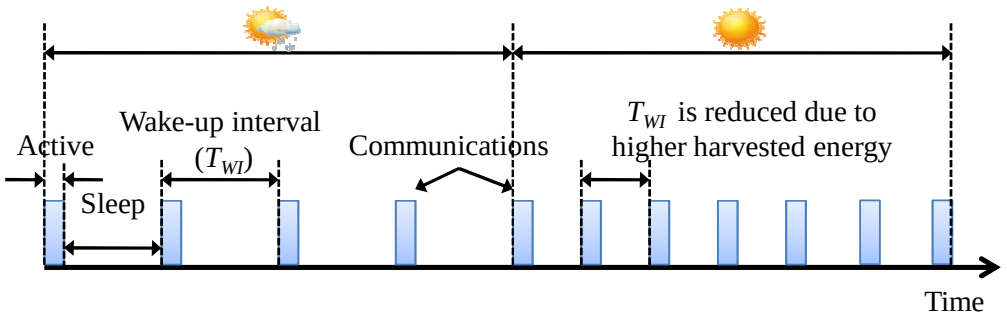

FIGURE 1.5: Duty cycle power manager. The average consumed energy of the node can be adapted by changing its wake-up interval according to the harvested energy.

(or clock frequency) and constellation size based on prediction results. It can be observed that the cooperative architecture is able to achieve up to 40% energy reduction when compared to non energy saving systems.

1.3.3 Duty Cycle Power Manager

This approach directly controls the MAC protocol, which is a source of waste for the radio bearing the channel as transmitting packets [22]. MAC protocols are specifically designed to turn WSN nodes alternately between active and sleeping periods. During the active period, nodes are able to transmit or receive data, but during the sleeping period, nodes are completely turned off for energy saving. Therefore, the global consumed energy of the node can be adapted by a power manager by changing the sleeping period (or wake-up interval) of MAC protocols as shown in Fig. 1.5. Different MAC protocols for WSNs can be found in [22]. However, we focus on the specific family of duty cycle protocols that can be used by a power manager in EH-WSNs. These duty cycle MAC protocols can be roughly categorized into two categories [54]: synchronous and asynchronous protocols.

Synchronous approaches such as S-MAC [55], T-MAC [56], R-MAC [57] and DW-MAC [58] synchronize neighboring nodes in order to align their active or sleeping periods. Neighbor nodes start exchanging packets only within the common active time, enabling a node to sleep for most of the time within an operational cycle without missing any incoming packet. Generally, these approaches aim to reduce the global consumed energy by reducing the idle listening. However, the required synchronization introduces extra overhead and high complexity. Moreover, a node has to wake up multiple times if its neighbors are on different periods. These disadvantages limit the use of synchronous MAC protocols in EH-WSNs.

Existing asynchronous approaches such as B-MAC [59], X-MAC [60], TICER [61], RICER [61] and WiseMAC [62], on the other hand, allow nodes to operate independently, with their own wake-up interval. Such protocols typically employ a low-power listening, in which, prior to data transmission, a sender transmits a preamble lasting at least as long as the sleep period of the receiver. When the receiver wakes up and detects the preamble, it stays awake to receive the data. These protocols achieve high energy efficiency and remove the synchronization overhead required in synchronous approaches. Moreover, they are mainly optimized for low traffic [22] and therefore, suitable for EH-WSNs which usually have low data rate [4].

Compared to other approaches, duty cycle power managers have two main advantages when applied in EH-WSNs. Firstly, they do not require complex hardware as DVFS, which have to support multiple system voltage and frequency levels. Secondly, duty cycle power manager directly control the MAC protocol, which is generally the most consumed energy in EH-WSNs instead of optimizing at higher layers as DPM. Therefore, an efficient duty cycle power manager can reduce the global consumed energy to increase the QoS while following the ENO condition. These advantages make duty cycle adaptation the most popular technique for PMs embedded in EH-WSNs [63][64][65][4].

In this thesis, a set of novel duty cycle PMs for EH-WSNs are presented. PMs adapt the average consumed energy of the node by changing its wake-up interval. Our PMs offer the following advantages compared to state-of-the-art PMs:

- As there are many attentions on EH-WSNs using solar energy, our PMs are rather more generic as they can be easily applied with different kinds of energy sources.
- The ENO condition over a long period must be satisfied for long-term operations in EH-WSNs. To achieve this, the ENO is periodically considered every period depending on behaviors of harvesting energy sources. It can be few minutes for continuous energy sources where harvested energy is available most of the time (e.g. light energy in a hospital, thermal energy from an industrial machine) or up to 24 hours for periodic energy sources where harvested energy can be scavenged a certain period (e.g. solar energy in the outdoor environment, light energy in an office).

- Our PMs maximize the QoS while satisfying ENO condition. This is required in most of monitoring applications to increase the system performance in terms of data throughput and latency.
- Finally, our PMs are low complexity, have small memory footprint, and can be implemented on a real EH-WSN node.

Following these features, the thesis outline and contributions are presented in the next section.

1.4 Thesis Outline and Contributions

Chapter 2: Energy Neutral Design Framework for Autonomous Wireless Sensor Network.

In this chapter, principles of potential harvesting energy sources for WSN are firstly presented, followed by a brief introduction of state-of-the-art platforms. Our efficient energy harvesting system, named MESC (Multiple Energy Sources Converter), which is compatible with various environmental sources such as light, heat, or wind energy is proposed. Our platform takes advantage of double level capacitors not only to prolong the system lifetime, but also to enable robust booting from the exhausting energy of the system. Moreover, a precise system design model providing a methodology to optimize the size of storage devices and the quality of service of a WSN node according to the consumed and the harvested energy is also proposed. Experiments to validate this model are performed on a real WSN platform with both photovoltaic cells and thermal generators in an indoor environment. The main contributions in this chapter are:

- Multiple energy sources converter (MESC) which can be used with different energy sources. Its energy storage is composed of two capacitors to provide a fast booting capability.
- Energy neutral design framework for optimizing the size of two capacitors in order to not only satisfy ENO but also to maximize the QoS of the EH-WSN node.

Chapter 3: Energy Monitor and Energy Predictor for Supercapacitor-based Energy Storage.

To provide energy aware capability, an energy monitor is embedded in EH-WSN. By only monitoring the voltage of a supercapacitor used for the energy storage (StoreCap) and tracking all activities of the node during a time slot, energy profiles such as the harvested energy, consumed energy and stored energy are provided. Moreover, an energy predictor using adaptive filter is also proposed to provide the prediction of harvested energy in a near future. Both energy monitor and energy predictor aim to low resource designs and energy sources independence. Therefore, they provide practical implementations on real EH-WSN nodes with different kinds of energy sources such as solar, thermal and wind energy. The contributions in this chapter are summarized as follows:

- Energy monitor for supercapacitor-based EH-WSNs.
- Energy predictor using adaptive filter.

Chapter 4: Duty Cycle Power Manager for Continuous Energy Sources.

In this chapter, a set of power managers are proposed for WSN applications powered by continuous energy sources such as light energy in hospitals or heat energy from industrial machines. As energy can be scavenged most of the time without interruption, the EH-WSN node can consume energy equal to its harvested energy during a defined time slot. Based on this principle, two different approaches are proposed in this chapter. First, an adaptive controller Proportional Integral Derivative (PID) is used as the PM, named PID-PM, to converge the voltage of StoreCap to ENO condition. PID-PM adapts the wake-up interval of the node (T_{WI}) only according to the change of current voltage. This shows an interest of our approach as monitoring harvested as well as consumed energy is not required. However, PID-PM suffers from a trial-and-error process before converging to ENO, which is mandantory in any adaptive controller. Therefore, the second approach is proposed based on the energy monitor proposed in Chapter 3. Not only based on the current voltage, estimations of harvested and consumed energy are also considered to determine the next wake-up interval. As a consequence, the energy monitor-based power manager (EM-PM) brings faster convergence to ENO than PID-PM. Main contributions described in this chapter are:

- PID-PM: Power manager with a PID controller.
- EM-PM: Power manager with the energy monitor.

Both PID-PM and EM-PM are low power, low complexity, energy sources independent, and can be easily implemented on a real wireless node with different harvesters.

Chapter 5: Power Manager for Periodic Energy Sources.

In contrast to energy sources assumed in Chapter 4, periodic energy sources only provide energy during an energy harvesting interval (T_{EI}) instead of during the next non-energy harvesting interval (T_{NEI}). This behavior is repeated every cycle $T_C = T_{EI} + T_{NEI}$. To satisfy the ENO after a cycle T_C of the periodic energy sources, the PM has to buffer harvested energy during T_{EI} and then, uses it during T_{NEI}. Therefore, a PEriOdic power manager (PEO-PM) is proposed and validated with light energy in our office. Not only satisfying ENO, PEO-PM is able to balance the Quality of Service (QoS) during the whole cycle T_C.

Another issue addressed in this chapter especially when considering a multi-hop EH-WSN is the effect of wake-up interval variations to the global QoS. Due to its low harvested energy, a relay node is impractical to synchronize with a transmitter if its wake-up interval regularly changes and therefore, degrading the global QoS. Therefore, a new power manager, named Wake-up Variation Reduction Power Manager (WVR-PM) is proposed. As the wake-up interval does not change for a long period, the synchronization among EH-WSN nodes is maintained during this period, and therefore, guaranteeing global QoS. Moreover, a new Synchronized Wake-up Interval MAC protocol (SyWiM) is also proposed to take advantage of the fact that the wake-up interval of the node is rarely changed. Based on this information, the transmitter can wake-up at the right time to communicate with the receiver. The main contributions proposed in this chapter are:

- A power manager for periodic energy source (PEO-PM).
- A wake-up variation reduction power manager (WVR-PM).
- A WiseMac-based RICER (W-RICER).

Finally, conclusions and perspectives are given at the last chapter of this thesis (**Chapter 6: Conclusions and Perspectives**).

Chapter 2

Energy Neutral Design Framework for Autonomous Wireless Sensor Network

2.1 Energy Sources for Wireless Sensor Network

In this section, an overview of potential energy sources for WSN is presented. According to our knowledge, popular sources of ambient energy considered suitable for WSN are solar, vibration, wind and thermal energy. In the following subsections, basic understanding of conversion principles and a brief survey of research efforts in these areas are described.

2.1.1 Solar Energy

Solar energy is directly extracted by the energy radiated from the sun or fluorescent lights in an office. Technologies to produce solar energy are widely classified as passive and active solar depending on the way they capture, convert and distribute solar energy. Active solar techniques include the use of photovoltaic panels and solar thermal collectors to harness the energy. Passive solar techniques include orienting a building to the sun, selecting materials with favorable thermal mass or light dispersing properties, and designing spaces that naturally circulate air.

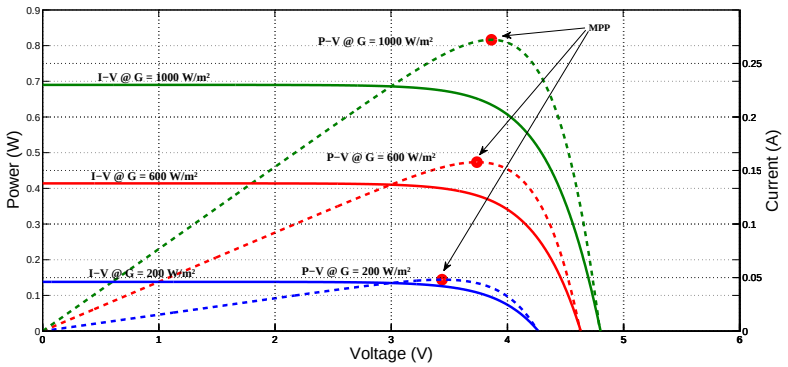

FIGURE 2.1: Maximum Power Point (MPP) of a PV in three different irradiance conditions (G) [1]. MPPT mechanism is designed to provide highest power from PVs.

In the context of small devices as WSN nodes, solar energy with photovoltaic cells (PVs) is the most popular method for supplying additional energy. It has been shown that among energy sources, solar provide the highest power density [66]. Moreover, PVs are small in size, cheap and easy to implement when compared to other strategies. Another advantage of solar energy is that the available energy can be predicted at a given time [33]. This feature helps the PM achieving ENO in a more efficient way with a low error energy predictor. A typical solar powered WSN platform is Heliomote where PVs are directly connected to rechargeable batteries used for the storage device [26]. This design is simple but inefficient as the energy extracted from PVs is much less than its maximimum value.

To increase the energy conversion efficiency, a low-power Maximum Power Point Tracking (MPPT) has been proposed. This technique aims to automatically find the voltage V_{MPP} or current I_{MPP} at which PVs provide the maximum output power P_{MPP} even in non-optimal weather conditions as illustrated in Fig. 2.1. A small photosensor is used in AmbiMax platform to estimate the light condition and force the PVs working around its MPP [67]. Other MPPT techniques specially designed for PVs are discussed in [68].

2.1.2 Thermal Energy

In this kind of energy, the difference of temperature between two surfaces of metals or semiconductors causes a voltage. Thermal energy can be extracted by using a thermo-generator (TEG) [69]. The hot surface of the TEG is attached to a heat source while the cold surface is commonly chosen to provide the heat spreading effect towards a heat sink. The thermal gradient results in an output voltage by the Seebeck effect and hence,

generates thermal energy. A commercial product exploiting thermal energy is Micropelt, which is shown in Fig. 2.2. Its output interface is compatible with the popular wireless evaluation board TI eZ430-RF2500T. Although thermal energy is often unpre-

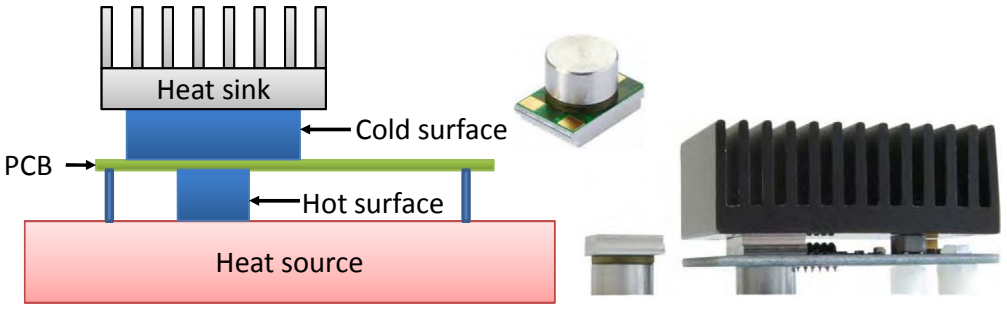

FIGURE 2.2: Typical setup for thermal-powered WSN.

dictable and uncontrollable, monitoring applications based on thermal-powered WSN usually only require tracking data whenever the harvested energy from TEG is available. One example involves the health monitoring of industrial engines, which can exploit excess or wasted heat when they are running. Another example concerns the monitoring of patient health in a hospital with the heat from body skin.

2.1.3 Wind Energy

The wind-powered WSN is limited to special applications due to the size of the turbine, which is used to harvest wind energy. Although it is less attractive compared to solar or thermal-based WSN, some efforts have been conducted to generate wind power at a very small scale recently. As shown in [25], a micro turbine with high efficiency conversion is quite promising. Its overall volume is below $300cm^3$ and suitable for powering a small WSN node in outdoor environment. This turbine can generate up to 10mW within a wind speed of 16km/h.

In order to maximize the harvested energy from the wind turbine over a wide range of operating conditions, a MPPT is also applied [67]. Moreover, an effective power-saving architecture has been proposed for the control circuit to turn the whole harvester off during the periods of wind absence. Experimental setup for wind energy can be found in Fig. 2.3. A low-power diode bridge is used to converter the AC voltage at the output of the turbine into a DC voltage for powering the WSN node.

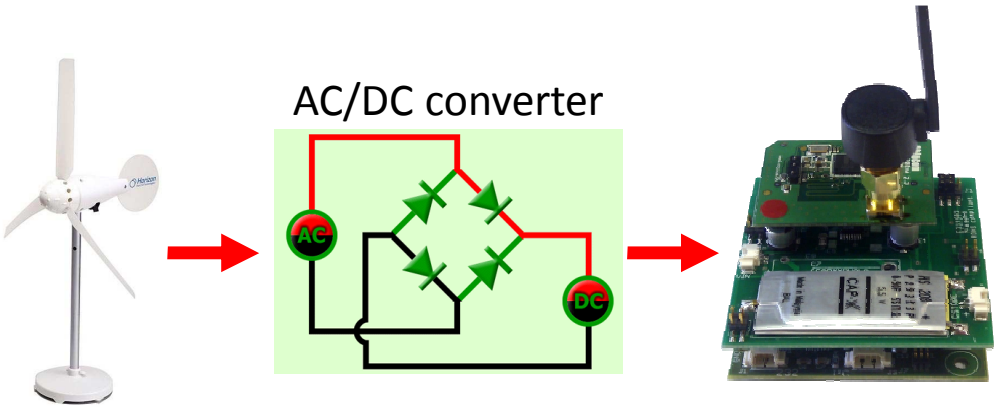

FIGURE 2.3: Experiment setup for wind-powered WSN. A diode bridge is used to convert the voltage generated by the wind turbine from AC to DC.

2.1.4 Other Energy Sources

Other energy sources, which seem to have great potential, such as vibration and fuel energy are discussed in this section. Vibration energy available for energy harvesting wireless sensor node can be found in buildings or human motions. There are three kinds of converters to extract vibration energy: electromagnetic, electrostatic and piezoelectric converters [70]. In the first case, the relative motion of a coil in a magnetic field causes an output voltage. Electrostatic converters consist of two capacitor plates and a voltage is created when these plates are moved. Finally, piezoelectric converters exploit the ability of some materials like crystals or ceramics to generate a voltage when there is a mechanical stress. Simulations and measurements in [70][71][72] show that piezoelectric converters provide the highest power density, up to $200\mu\text{W}/cm^3$ [66]. Therefore, many vibration-based WSNs are using piezoelectric converters for harvesting energy. A WSN node proposed in [73] can also be solely powered by the short duration vibrations when a vehicle passes over can be used for traffic monitoring applications. A vibration-based platform using a piezoelectric push-button in [74] shows that vibration energy when the button is depressed is sufficient to transmit a 24-bit frame. These results open new opportunities for autonomous WSNs using vibration energy.

Energy from fuel cells is useful when the energy storage devices (rechargeable batteries or supercapacitors) are going to deeply discharge and the ambient energy is not available. The WSN node then, activates the fuel cell interface in order to rapidly recharge its storage and avoid the system shutdown. Fuel cells are rechargeable electrochemical energy conversion devices where electricity and heat are produced as long as hydrogen

is supplied to react with oxygen [75]. The advantage of fuel cells is both energy storage and power delivery is much higher than traditional storage devices (batteries and supercapacitors). However they require hydrogen that complicates their deployment. The WSN using fuel cells is therefore, only available in research environment. Some typical platforms in this field can be found in [75] and [76] .

2.2 Hardware Design Challenges for EH-WSNs

Environmental energy can be converted from a wide range of harvesters such as photovoltaic cells (PVs) [26], thermal generators (TEGs) [27] or wind turbines [25]. However, energy harvesting (EH) WSNs need to cope with different shapes of the energy extracted from harvesters. While indoor/outdoor PVs provide high voltage but low current, TEGs output low voltage but high current. Meanwhile, wind turbines produce an AC output which needs to be adapted.

Another challenge in EH-WSNs is how to rapidly power on the system from its empty energy state. When the system must boot from exhausted energy, it has to wait for a sufficient voltage of the storage device to power on electronic devices. Moreover, the buffered energy must be enough for booting process at this voltage. For a standalone storage device, if the capacity is big, it takes a long time to charge the storage device to its powered voltage level. In contrast, if the capacity is small, the charging time is reduced but it cannot store enough energy for a long period without harvesting. As a consequence, a better design is the use of double layers for the storage device. The first one, with small capacity, directly powers the whole system. The second one, with bigger capacity, is connected to the first one and allowed to be charged as soon as the first storage device reaches the regulated voltage. This structure benefits from a short charging time for the small capacitor and is able to store a lot of energy in the second one [77].

Moreover, the operational lifetime of the energy storage device is an important feature when designing a long-term energy harvesting platform. Rechargeable batteries which are compatible with battery powered WSNs can be easily used as energy storage devices. However, the limited recharge cycles of batteries (500 cycles for a Lithium battery [78]) only provides around two years lifetime for a daily recharge system. Moreover, a

battery-based WSN requires an additional charging control circuit to avoid overflow or underflow, increasing the hardware footprints. Supercapacitors which have more than half a million recharge cycles and over 10-year operational lifetime [78] are widely used in energy harvesting WSNs [78][79]. Unfortunately, the leakage energy of a supercapacitor is higher than a battery [80] and therefore, needs to be properly considered in the design of a supercapacitor-based EH-WSN.

Instead of minimizing the consumed energy as in case of battery-powered system, a self-powered WSN node with ambient energy adapts the consumed energy by changing its quality of service (QoS) according to the available harvested energy when it is deployed. For an autonomous node, it is requisite to ensure that the consumed energy is equal to the harvested energy over a long period. This leads to Energy Neutral Operation (ENO) [33] with a theoretical infinite system lifetime. The size of the storage devices needs to be meticulously considered to satisfy ENO condition when designing an efficient EH-WSN node. As the harvested energy is not always available, it has to be buffered in the storage device during harvesting interval and is used during non-harvesting interval. If there is not sufficient space, a part of harvested energy is discarded and degrades the average QoS. However, increase the size of supercapacitor-based storage may not improve the QoS as the total consumed energy is also increased due to the leakage energy.

In this chapter, a new Multiple Energy Sources Converter (MESC) compatible with different kinds of harvesting devices such as PVs and TEGs is proposed. Our design is simple, flexible and easy to implement by using available commercial components. Two separate capacitors are used for energy storage to provide fast booting capability and prolong the system lifetime. While most of related platforms focus on maximizing the harvested power, there is a few concerns on sizing storage devices (supercapacitors in our platform), which directly impacts the system QoS. Therefore, a new energy neutral design framework to optimize the size of capacitors in MESC is also proposed as a second contribution. The objective is not only to satisfy ENO condition but also to provide a maximum QoS according to the consumed energy and the harvested energy. Two different kind of energy sources are considered in the design framework including continuous and periodic sources.

The rest of this chapter is organized as follows. In Section 2.3, state-of-the-art WSN platforms are presented. The hardware architecture and electrical characteristics of MESC

are proposed in Section 2.4, followed by the energy neutral design framework in Section 2.6. Experimental results with both thermal and solar energy sources used to validate our framework and optimize the size of supercapacitors are presented in Section 2.7. Finally, this chapter ends with conclusions.

2.3 State-of-the-Art WSN Platforms

In recent years, a large number of energy harvesting wireless sensor platforms ranging from academia to industry have been proposed. The independency of recharging or replacing batteries significantly increases the autonomy of the WSN nodes. This advantage makes energy harvesting WSN widely used in remote places where cables are becoming impractical and costly to draw such as volcano monitoring [81] or glacial movement monitoring [82]. In this section, an overview of existing platforms, which are classified into two categories, named single-path and dual-path architectures, is presented.

2.3.1 Single-Path Architecture

In this traditional architecture, there is only a main energy storage which can be a battery, a supercapacitor or both of them. All energy from harvesters is used to charge the energy storage for powering the WSN node through a DC/DC converter. The energy flow is depicted in Fig. 2.4. A Maximum Power Point Tracking (MPPT) circuit can also be integrated to the energy adapter in order to normalize the output energy to DC and to increase the conversion efficiency. This architecture is simple and easy to implement but suffers from a long booting time. As the DC/DC converter requires a minimum input voltage (e.g. 1.8V with TPS61030), it takes a long time to charge the empty energy storage with big capacitance to this voltage. To reduce this problem, the energy storage is usually charged to a certain voltage before deploying the nodes. Some typical platforms belonging to this category are listed in the following.

Heliomote [26] is one of the first solar energy harvesting WSN systems. Two small PVs are directly connected to rechargeable batteries through a protection diode. This solution is simple but inefficient as the harvested energy is reserved only when the output voltage from PVs is 0.7V higher than the battery voltage due to the diode drop. Moreover, batteries have limited recharge cycles [78] so that the system lifetime is reduced to less

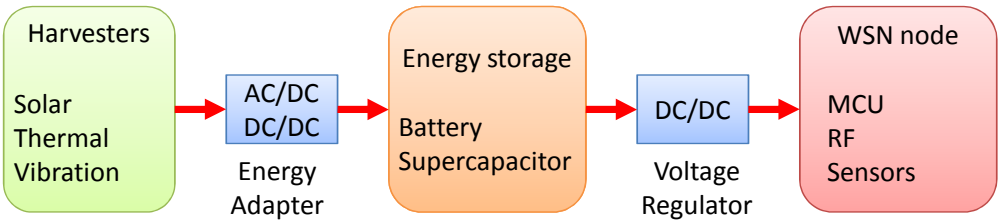

FIGURE 2.4: Single-path architecture for EH-WSN.

than two years for a daily recharge. Although Heliomote is specifically designed for solar energy, a MPPT circuit is not included. To increase the conversion efficiency, two NiMH batteries are used for the energy storage whose voltage varies between 2.2V and 2.8V. Therefore, with a diode used to prevent reverse current flow into the solar panel, the output voltage of the PVs remains close to the optimal point (from 2.9V to 3.5V). A system design model presented in [33] provides a framework to estimate the battery size as well as the average QoS of a WSN node in the ENO mode. However, this model is only applied for a periodic solar energy source.

Prometheus [79] has a similar design to Heliomote but a hybrid energy storage. It is a combination of a supercapacitor and a rechargeable battery to overcome the limited system lifetime of Heliomote [26]. When the supercapacitor is fully charged, the surplus energy will charge the battery. Otherwise, when the supercapacitor voltage is below a predefined threshold, the demanded energy is driven from the battery. By this way, the energy consumed by the WSN node is mostly served by the supercapacitor and access to the battery is reduced. This solution takes advantage of more than half a million recharge cycles of a supercapacitor [78]. Therefore, the battery lifetime can be extended up to four years under an average of 10% load. Unfortunately, supercapacitors have higher leakage current compared to rechargeable batteries. Moreover, the larger the capacity is, the greater the leakage current is. Therefore, an energy model is proposed in [79] to provide a trade-off between the size of the supercapacitor, the leakage energy and the average consumed energy of a WSN node. However, this energy model aims to maximize the system life time but does not satisfy the ENO condition. Prometheus also lacks a MPPT circuit and requires a high start-up voltage, which is similar to Heliomote.

Everlast [78] is an EH-WSN platform which only uses a supercapacitor as its energy storage. By removing the battery, the system lifetime is extremely increased. Authors claimed that Everlast can operate for an estimated lifetime of 20 years without any maintenance. Moreover, a MPPT is implemented by software to improve the output

power from PVs. The MPPT algorithm is implemented on the microcontroller with an I-V tracer. This accurate MPPT increases the conversion efficiency of PVs up to 89%. Another improvement in this work is the use of a pulse-frequency modulated (PFM) to transfer the energy from PVs instead of directly connecting them to the energy storage. Since the supercapacitor is seen as a short circuit to the PVs when they are connected together, the voltage of PVs is quickly fallen to the voltage of the supercapacitor which is usually far from the optimal operating point for PVs. By giving a series of pulse, the switch in PFM regulator keeps voltage of PVs around the MPP. This solution enables charging the supercapacitor up to 400% faster than direct charging as Heliomote or Prometheus. Unfortunately, Everlast requires a high harvested power in order of W due to the high speed operations of its MPPT, and is therefore, not a suitable choice for indoor harvesting systems where harvested power is only in order of mW. Another lack in this work is a design framework for meticulously sizing the supercapacitor for the energy storage.

2.3.2 Dual-Path Architecture

In a dual-path architecture, the fundamental difference compared to single-path architecture is the use of an energy flow controller. A primary and a secondary storage (PS and SS) are used to buffer harvested energy instead of only one storage as in case of single-path architecture. The basic blocks of the dual-path architecture are presented in Fig. 2.5. When environmental energy is available, all harvested energy will charge the PS for powering the WSN node. As soon as the PS is fully charged, surplus energy is driven into the SS. Otherwise, when the environment energy is insufficient, the remaining energy is taken from the SS to the PS for ensuring continuous operations of the WSN node. The advantage of this architecture is a fast booting from both empty PS and SS. Due to the small capacity of the PS, it is quickly charged to a minimum voltage sufficient to enable the voltage regulator and then, the WSN node can be activated. Moreover, SS has a big capacity to provide long-term operations during the period of energy absence.

DuraCap [77] is an example of a supercapacitor-based energy storage using dual-path architecture. This platform addresses two problems in solar-powered WSN including the booting process and MPPT with different PVs. Harvested energy is firstly charged in

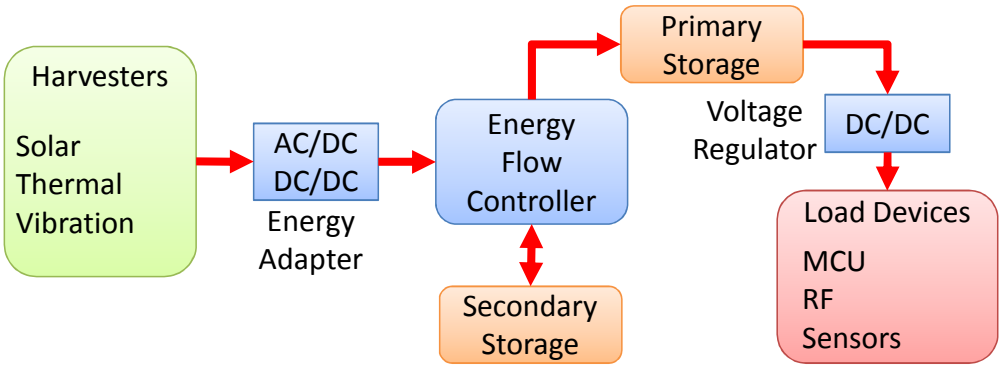

FIGURE 2.5: Dual-path architecture for EH-WSN. Energy from harvesters is distributed to both primary and secondary storages by the energy flow controller.

a small capacitor for booting the WSN node before fulfilling an array of bigger supercapacitors. A PFM regulator and an I-V tracer similar to Prometheus are implemented to perform MPPT function. Another improvement in this platform is a bound-control circuit using a low-powered comparator to generate the control signals for the PFM regulator. The MCU is not required to be active all the time for performing MPPT in software as in case of Prometheus, and therefore, reduces the global consumed energy. When a new PV is plugged-in, the MCU temporarily disconnects it from the system to track the I-V curve. As soon as the MPP is determined, the MCU only needs to send two non-volatile values to set the upper and lower-bound for the comparator in the bound-control circuit. Then, the PFM regulator enables the new configuration to accomplish the MPPT function. This structure is extended in EscaCap [83] with a dynamic configuration for the SS. The array of supercapacitors can be connected in series or parallel by means of a switch array. Experimental results show that EscaCap efficiently reduces the leakage energy and improves the charging speed.

As energy harvesting for single source, especially for solar, has been well investigated, recent works deal with the combination of several sources. When considering stationary outdoor applications, the most popular sources are solar and wind energy due to their wide availability and high power. Moreover, there seems to be a mutual complementarity between these sources: strong winds usually occur when the weather is bad rather than in sunny days, or during the night-time where solar energy is not available [84]. These reasons make solar and wind energy be widely chosen in a multi-source platform such as Ambimax [67] and Capnet [85]. However, with only a single energy storage, they suffer from booting time from an exhausted energy as explained in Section 2.3.1. Combined with the dual-path architecture, a multi-source, multi-storage EH-WSN platform

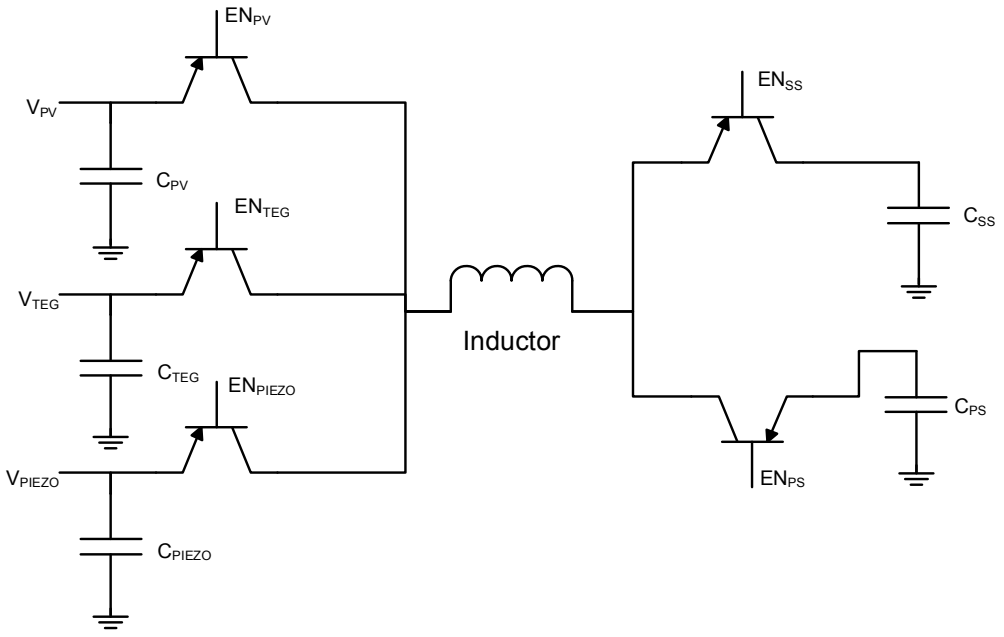

FIGURE 2.6: Multi-sources architecture for photovoltaics (PV), themoelectrics (TEG) and piezoelectrics (PIEZO) using a sharing inductor [2]. At a given time, only one harvester is connected to the inductor by selecting EN_{PV}, EN_{TEG} or EN_{PIEZO}.

is proposed in [86]. A supercapacitor and a rechargeable battery are used for the PS and SS, respectively. The power management circuit in this work acts as the energy flow controller illustrated in Fig. 2.5. Moreover, to increase the lifetime of the battery, the charge/discharge control circuit is designed to provide overcharge and undercharge protection.

To reduce the hardware cost due to the number of external off-chip components when multiple energy sources are used, an inductor sharing-based architecture is proposed in [2]. Three different harvesters are supported in this platform: PV, TEG and piezoelectrics (PIEZO) for vibration energy. Each harvester is equipped by a power converter to normalize the output energy. Since all of these converters are designed to operate in the discontinuous conduction mode (DCM), there is only one harvester connected to the inductor at a given time instead of the combination of all input energy sources as in [86]. In this design, a switch matrix has been used that can be reconfigured into all of the power converters. When a converter is disconnected from the inductor, harvested energy still keeps charging its temporary capacitor until its schedule (C_{PV}, C_{TEG} and C_{PIEZO}). Energy in this capacitor is then, immediately transferred through the inductor to the energy storage, including both primary storage (C_{PS}) and secondary storage (C_{SS}). Therefore, there is no wasted energy during the idle period of each converter.

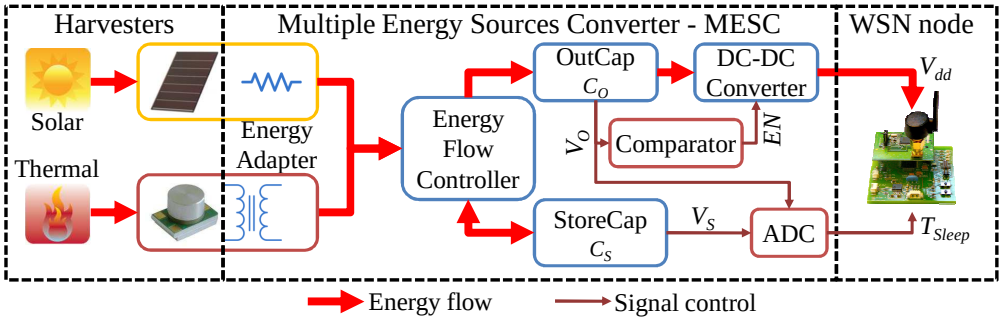

FIGURE 2.7: MESC hardware architecture. The harvested energy is normalized by the energy adapter and is distributed to OutCap and StoreCap by the energy flow controller. The comparator enables powering the system when there is sufficient energy in OutCap. Both V_O and V_S are connected to an ADC for monitoring the state-of-charge of OutCap and StoreCap for further processing (e.g. booting, adaptations ...).

Following this trend, we propose a Multiple Energy Sources Converter (MESC). Our platform is simple, flexible and easy to implement with commercial off-the-shelf (COTS) components. For higher efficiency, a dual-path architecture with two separate capacitors for the energy storage are applied in MESC. This structure not only provides a long system lifetime but also supports fast booting capability. However, the MPPT technique is not used in our platform because it is directly linked to a particular harvester. While PVs for solar energy have the MPP from 70% to 80% [68], TEGs for thermal energy have the MPP around 50% [2] of the open circuit. In this work, we focus on the system design model providing a methodology to optimize the size of the supercapacitor-based energy storage in order to satisfy ENO condition and maximize the system QoS. Both periodic and continuous energy sources are considered in our design model.

2.4 System Architecture and Operation Principles

The hardware architecture of MESC is shown in Fig. 2.7. Energy adapters are added to normalize the shape of output energy from multiple harvesters. For instance, PVs usually have high open circuit voltage (e.g. 5V with two PVs in series [26]) to simplify the energy converter with a resistor to limit the output current. Meanwhile, TEGs for heat energy bring a very low output voltage (e.g. 20mV [87]). In this case, a step-up transformer is added to amplify this output voltage. A combination of a diode-bridge and a step-up transformer can be used for a wind generator due to its low AC-voltage output. Energy adapters should be low-powered devices to minimize power losses. For instance, Schottky

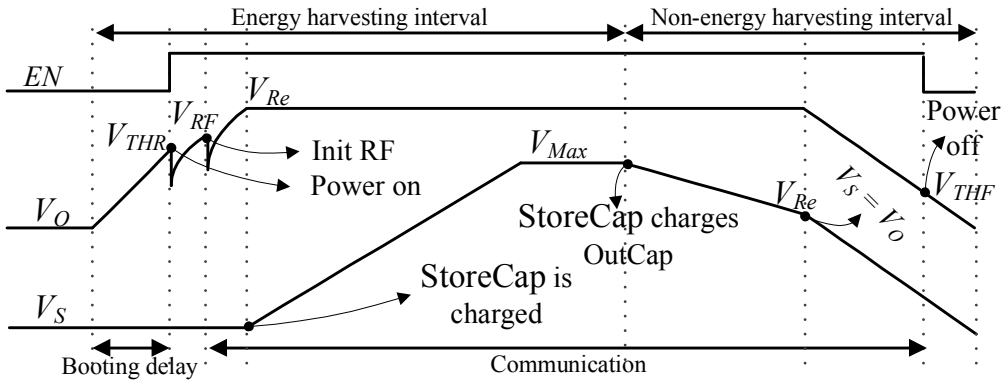

FIGURE 2.8: System operation diagram of MESC (time and voltage are not scaled). During the harvesting energy interval, the WSN node is kept shut down until V_O reaches V_{THR}. During the non-harvesting energy interval, the WSN node is turned off when V_O decreases below V_{THF}.

diodes (BAT47) for the diode bridge [25] and Coilcraft step-up transformers (LPR6235) are dedicated to low-powered systems and therefore, can be used in EH-WSNs.

Two separate capacitors are used for the energy storage and are charged by the energy flow controller. The output capacitor (OutCap) is connected to a DC/DC converter to provide the voltage supply to the wireless node. The second one is a supercapacitor (StoreCap) which acts as the main energy storage. OutCap has charging priority but small capacitance compared to the StoreCap. As a result, this design provides a fast booting capability due to short charging time of the small capacitor. Finally, to avoid the decreased radio range caused by decreased voltage of the OutCap, a DC/DC converter is used to provide a constant 3.3V output which is commonly compatible with WSN nodes.

Coordination of the control signals to operate the system is explained in Fig. 2.8. At the beginning, the system is powered off and storage devices are empty. All energy from harvesting devices will charge the OutCap. When V_O reaches the rising threshold (V_{THR}), the available energy in OutCap is sufficient for booting the system. Therefore, a comparator brings the enable signal EN from low to high for powering the WSN node. However, the available energy in the OutCap at V_{THR} is only enough for booting the system and initializing some basic modules of the microcontroller (MCU) such as I/O, Timer and ADC. Therefore, the MCU runs into sleep mode, periodically monitors V_O using a low ADC, and then initializes the radio chip as soon as V_O reaches V_{RF}.

The energy flow controller keeps on charging OutCap to its regulated voltage (V_{Re}). After V_O has reached regulation, StoreCap is allowed to be charged. However, when V_S

is charged to its maximum voltage (V_{Max}), there is no space for the harvested energy. Therefore, the WSN node should utilize all harvested energy to increase the QoS and also avoid wasted energy. When there is no more energy from harvesters (non-harvesting energy interval in Fig. 2.8), V_S charges V_O to V_{Re} as long as V_S is greater than V_{Re}. However, when V_S is less than V_{Re}, V_S and V_O decrease together and the system is powered off when V_O is under the falling threshold V_{THF}.

2.5 Leakage Energy and DC/DC Converter Efficiency

The electrical characteristics of MESC including the leakage energy and the DC/DC converter efficiency are estimated from experimental measurements. A CapXX supercapacitor of $0.9F$ [88] is used for StoreCap (C_S). At the beginning of the measurement, V_S is $4.925V$ and the WSN node is disconnected from MESC. Due to the leakage energy, V_S is linearly reduced to $4.825V$ after $10000s$. Therefore, the total leakage energy for a period T can be estimated by

$$E_{Leak} = P_{Leak}T, \tag{2.1}$$

where P_{Leak} is the leakage power defined as follows:

$$P_{Leak} = \frac{1}{2}(0.9F)\frac{(4.925V)^2 - (4.825V)^2}{(10000s)} = 43(\mu W) \tag{2.2}$$

This leakage power comes mainly from the 0.9F supercapacitor used for StoreCap. By characterizing this StoreCap alone, its leakage power is estimated around 30μW. Therefore, the total leakage power of remaining components in MESC including OutCap, the energy flow controller and the comparator is approximated to 13μW.

The DC/DC converter is designed to provide stable output voltage to the WSN node. Unfortunately, its efficiency not only depends on the input voltage but also on the output current. For instance, the TPS61030 component used in this work, has efficiency in range of $[80-93]\%$. It is impractical to achieve this efficiency precisely as the input voltage from OutCap usually changes due to environmental conditions and the output current depends on activities of the WSN node (transmission, reception or sensing). Therefore, the average DC/DC converter efficiency (η) has been characterized in our design model. Two different scenarios with the same PowWow WSN node [89] are setup to evaluate η. In the first scenario, the power supply of the node (V_{dd}) is directly connected to

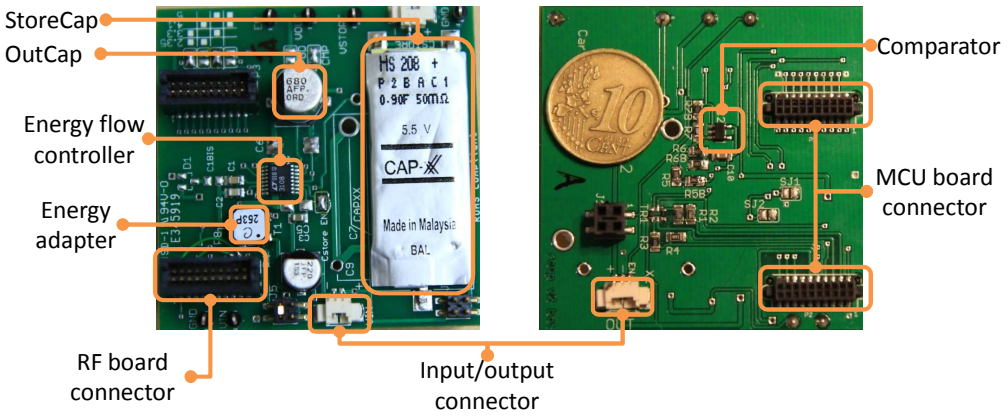

FIGURE 2.9: Hardware design of MESC.

V_O without using the DC/DC converter. In the second one, V_{dd} is connected to the output of the DC/DC converter. The average consumed energy for both scenarios is 830μJ and 971μJ, respectively. As a consequence, the average converter efficiency can be approximated to $\eta = 0.85$.

An overview of the hardware design of MESC can be found in Fig. 2.9. The LTC3108 component is used as an energy flow controller to drive the energy extracted from harvesters. It provides a complete solution for EH-WSNs with two outputs. The first output is connected to OutCap for powering the WSN node while the second one is connected to StoreCap for energy storage. The energy adapter is designed as a multi-choice footprint which can be soldered by a resistor in case of PVs or a step-up transformer in case of TEGs. The low-powered MAX917 component is used for the comparator. Its falling threshold (V_{THF}) can be chosen as the minimum input voltage of the DC/DC converter, while the rising threshold (V_{THR}) is in the range of $[V_{THF}, V_{Re}]$. In the current version of MESC, $V_{THF} = 1.8$V and $V_{THR} = 2.9$V. Determining C_O and C_S in order to satisfy ENO and maximize QoS is described in the next section. To provide harvesting energy aware capability, a low complexity software-based energy monitor will be proposed in Chapter 3. By reading the voltage of the StoreCap and tracking all activities of the WSN node, the harvested energy as well as the consumed energy can be estimated. A low-powered battery monitor IC in [26] is not required in our platform since the available energy in a supercapacitor can be easily estimated by measuring its voltage.

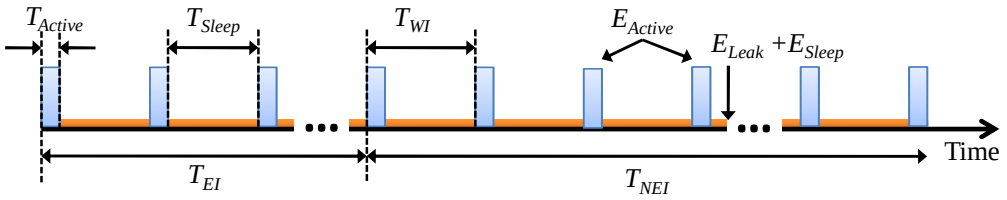

FIGURE 2.10: Communication of the WSN node during a cycle of the periodic source including the harvesting and non-harvesting energy interval (TEI and T_{NEI}). However, the harvested energy is only available during T_{EI}.

2.6 Energy Neutral Design Framework

In this section, the implications of MESC when it is used as a plug-in for a practical energy harvesting WSN node are considered. In particular, the size of energy storage devices (C_O and C_S) and the system QoS at the design phase are discussed.

First of all, we present how to efficiently determine the size of OutCap (C_O). For a complete booting of the WSN node from the exhaustion of energy, the buffered energy in OutCap must satisfy the following constraint:

$$\frac{\eta}{2} C_O (V_{THR}^2 - V_{THF}^2) > E_{Reset} \tag{2.3}$$

where E_{Reset} is the energy consumed by the WSN node during the booting process. The booting process is enabled as soon as V_O reaches V_{THR}. An amount of consumed energy E_{Reset} causes a voltage drop of V_O. However, V_O must be higher than V_{THF} for a successful booting. The constraint in (2.3) means that energy buffered in C_O from voltage level V_{THF} to V_{THR} must be sufficient for the booting process.

Once the system has booted, the WSN node periodically performs communication in the active period (T_{Active}) and then stays in low power mode during the sleep period (T_{Sleep}) until the next wake-up interval (T_{WI}) as shown in Fig. 2.10. Therefore, T_{WI} can be considered as the QoS of the system. The lower T_{WI} is, the better QoS is. The size of C_S to maximize QoS, or minimize T_{WI}, depends on the behavior of harvesting sources, the consumed energy as well as the harvested energy. Let us show their relations in the following subsections.

2.6.1 Periodic Energy Source

In this subsection, it is assumed that the energy is only harvested during an energy interval (T_{EI}) but not during a non-energy interval (T_{NEI}) (e.g. solar energy in an outdoor environment). This behavior is periodically repeated. A proposed technique to estimate T_{EI} and T_{NEI} can be found in [4]. Fig. 2.10 shows one cycle of the periodic energy source where the WSN node is required to send data each wake-up interval T_{WI} during the whole cycle. Therefore, during the T_{EI}, a part of the harvested energy must be reserved in StoreCap for activities of the wireless node during the T_{NEI}. The total harvested energy buffered in StoreCap during T_{EI} is estimated as

$$E_{EI} = P_H T_{EI} - \frac{1}{\eta}\left(\frac{T_{EI}}{T_{WI}} E_{Active} + P_{Sleep} T_{EI}\right) - P_{Leak} T_{EI} \tag{2.4}$$

where P_H is the harvested power, T_{EI}/T_{WI} is the number of wake-up times during T_{EI}, E_{Active} is the consumed energy of the WSN node for each wake-up, P_{Sleep} is the consumed power in sleeping mode and P_{Leak} is the leakage power of the whole system. The first term is the harvested energy during the energy interval, while the second one represents the consumed energy of the WSN node including active and sleeping period. From Fig. 2.10, the total sleep time of the node is

$$\sum T_{Sleep} = T_{EI} - \frac{T_{EI}}{T_{WI}} T_{Active} \tag{2.5}$$

However, the second term in (2.5) is in order of ms (as T_{Active} is only μs), which is negligible compared to the first term (in order of hour). Therefore, total leakage energy is estimated as $P_{Leak}T_{EI}$, where T_{EI} is approximated as the total sleep time of the node during harvesting energy interval. In order to buffer this amount of energy (E_{EI}), the size of StoreCap must satisfy

$$\frac{1}{2} C_S (V_{Max}^2 - V_{THF}^2) > E_{EI} \tag{2.6}$$

where V_{Max} is the maximum voltage of the StoreCap. Meanwhile, the consumed energy during the T_{NEI} is

$$E_{NEI} = \frac{1}{\eta}\left(\frac{T_{NEI}}{T_{WI}} E_{Active} + P_{Sleep} T_{NEI}\right) + P_{Leak} T_{NEI} \tag{2.7}$$

To achieve theoretical infinite lifetime of the WSN node, the ENO condition after a cycle including T_{EI} and T_{NEI} needs to be satisfied. For that, we must have $E_{EI} = E_{NEI}$, and so

$$T_{WI} = \frac{(T_{EI} + T_{NEI})\, E_{Active}}{\eta P_H T_{EI} - (\eta P_{Leak} + P_{Sleep})\,(T_{EI} + T_{NEI})} \tag{2.8}$$

This result presents the trade-off between the QoS of the system (T_{WI}), the consumed energy in the active period (E_{Active}) and the harvested power (P_H). Obviously, the lower E_{Active} and the higher P_H will decrease T_{WI} and therefore, increase the system QoS. Moreover, (2.4) and (2.6) present how C_S can be determined to maximize QoS during the design phase. The increase of P_H requires more space in StoreCap otherwise, a part of harvested energy is discarded. Instead of having E_{EI} , only $\frac{1}{2}C_S\left(V_{Max}^2 - V_{THF}^2\right)$ can be used for operations during non-harvesting energy interval (T_{NEI}). The consumed energy during T_{NEI} has to be reduced for ensuring ENO condition but, it also reduces the overall system QoS. It is interesting to notice that only the minimum C_S satisfying (2.6) provides the maximum QoS. Bigger capacitance would not improve the QoS due to higher leakage energy. Moreover, it is obvious that V_S at the end of a cycle should be equal to the value at the beginning of this cycle when ENO is satisfied. Unfortunately, the minimum V_S during non-harvesting energy interval (T_{NEI}) is V_{THF} which means that the ENO is only considered when $V_S > V_{THF}$ during harvesting energy interval (T_{EI}). A simple solution is to charge V_S to V_{THF} before its deployment. Otherwise, the ENO cannot be satisfied until V_S reaches V_{THF}.

2.6.2 Continuous Energy Source

In constrast with energy sources presented in the previous subsection, a continuous energy source (e.g. heat energy from an industrial machine, light energy in a hospital) usually provides harvested energy most of the time. A proposed WSN behavior when using this energy source is that the WSN node always maximizes the QoS of the system without the need of buffering energy in StoreCap. In this context, the ENO condition is only considered during the harvesting energy interval. Therefore, from (2.4), let $T_{NEI} = 0$, we have

$$T_{WI} = \frac{E_{Active}}{\eta\,(P_H - P_{Leak}) - P_{Sleep}} \tag{2.9}$$

TABLE 2.1: Energy consumption of the PowWow platform [6]

	Symbol	Value
Calculation Before Transmission	E_{CBT}	9.7μJ
Transmit/Receive wake-up Beacon	E_{WUB}	51μJ
Data Transmission	E_{DT}	80μJ
Data Reception	E_{DR}	100μJ
Clear Channel Assessment	E_{CCA}	18μJ
Transmission power	P_{Tx}	66.33mW
Reception power	P_{Rx}	76.89mW
Sleep power	P_{Sleep}	85.8μW

This result shows that the ENO condition is satisfied at anytime of the energy interval because T_{WI} is independent of T_{EI}. As a consequence, the size C_S is not important in this design because there is no surplus energy to charge the StoreCap. This behavior is also useful when C_S is fully charged ($V_S = V_{Max}$ in Fig. 2.8). Since there is no more space for storing the harvested energy, the wireless node can maximize the QoS according to the harvested energy to avoid wasting energy. Moreover, (2.9) can be used to estimate the QoS of the system according to E_{Active} and P_H when the environmental energy is available.

Our design framework presents a trade-off to design an efficient MESC for a particular sensor node. It is obvious that when energy is only available for a certain period, harvesting node has to buffer a part of harvested energy for continuous operations during the non-harvesting energy interval. Therefore, the size of the supercapacitor must be optimized not only to sufficiently buffer the harvested energy but also to minimize the leakage energy. However, when harvested energy is available most of the time, the wireless node consumes energy as much as it can harvest while respecting the ENO condition. In this context, the smaller size of StoreCap provides a better QoS as it reduces the leakage. Next section shows in details how capacitors are optimized when MESC is used for powering a PowWow WSN node.

2.7 Experimental Result

2.7.1 Measurements Setup

Our experimentations to validate the system design model are performed using the PowWow WSN platform [89] which is based on the MSP430 microcontroller and the CC2420

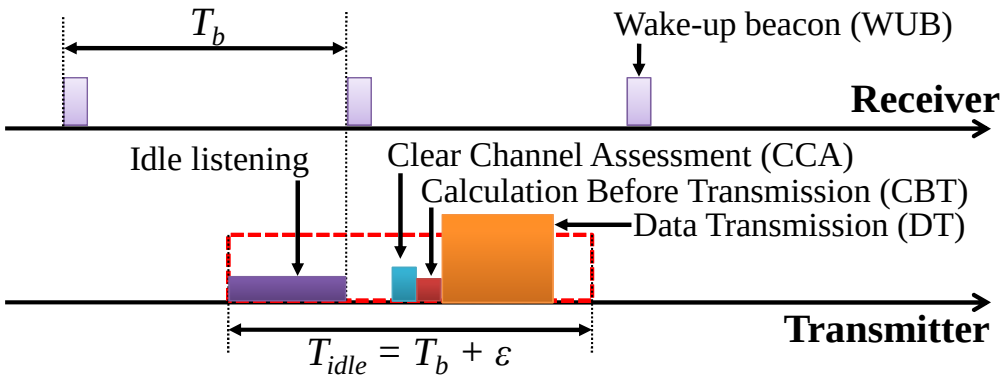

FIGURE 2.11: RICER-based protocol for communications between two nodes. When waking up, the transmitter waits for a wake-up beacon (WUB) from the receiver. After receiving a WUB, the transmitter sends a data packet (DT) after Clear Channel Assessment (CCA) and Calculation Before Transmission (CBT).

RF transceiver. MESC is configured to provide $V_{Re} = 3.3$V and $V_{RF} = 3$V The comparator is designed to provide $V_{THR} = 2.8$V and $V_{THF} = 1.8$V. The maximum voltage which is allowed for C_S is set to $V_{Max} = 5.2$V. $T_{EI} = 36000$s and $T_{NEI} = 50400$s for a spring day of 24 hours.

For communications among nodes, asynchronous protocols have shown their energy efficiency for a low traffic EH-WSN [22]. These protocols are based on a non-scheduled preample sampling that saves wasted energy due to the synchronization between many nodes. Some typical protocols in this field are RICER (Receiver Initiated Cycled Receiver) [61], TICER (Transmitter Initiated Cycled Receiver) [61], WiseMAC (Wireless sensor MAC) [62] and TAD-MAC (Traffic-Aware Dynamic MAC) [90]. A meticulous choice of the MAC protocol is a key to improve the QoS of the EH-WSNs due to its direct impact on the consumed energy (E_{Active}). TAD-MAC was shown to be an ultra low power and energy efficient protocol for wireless body area sensor networks. Therefore, it can be used for a single-hop EH-WSN with a low variation on the wake-up interval of many nodes. Meanwhile, WiseMAC is able to deal with the variation in a multi-hop network by exploiting the knowledge of the schedule of neighbor nodes to provide a minimized preamble sampling. In a general network, either RICER or TICER can be used. For ensuring the data transmission, the preamble must be long enough in order to have a successful rendez-vous.

In this work, a simple MAC protocol based on RICER [61] illustrated on Fig. 2.11 is used. This protocol has been validated on the PowWow platform and the energy consumed by different states of the protocol stack was fully characterized [6]. The receiver, powered by

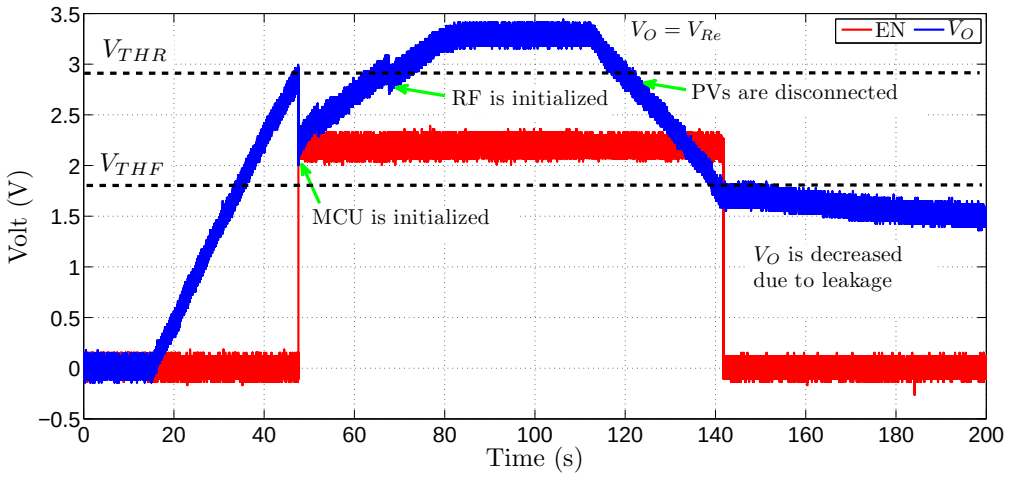

FIGURE 2.12: Booting process with light energy in an office.

batteries and connected to a host computer, periodically sends a wake-up beacon (WUB) each T_b = 50ms. When a transmitter wants to send a data packet, it has to wait for the WUB from the receiver (idle listening). After receiving the WUB, the transmitter performs a Clear Channel Assessment (CCA), Calculation Before Transmission (CBT) and a data packet transmission (DT). In order to deal with clock drift, the maximum idle listening period at transmitter (T_{idle}) must be slightly higher than T_b and is set to 52ms. Acknowledgement packets (ACK) are not used in this protocol as retransmission is not implemented at the transmitter. To evaluate the average consumed energy for each wake-up of the node, Table 2.1 summarizing the consumed energy of each state is used. For a long time measurement, we assume that $\overline{T_{idle}} = T_b/2$ as the average of idle listening time and therefore,

$$E_{Active} = P_{Rx}\overline{T_{idle}} + E_{WUB} + E_{CCA} + E_{CBT} + E_{DT} = 2081\mu J \tag{2.10}$$

To determine C_O, the consumed energy for booting a PowWow node (E_{Reset}) has been experimentally measured to 1094μJ. Therefore, from (2.3), C_O must be at least greater than 560μF. From the list of available capacitors and also to provide fault tolerance, a low leakage 680μF is used for the OutCap.

2.7.2 Fast Booting Capability

Fig. 2.12 shows the booting process with data extracted from a LeCroy oscilloscope when a PowWow node is powered by two PVs of size 4x6cm and is setup in our office. At the

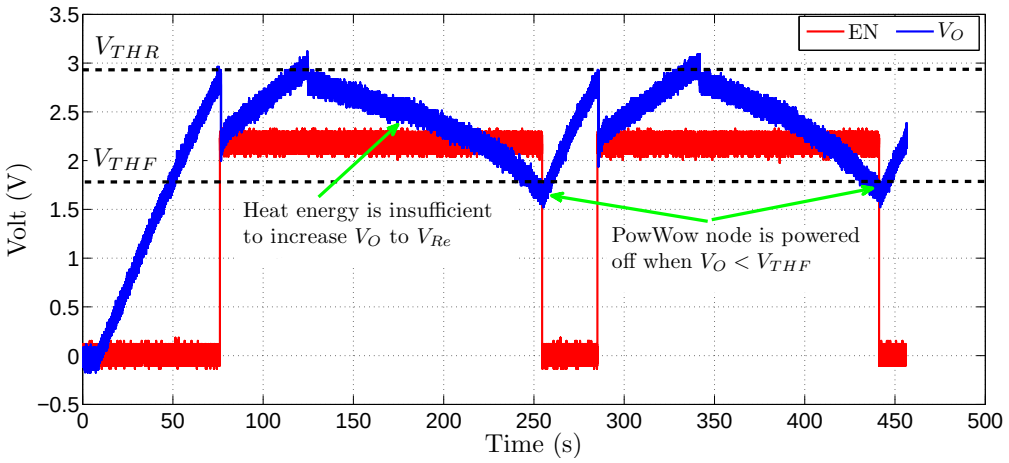

FIGURE 2.13: V_O with thermal energy. After initializing the RF transceiver, the thermal energy is only enough to charge V_O to V_{Re}. More harvested power is required to satisfy ENO of EH-WSN node.

begining, both C_O and C_S are empty. When PVs are connected to the PowWow node, V_O is rapidly increased. As soon as V_O reaches V_{THR} = 2.9V, the EN signal is enabled to power the node. Then, a voltage drop can be observed on V_O due to the consumed energy of booting process. However, V_O is still higher than V_{THF} = 1.8V. From this point, the MCU stays in low power mode and wakes up every 4s to read V_O through a low power ADC channel. As it can be seen on Fig. 2.12, V_O is slower increased when the MCU has booted since a part of harvested energy is consumed by the MCU. As soon as V_O is higher than $V_{RF} = 3V$, the RF chip can be initialized to successfully complete the booting process. If a bigger capacitance is used for V_O the booting time is longer due to the delay to charge V_O to V_{THR}. By using (2.3), we can optimize C_O to minimize the booting time which is about 50s in this measurement, as shown in Fig. 2.12.

Another promising energy source is the heat energy from industrial machines. WSNs with thermal energy can be used for monitoring health condition of these machines. By analyzing their temperature, vibration, strain, and pressure in real time, engine maintenance will not be required until these data show it is necessary, rather than regularly scheduled, therefore, saving a great deal of cost. A TEG of size 30x30x3.3mm is used in this study. The hot surface is attached to a laptop adapter as the heat source while the cold surface is chosen to provide the heat spreading effect towards a heat sink. The temperature gap between the working PC adapter and the ambient air provides around 30mV output by the TEG.

Fig. 2.13 shows the voltage of the OutCap when a PowWow node is used with a TEG.

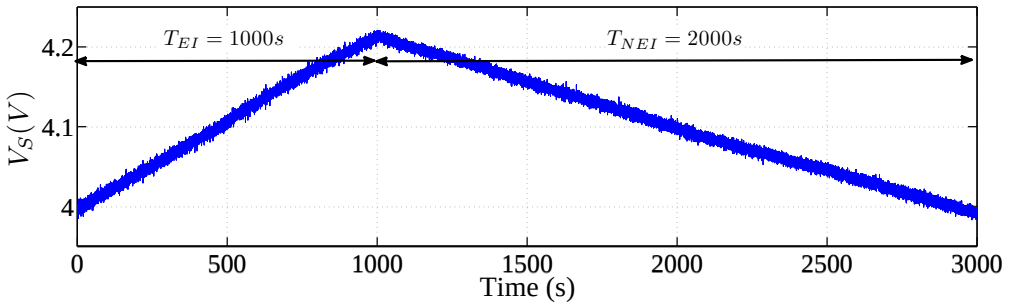

FIGURE 2.14: V_S of a PowWow node powered by two PVs when T_{WI} = 52s. The harvested energy buffered during T_{EI} = 1000s is used in the next 2000s when the environmental energy is no more available (T_{NEI}).

Due to lower harvested energy, a longer booting time is required compared to solar-powered node. After about 80s, the MCU is powered on when V_O = V_{THR}. V_O keeps increasing as the harvested energy is still greater than consumed energy of the PowWow node which is so far, only related to the MSP430. However, after initializing the RF transceiver CC2420, the harvested energy is less than the total consumed energy of the node including both MSP430 and CC2420. Therefore, V_O is decreased instead of continuously increasing to V_{Re}. The PowWow node is completely powered off when V_O = V_{THF}. The node wakes up again when there is enough buffered energy in the OutCap until its next shut down. Although booting process is successful, heat energy in this measurement is insufficient to satisfy ENO. A simple solution is to add one more TEG to increase the input power which can be found in [91].

2.7.3 Design Framework Validation

In this section, measurements to validate our design framework with two kinds of energy sources are presented. The PowWow node is now powered by two PVs of size 4x6cm setup in an office where the light condition is around 800lux. The measured harvested power at this condition is 574μW in average and can be considered as a periodic energy source. Therefore, from (2.8), T_{WI} = 52s. The Fig. 2.14 shows a short measurement of V_S when T_{EI} = 1000s and T_{NEI} = 2000s. As it can be observed, the energy saved in the first 1000s is enough for the next 2000s. If a higher QoS is required, either more energy must be scavenged (e.g. bigger PVs) or the consumed energy during the active period (E_{Active}) must be reduced.

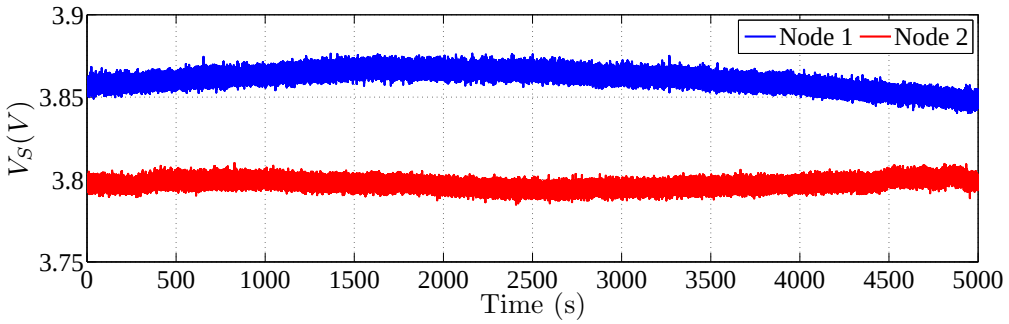

FIGURE 2.15: V_S of two different PowWow nodes when $T_{WI} = 5.7$s. V_S almost does not change due to the equality of harvested energy and consumed energy.

Fluorescent light conditions in a hospital or an industrial environment is a potential energy source for monitoring applications using energy harvesting WSNs. This kind of energy source can provide a theoretical infinite T_{EI} because the indoor lights are usually switched on all the time. Therefore, it can be considered as a continuous energy source. Considering two PVs used in the previous measurement, and using (2.9) to simulate this situation, T_{WI} is reduced to 5.7s. Fig. 2.15 presents the V_S for two nodes with different start up voltage in this context (3.87V for the first node and 3.80V for the second node). V_S is almost constant because, from (2.9), the ENO condition is always satisfied. Experimental results presented in Fig. 2.14 and Fig. 2.15 show the high accuracy of our system design model as the node behavior exactly satisfies the proposed application and the ENO condition.

2.7.4 Maximize QoS in ENO

In this section, our design framework is used to determine C_S in order to maximize the QoS in ENO for EH-WSN nodes. The leakage power of the whole system is modeled by

$$P_{Leak} = 13 + \frac{C_S}{0.9F} 30(\mu W) \tag{2.11}$$

The leakage power of C_S is linearly increased with its capacitance and is modeled based on the leakage power of a CapXX 0.9F characterized in Section 2.4. Meanwhile, the leakage power of remaining components of MESC is estimated to 13(μW).

First of all, from (2.8) for a periodic energy source, the harvested power must be at least greater than 500(μW) to achieve a valid value of T_{WI} (the denominator must be greater than zero). Lower harvested powered can not satisfy the ENO condition. In this

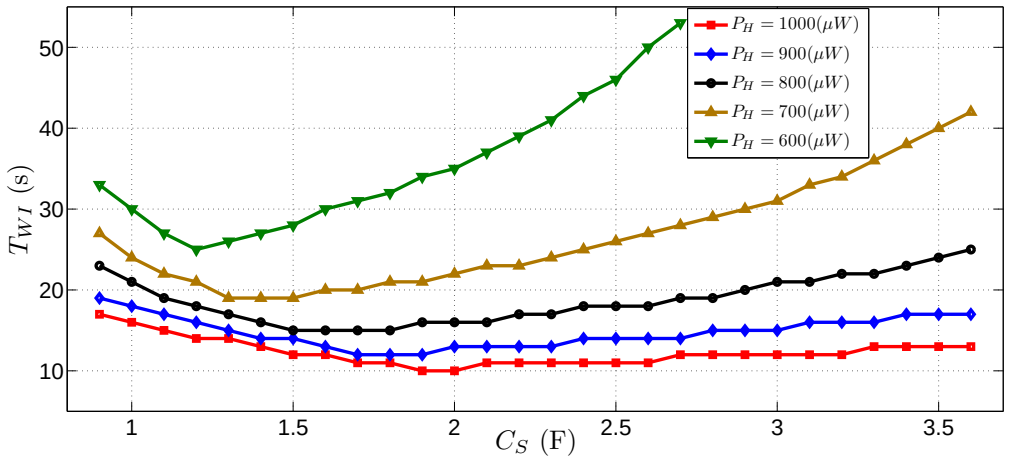

FIGURE 2.16: Average wake-up interval (T_{WI}) according to different harvested power (P_H) and storage capacitance (C_S) with a periodic energy source on OMNET++ simulation.

context, the harvested energy is less than the total consumed energy even if the WSN node always stays in sleeping mode without any communication. Fig. 2.16 presents the average T_{WI} according to different levels of harvested power (P_H) and capacitance of the storage (C_S). As it can be observed when $P_H = 600\mu$W and $C_S = 0.9$F, from (2.8), the wake-up interval during T_{EI} can reach 23s. Unfortunately, the condition (2.6) is false, C_S is fully charged to V_{Max} and then, all of harvested energy is discarded. To ensure ENO, the performance during T_{NEI}, when there is no more harvested energy, must be reduced to 49s. Therefore, the average wake-up interval is only 33s as it can be found in Fig. 2.16. When the size of C_S is increased to 1.1F, the system has more space to store the harvested energy and the wake-up interval during T_{NEI} is reduced to 28s. However, due to higher leakage, the performance during T_{EI} is reduced to 25s resulting to an average wake-up interval of 27s. In this case, just a small part of harvested energy is wasted. The best performance with minimum wake-up interval is achieved ($T_{WI} = 25$s) when $C_S = 1.2$F. All harvested energy is stored in the storage and is used for packet transmissions. Increasing the size of C_S greater than 1.2F is inefficient as the global consumed energy is also increased due to leakage energy and the wake-up interval has to increase to satisfy ENO. Although there is no wasted harvested energy when $C_S = 1.8$F, the overall QoS ($T_{WI} = 32$s) is still lower than the case when $C_S = 1$F ($T_{WI} = 30$s).

When the harvested power is increased, the average wake-up interval is reduced to provide better QoS as presented in Fig. 2.16. For each level of harvested power, there is an optimized C_S which provides the highest QoS with minimum T_{WI}. However, the impact of leakage energy on the average wake-up interval is reduced with high harvested power.

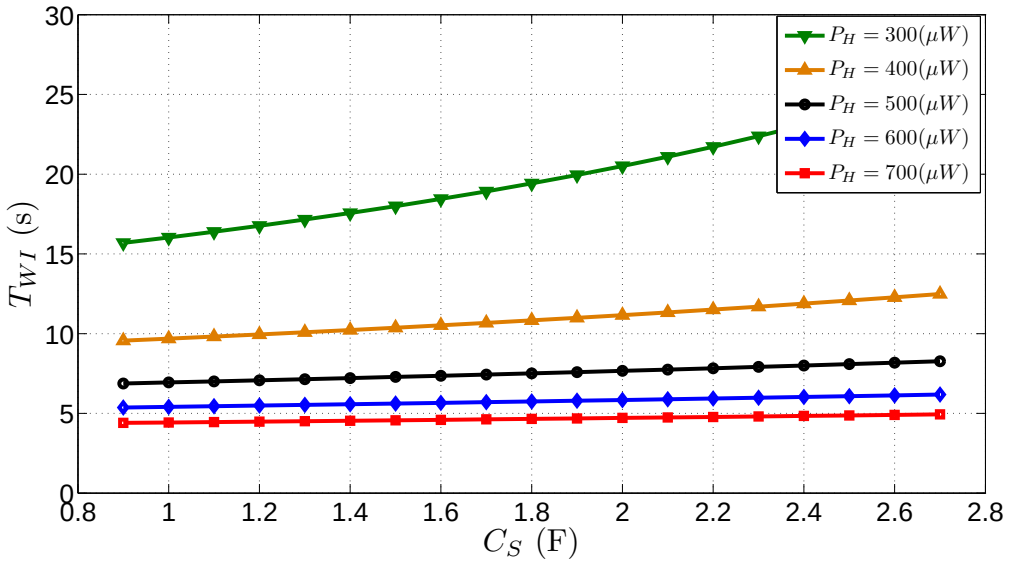

FIGURE 2.17: Average wake-up interval (T_{WI}) according to different harvested power (P_H) and storage capacitance (C_S) with a continuous energy source.

When $P_H = 1000\mu$W for instance, the minimum T_{WI} is 15s when $C_S = 1.8$F. However, when C_S is increased to 2.6F, T_{WI} is only reduced to 18s. Based on these results, if the harvested power is estimated in range of $[800 - 1000](\mu$W), two capacitors 0.9F can be used to provide 1.8F for the energy storage. From the datasheet of a harvester, its generated power (P_H) can be estimated and from our design framework, an optimized capacitance (C_S) can be determined to provide a maximized QoS in ENO for EH-WSN nodes.

For a continuous energy source, the harvested power should be greater than 200μW to satisfy the ENO as the denominator in (2.9) must be greater than zero. As it can be observed from Fig. 2.17, the leakage energy due to bigger capacitance has a linear impact on the wake-up interval of the node. This problem is discussed in Chapter 4 where an Energy Monitor-based Power Manager (EM-PM) adapts the wake-up interval of a thermal-powered PowWow node in real-time. The average performance is reduced by about 1s when two 0.09F capacitors, instead of only one, are used for C_S. However, the wake-up interval is more stable with higher capacitance as the EM-PM does not regard the small change on V_S, which is the main input to perform adaptations. In contrast, with lower capacitance, the EM-PM is more sensitive to the change of V_S which results in more variations of the wake-up interval. This behavior should be taken into account when designing MAC protocols. For instance, TAD-MAC requires a stable wake-up of the transmitter to optimize the wake-up interval of the receiver. Meanwhile, WiseMAC

is able to deal with variations of the wake-up interval. Finally, the impact of leakage energy is also reduced when more energy can be harvested.

2.8 Conclusions

In this chapter, the Multiple Energy Sources Converter (MESC) which is compatible with different environmental sources has been proposed. It is flexible and provides a complete solution for EH-WSN. The system has robust booting and durable energy storage by using two capacitors for the energy storage devices. Moreover, the precise energy neutral design framework provides various considerations for an efficient EH-WSN platform such as the size of energy storages to maximize the QoS of the system according to the consumed energy, and the harvested energy when the node is operating in ENO. Following chapters will focus on a dynamic power manager which adapts the system QoS according to harvested energy. To achieve this, an energy monitor providing energy profiles such as the harvested energy, consumed energy as well as the energy in storage devices in running phase must be embedded. When supercapacitors are used for the energy storage, our design takes advantage of a simple energy monitor which is proposed in Chapter 3. By only reading the voltage of StoreCap and tracking all activities of a EH-WSN node, these energy profiles are estimated. Moreover, an energy predictor using the adaptive filter is also proposed to provide the prediction of the potential harvested energy. Based on these information, the power manager is able to perform adaptations in order to achieve ENO on a EH-WSN node.

Chapter 3

Energy Monitor and Energy Predictor for Supercapacitor-based Energy Storage

3.1 Introduction

Wireless Sensor Networks (WSNs) provide a powerful combination of distributed sensing, computing and wireless communication that can be useful in various monitoring applications [12]. In order to design autonomous WSNs, energy harvesting (EH) and supercapacitor-based energy storage are considered as a promising approach. Moreover, a power manager (PM) is also embedded inside the wireless node to respect the Energy Neutral Operation (ENO) [33]. In the cooperation with the PM, an energy monitor is designed to provide energy profiles including the harvested energy ($\tilde{e}_H$), the consumed energy ($\tilde{e}_C$), the leakage energy ($\tilde{e}_{Leak}$) as well as the available energy in the storage device ($\tilde{e}_S$). These data will be used by the PM to dynamically adapt activities of the wireless node while respecting ENO condition. Fig. 3.1 shows how the energy monitor is embedded in the EH-WSN dual-path architecture. The energy monitor is not required for tracking the energy in the primary storage (PS) as it is usually filled up by the SS resulting in an almost constant energy in the PS during the whole operation time of the WSN node. Moreover, energy in the PS is negligible as it has a small capacity compared to the secondary storage (SS).

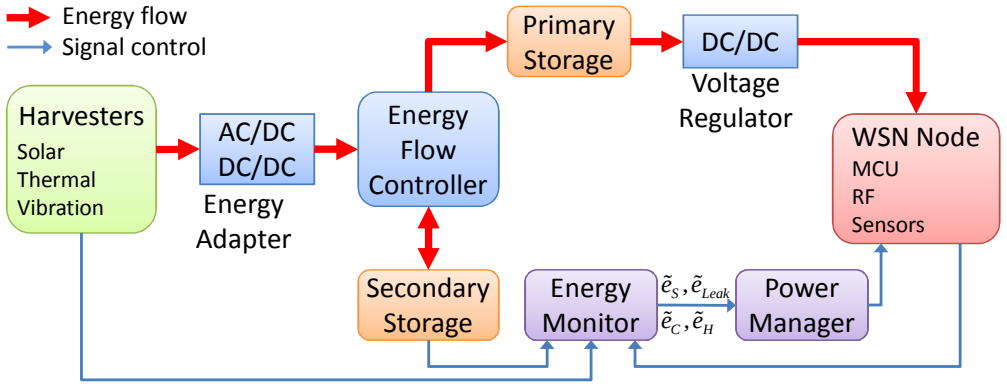

FIGURE 3.1: Energy monitor in the dual-path architecture.

The energy monitor is an essential component to provide energy-aware capability in EH-WSN. It can be implemented either by hardware or software components. The basic principle of hardware-based approaches is based on real-time monitoring of the current and voltage and then, the energy consumed by the WSN or energy extracted from harvesters is computed. Therefore, hardware-based energy monitors are able to be applied for any platform with different harvesters. Meanwhile, software-based approaches usually have platform dependencies and need to characterize the consumed energy of the platform before implementation. However, most of current energy monitors are designed for battery-based systems. The first contribution in this chapter is an efficient energy monitor, which is specifically designed for supercapacitor-based EH-WSN. Our energy monitor only needs to read the voltage of the SuperCap, which is used for the SS, and keeps tracking activities of the wireless node to provide the estimation of harvested as well as consumed energy. Therefore, our energy monitor can be applied for different energy sources.

Moreover, an energy predictor to provide the estimation of incoming harvested energy is also useful for the PM. With the energy predictor, a predictive PM can optimize activities of the wireless node in the near future. However, proposed energy predictors are focused on solar-based WSNs to exploit from the diurnal cycle of solar energy. On the current day, the harvested energy at a given time is expected to be similar to the harvested energy at the same time on the previous day. Therefore, historical values of harvested energy for many days are maintained to predict the future energy profiles. The second contribution in this chapter is a low complexity energy predictor for multiple harvesting sources such as solar, light and wind energy using the adaptive filter is proposed. Our energy predictor has a dynamic configuration in run-time to reduce the prediction error.

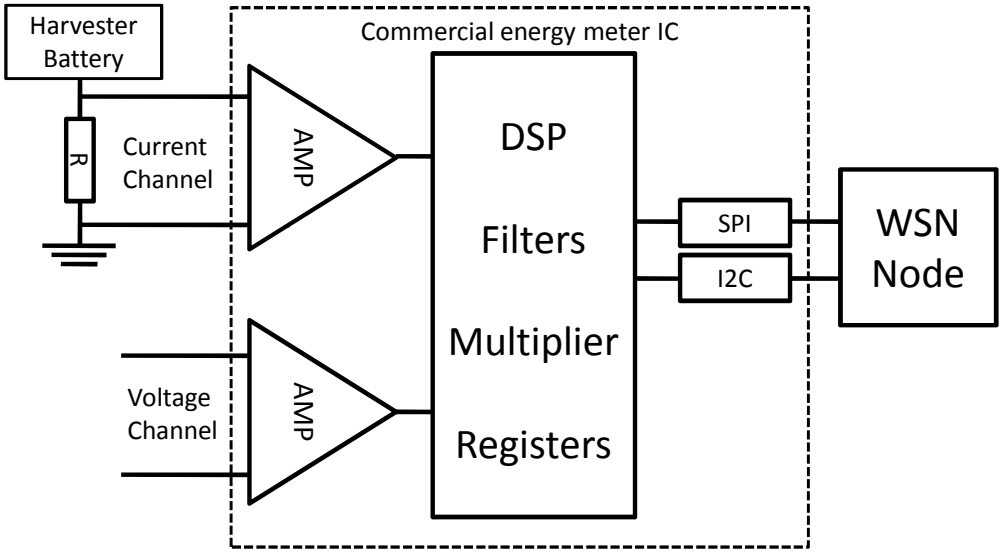

FIGURE 3.2: Generic architecture of a hardware-based energy monitor.

Based on only one previous value of the harvested energy, the energy predictor estimates the next one and therefore, has a low memory requirement.

The rest of this chapter is organized as follows. In Section 3.2, state-of-the-art energy monitors, which are classified in hardware-based and software-based energy monitors, are presented. Our proposed energy monitor designed for supercapacitor-based EH-WSNs is described in Section 3.3. Then, state-of-the-art energy predictors are presented in Section 3.4, followed by the design of our energy predictor in Section 3.5. Simulation results with both solar, light and wind energy are depicted in Section 3.6. Finally, this chapter ends with conclusions.

3.2 State-of-the-Art Energy Monitor

3.2.1 Hardware-based Energy Monitor

This kind of solution benefits from various commercial energy meter ICs. The basic principle is to measure the voltage drop around a shunt resistor R connected to the power supply of the circuit as shown in Fig. 3.2. The consumed current (I_C) is derived by dividing this voltage drop (V_{dr}) by the resistance R. Then, the supply voltage (V_{dd}) read by an analog-to-digital converter (ADC) can be multiplied by I_C to obtain the power usage. These computations are usually done on the MCU. This approach can be found in [26] where a low-power monitor IC (DS2438) is used to perform the role of energy

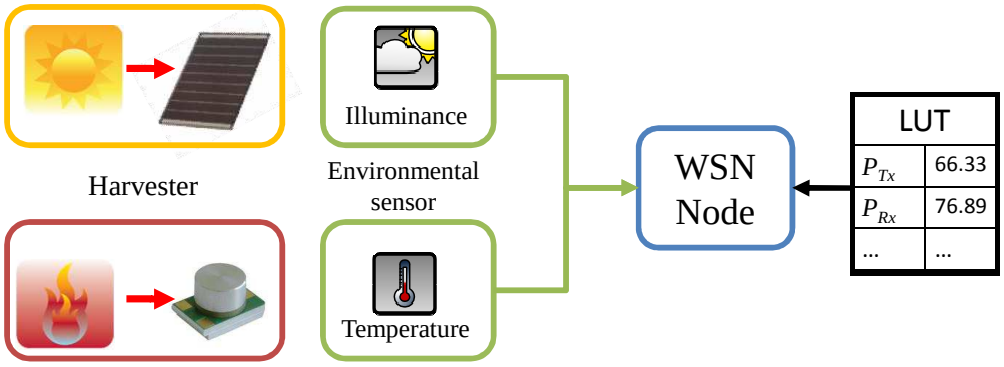

FIGURE 3.3: Generic architecture of a software-based energy monitor.

monitor. Information regarding instantaneous solar power availability, battery terminal voltage and accummulated current are provided by a one-wire interface (SPI or I2C).

However, on-board ADC in [26] is only 10 bits which limits the resolution. To achieve higher resolution, a scalable power observation tool (SPOT) taking advantage of a voltage-to-frequency converter (VFC) to read the voltage drop from a shunt resistor is proposed in [92]. Since VFC is entirely an analog device, it provides an infinite resolution. In order to minimize MCU overhead, an internal 32-bit counter is used to directly provide the energy measurement. In this way, SPOT is well adapted for a WSN node to monitor its harvested and consumed energy. Moreover, with extremely high sampling frequency (20kHz) compared to monitor IC (36.41Hz with DS2438 [26]), SPOT is able to follow the change of current during a short active period of the WSN node instead of an assumed constant current in [26].

3.2.2 Software-based Energy Monitor

Software approaches do not require sophisticated hardware designs. However, some offline characterizations need to be performed before the implementation. A simple energy monitor presented in [4] is based on a small illuminance sensor and the consumed energy profiles for each actitivity of the WSN such as sensing and RF transmission. Experimentations are performed on a WSN platform (TI ez430) equipped with a small PV in size of 2.25x2.25in. The harvested energy is approximated by a function of the light intensity from the illuminance sensor (expressed in lux). Meanwhile, the consumed energy is the average current delivered from the battery during a period and is computed independently for sensing, transmitting and receiving a data packet. This solution can

be extended to different kinds of harvesters and is depicted in Fig. 3.3. However, an environmental sensor is required to estimate the harvested energy (e.g. illuminance sensor for solar energy, temparature for thermal energy) and a look up table (LUT) is used to estimate the consumed energy of the WSN node.

While state-of-the-art energy monitors are designed for battery-based systems, our proposed energy monitor is dedicated for supercapacitor-based EH-WSNs. This energy monitor also benefits from a LUT to provide a precise consumed energy of the WSN node. When a supercapacitor is used for energy storage, harvested energy can be estimated by reading the voltage of supercapacitor without any environmental sensor. Therefore, our approach can be easily applied for different energy sources.

3.3 Supercapacitor-based Energy Monitor

In this section, an energy monitor embedded in supercapacitor-based EH-WSN is proposed. The time domain is divided into slots of duration $T_S(n)$ and the energy monitor is carried out at the end of each slot. By reading the current voltage of the supercapacitor (V_S) used for the SS (StoreCap) and looking into a table characterizing consumed energy of atomic functions, following discrete energy values are evaluated:

- $\tilde{e}_S(n)$, $\tilde{e}_{Leak}(n)$: available energy in StoreCap at the end of slot n and leakage energy of the whole system during slot n, provided by the stored energy model.
- $\tilde{e}_C(n)$: consumed energy of the wireless node during slot n, provided by the consumed energy model.
- $\tilde{e}_H(n)$: harvested energy during slot n, provided by the harvested energy model.

3.3.1 Stored Energy Model

The ideal capacitor only charges and discharges electrical energy without any dissipation. Actually, the imperfection of capacitors creates resistance. This is specified as the equivalent series resistance (ESR) of a capacitor. This resistor consumes a part of capacitor energy. Fig. 3.4 shows the equivalent circuit used to analyze the energy in the capacitor

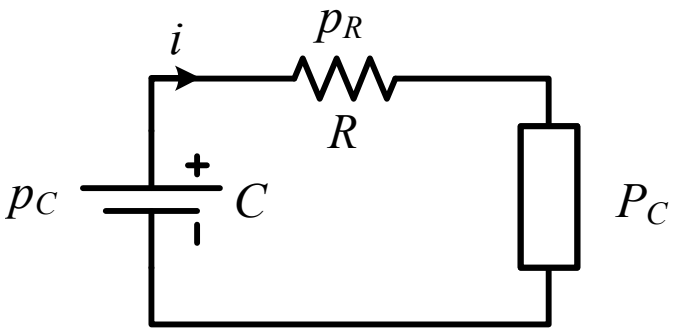

FIGURE 3.4: Generic model for the supercapacitor.

with assumption that the load power is constant. The power drawn from the capacitor must be equal to the power consumed by the load and resistor ESR as follows:

$$p_C(t) = -(P_C + p_R(t)) \tag{3.1}$$

where $p_C(t)$ is the power drawn from capacitor:

$$p_C(t) = CV_C(t)\frac{dV_C(t)}{dt} \tag{3.2}$$

and $p_R(t)$ is the power loss from ESR resistor:

$$p_R(t) = i^2(t)R \tag{3.3}$$

and P_C is the power consumed by the wireless node, which is assumed as a constant value. Therefore, it can be approximated as the average consumption energy during a time slot lasting for T_S:

$$P_C = \frac{\tilde{e}_C(n)}{T_S} \tag{3.4}$$

From results in [93], the instantaneous current is evaluated as:

$$i(t) = C\frac{dV_C(t)}{d(t)} = \frac{-V_C(t) + \sqrt{V_C^2(t) - 4RP_C}}{2R} \tag{3.5}$$

Sampling the voltage across the capacitor many times during slot n, we can approximate the average current $I(n)$. Therefore:

$$\tilde{e}_S(n) = \frac{1}{2}CV_S^2(n) - I^2(n)RT_S(n) \tag{3.6}$$

The first term in (3.6) is the energy stored in the capacitor that comes from (3.2) while the second one is the energy dissipated in R. However, the low consumed current of the WSN node (in order of mA) and low ESR (in order of mΩ) implies that the second term in (3.6) is in order of pJ, and is therefore, negligible when compared to the first one (in mJ). Consequently, the buffered energy in StoreCap can be approximated according to its voltage $V_S(n)$ and capacitance C_S as:

$$\tilde{e}_S(n) = \frac{1}{2}C_S V_S^2(n) \tag{3.7}$$

Meanwhile, the leakage energy of the whole system during slot n depends on C_S. As shown in [80], leakage energy is more severe for a larger capacitor than for a smaller one. However, for a specified C_S, leakage energy can be estimated by

$$\tilde{e}_{Leak}(n) = P_{Leak}T_S(n), \tag{3.8}$$

where P_{Leak} is the leakage power, which is considered as a constant.

3.3.2 Consumed Energy Model

In a WSN application, a node periodically wakes up and briefly turns on active mode for sensing and RF communication. It stays most of the time in sleeping mode for energy saving. Therefore, the total consumed energy during slot n can be divided into two parts: $\tilde{e}_{Active}(n)$, the consumed energy in active time, and $\tilde{e}_{Sleep}(n)$, the consumed energy in sleeping time. As the consumed current is nearly constant in sleep mode, $\tilde{e}_{Sleep}(n)$ can be easily estimated based on the sleep power P_{Sleep} as

$$\tilde{e}_{Sleep}(n) = P_{Sleep}T_{Sleep}(n) \approx P_{Sleep}T_S(n) \tag{3.9}$$

The total sleeping time during slot n ($T_{Sleep}(n)$) is approximated to $T_S(n)$ as the total active time is negligible (in order of ms) compared to the sleeping time (in order of s).

However, it is more complex to estimate $\tilde{e}_{Active}(n)$ based on the power as many different scenarios in the active time results in a variation of the consumed current of the WSN node. Therefore, to obtain more accurate measurements, it is necessary to identify the consumed energy of many scenarios according to a specific WSN platform.

In this work, PowWow [89] platforms, which are based on the MSP430 microcontroller and the CC2420 RF transceiver, are used to evaluate our approaches. The consumed energy for these activities performed on PowWow platform has been already characterized and gathered into Table 2.1 which is used as a LUT. The microcontroller keeps tracking all activities of the node to estimate the consumed energy in active mode during a slot. Let's apply the energy monitor into two PowWow nodes performing communications based on the RICER protocol as shown in Fig. 2.11. In this example, when the transmitter wants to send a data packet, it has to wait for a Wake-Up Beacon (WUB) from the receiver. Once a WUB is received, the transmitter performs Clear Channel Assessment (CCA) and Calculation Before Transmission (CBT) before transmitting a data packet (DT). We define k the number of wake-up occurring during slot n. Therefore, the total consumed energy in active period of the transmitter can be expressed as

$$\tilde{e}_{Active}(n) = \sum_{i=1}^{k} t_{idle}(i) P_{Rx} + k(E_{WUB} + E_{CCA} + E_{CBT} + E_{DT}) \tag{3.10}$$

where $t_{idle}(i)$ represents the i^{th} idle listening time for the WUB. Meanwhile, the receiver sends its WUB every wake-up and waits for a potential packet. Therefore, the consumed energy at the receiver is

$$\tilde{e}_{Active}(n) = \sum_{i=1}^{k} (E_{WUB} + t_{DR}(i) P_{Rx}) + \theta E_{DR} \tag{3.11}$$

where t_{DR} is the idle listening time for a data packet from the transmitter, θ is the number of received packets during slot n. It is obvious that $\theta \leq k$, as a data packet is not always responsed after the receiver sends its WUB. Finally, the total consumed energy during slot n is estimated as

$$\tilde{e}_C(n) = \tilde{e}_{Active}(n) + P_{Sleep} T_S(n) \tag{3.12}$$

where $\tilde{e}_{Active}(n)$ is estimated from tracking all activities of a WSN node during slot n.

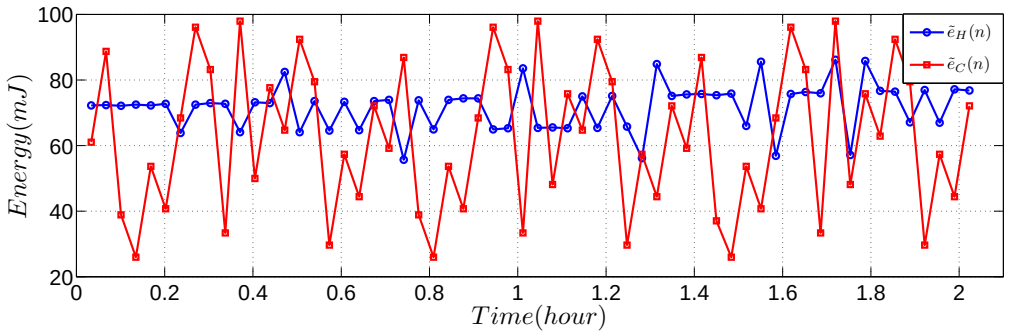

FIGURE 3.5: Harvested and consumed energy profiles in a PowWow node.

3.3.3 Harvested Energy Model

Following the energy flow principles explained in Section 2.4, the harvested energy is distributed into two parts by the energy flow controller (see Fig. 2.7). While the first part is directly consumed by the DC/DC converter to power the wireless node, the second one is stored into the StoreCap and is consumed by the leakage energy. Therefore, the harvested energy during slot n can be estimated by

$$\tilde{e}_H(n) = \frac{1}{\eta}\tilde{e}_C(n) + [\tilde{e}_S(n) - \tilde{e}_S(n-1)] + \tilde{e}_{Leak}(n) \tag{3.13}$$

where η is the DC/DC converter efficiency, $\tilde{e}_C(n)$ is the consumed energy of the wireless node, $[\tilde{e}_S(n) - \tilde{e}_S(n-1)]$ is the energy stored in the StoreCap during the slot n and $\tilde{e}_{Leak}$ is the leakage energy. When the harvested energy is greater than the sum of the consumed energy and the leakage energy, a part of harvested energy is consumed by the wireless node and leakage and therefore, only the surplus harvested energy charges StoreCap. On the other hand, when the harvested energy is less than the sum of the consumed energy and the leakage energy, all harvested energy is transferred to the load and the remaining energy is served by the StoreCap. In this case, the second term in (3.13), $[\tilde{e}_S(n) - \tilde{e}_S(n-1)]$, is negative.

Our software energy monitor only requires the voltage of StoreCap (V_S) and a LUT to estimate all energy profiles used for the PM such as the available energy in the StoreCap ($\tilde{e}_S$), the consumed energy ($\tilde{e}_C$) and the harvested energy ($\tilde{e}_H$). The main advantage of our approach is that no additional hardware device is required. Therefore, this energy monitor is independent of harvesters and can be extended to differerent energy sources (e.g. solar, thermal, wind energy). However, the energy monitor suffers from the noise when reading $V_S(n)$ and therefore, an average filter should be used to reduce this noise.

Fig. 3.5 presents $\tilde{e}_H(n)$ and $\tilde{e}_C(n)$ obtained with a PowWow node equipped with two 4x6cm PVs in an office. The energy monitor is activated every $T_S(n) = 2$ minutes. The average voltage of StoreCap used to evaluate all energy profiles is computed from three values of V_S. As it can be observed from Fig. 3.5, $\tilde{e}_C(n)$ has a high variation due to different t_{idle} in (3.10). Meanwhile, $\tilde{e}_H(n)$ presents a lower variation since light condition is almost constant during our measurement. This variation is considered as the mandatory error of our measurement method. Therefore, a PM using this energy monitor must has a fault tolerant scheme to overcome this problem.

3.4 State-of-the-Art Energy Predictor

In order to design an effective PM, some approaches benefit from an accurate energy predictor to estimate the energy that can be harvested in the near future. Based on several historical values of harvested energy, a potential energy can be predicted. When considering an EH-WSN node with limited resources, the energy predictor must have a low complexity and a small memory space for historical values. State-of-the-art prediction algorithms suitable to EH-WSNs can be divided into two categories: predictors based on analysis and predictiors based on learning.

3.4.1 Analysis-based Predictor

In the first category, we can find Exponentially Weighted Moving Average (EWMA) [63] and Weather Condition Moving Average (WCMA) [94] for solar energy. The principle of EWMA is to divide the time into several slots with the same duration and to apply a weighting factor to previous predicted values to estimate the energy that will be harvested during the next slot. With an array for previous predicted energy and an array for real harvested energy in a day, a full profile of the predicted energy in the next day can be provided by EWMA. However, EWMA has a low accuracy when a cloudy day is followed by a sunny day or vice versa. The WCMA overcomes this drawback by taking into account some previous harvested energy in a given day to estimate the weather condition. In this way, WCMA provides a better prediction as harvested energy close to the present value has a high relevance to the next value. However, both EWMA and WCMA have fixed internal parameters which are optimized for solar energy prediction.

3.4.2 Learning-based Predictor

In the second category, QLearning [95] and Neural Network algorithms [96] can be used for any harvesting device with learning phase to automatically configure their internal parameters. In QLearning algorithm, a decision maker agent, namely the learner, takes actions to the environment and receives reward. After several tries-and-errors, the agent gradually learns the best policy, which is the sequence of actions that maximizes the total reward. On the other hand, the neural network consists of many neurons whose connections are represented by weighted factors. During the training phase, these weighted factors are updated to respect an error less than a threshold. This phase is the disadvantage of both neural network and QLearning when compared to WCMA or EWMA as it requires an additional energy cost due to their high complexity.

These approaches can be used to design a predictive PM and optimize future activies of the EH-WSN node. However, while analysis-based predictors are specifically designed for solar-powered EH-WSN, learning-based predictors are expensive in term of memory space and complexity. In our approach, an energy predictor based on an adaptive filter is proposed. Not only low complexity with acceptable accuracy, our energy predictor also has a small memory space as only a previous harvested energy is used to estimate the future energy. Moreover, this energy preditor is able to extend to different energy sources as its internal coefficients are updated after each prediction to minimize the error. Simulation results show that our energy predictor using adaptive filter can be applied for both solar and wind energy with an average error less than 15%.

3.5 Energy Predictor using Adaptive Filter

In the PM designed for EH-WSN, the time axis is divided into slots of the same duration and the adaptation calculation is carried out at the end of each slot [33]. Therefore, the energy predictor is also periodically activated together with the PM to provide the predicted harvested energy profiles. We define the following discrete values used for the adaptive filter-based energy predictor (AF-EP):

- p, μ : order and the step size of the adaptive filter.
- $\tilde{e}_H(n)$: harvested energy during slot n provided by the energy monitor.

- $\tilde{E}_H(n)$: vector of p historical values,

  $\tilde{E}_H(n) = [\tilde{e}_H(n), \tilde{e}_H(n-1), ..., \tilde{e}_H(n-p+1)]$.

- $W(n)$: the vector of p coefficients of the AF-EP,

  $W(n) = [w_1(n), w_2(n), ..., w_p(n)]$.

- $\hat{e}_H(n)$: predicted harvested energy for slot n.

- $err(n)$: error of the prediction for slot n.

- $T_S(n)$: predictor interval or slot duration.

The architecture of the energy predictor using adaptive filter is presented in Fig. 3.6. A historical harvested energy profile is stored in the vector $\tilde{E}_H(n)$. Based on this profile, the predicted harvested energy for the next slot ($\hat{e}_H(n+1)$) is produced by a dot product between $\tilde{E}_H(n)$ and the coefficients of the adaptive filter ($W(n)$) as follows:

$$\hat{e}_H(n+1) = \tilde{E}_H(n).W(n) \tag{3.14}$$

After a slot duration T_S, an energy monitor is activated by a timer to estimate the harvested energy during slot $(n+1)$. The error of the prediction ($err(n+1)$), which is the difference between the predicted energy and the real energy as

$$err(n+1) = \hat{e}_H(n+1) - \tilde{e}_H(n+1) \tag{3.15}$$

is fed back to adjust coefficients of the AF-EP in the next slot $W(n+1)$. Meanwhile, $\tilde{e}_H(n+1)$ is used to update the next historical values ($\tilde{E}_H(n+1)$).

Algorithms to adjust the filter coefficients can be divided into two categories : the Least Mean Square (LMS) and the Recursive Least Square (RLS). Compared to the RLS algorithm, the LMS does not involve any matrix operation. Therefore, the LMS requires fewer computation resources and less memory compared to RLS. The implementation of the LMS is therefore, less complicated than the RLS. The standard LMS updates the coefficients of the adaptive filter as follows:

$$W(n+1) = W(n) + \mu err(n+1)\tilde{E}_H(n) \tag{3.16}$$

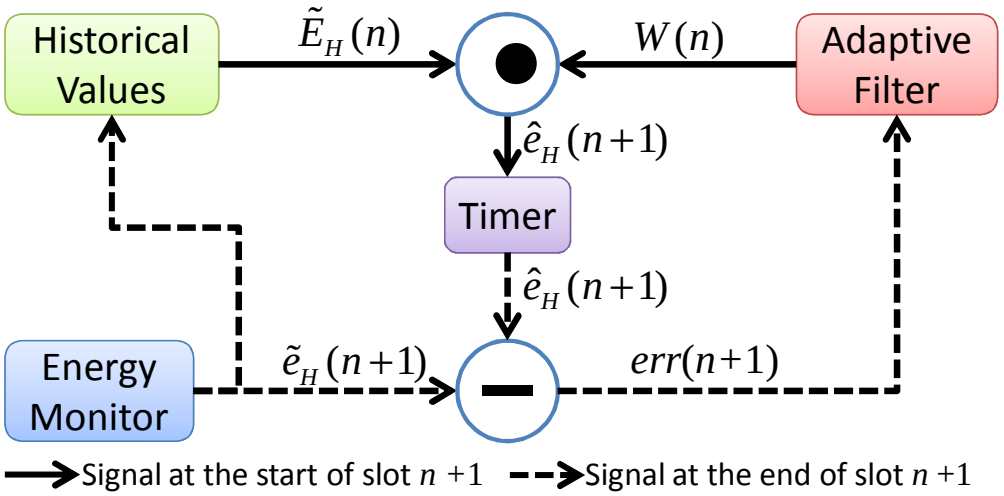

FIGURE 3.6: Energy predictor using adaptive filter architecture. Historical harvested energy profile is kept in a vector $\tilde{E}_H(n)$ to predict $\hat{e}_H(n+1)$ at the beginning of slot $(n+1)$. Until the end of slot $(n+1)$, $\tilde{E}_H(n)$ and $W(n)$ are updated from $err(n+1)$.

However, the main drawback of the standard LMSs is that it is sensitive to the change of the input vector $(\tilde{E}_H(n))$. Therefore, it is impractical to determine the optimized step size μ. The Normalized Least Mean Squares filter (NLMS) is a modified form of the standard LMS that overcomes this problem by normalizing the input vector. The NLMS algorithm updates the filter coefficients as

$$W(n+1) = W(n) + \frac{\mu err(n+1)\tilde{E}_H(n)}{\left\|\tilde{E}_H(n)\right\|^2} \tag{3.17}$$

where $\left\|\tilde{E}_H(n)\right\|$ is the modulas of vector $\tilde{E}_H(n)$, which is defined as

$$\left\|\tilde{E}_H(n)\right\| = \sqrt{\tilde{e}_H^2(n) + \tilde{e}_H^2(n-1) + ... + \tilde{e}_H^2(n-p+1)} \tag{3.18}$$

Unfortunately, the implementation of NLMS faces with divide-by-zero errors when (3.18) returns 0. This scenario occurs during the night in harvesting WNSs based on solar energy. Therefore, the predictor needs to check $\left\|\tilde{E}_H(n)\right\|$ before updating its coefficients. When $\left\|\tilde{E}_H(n)\right\| = 0$, the next value of harvested energy is simply predicted as zero.

3.6 Simulation Results

Our simulations are performed on a dataset downloaded from National Energy Renewable Laboratory (NERL) [97]. The visualization of the harvested power, which is another

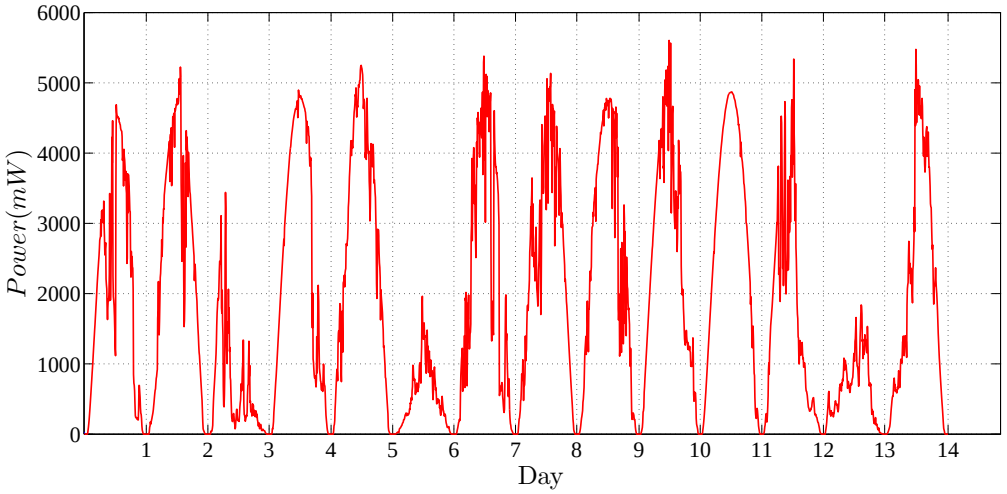

FIGURE 3.7: Harvested power profile over consecutive 14 days.

shape of harvested energy is shown in Fig.3.7. In order to obtain a higher accuracy of the results, only harvested energy profiles during the day are considered. The consecutive zero harvested energy during the night can affect the average error and therefore, are discarded. This simulation set-up is also used in [94].

The energy predictor should have the same activated period as the PM. Authors in [4] have shown that the optimized adaptation period is a few minutes or even a few seconds rather than 30 minutes as in [63]. Therefore, the predictor interval ($T_S(n)$) is set to 5 minutes for simulations carried out in this section. The metrics used to compare different energy predictors are defined as follows:

- $E_{avg}(\%)$: average error of the predictor, defined as

$$E_{avg} = \frac{1}{N}\sum_{n=1}^{N}\frac{|err(n)|}{\tilde{e}_H(n)} \tag{3.19}$$

  where N is the number of slots over 14 days and $|err(n)|$ returns the absolute value of the prediction error ($err(n)$).

- Mem (16-bit words): memory space for storing historical energy profiles.

- Mul: number of multiplications for the prediction algorithm.

The Fig. 3.8 shows the average error of the predictor for different filter order (p) and step size (μ) values. As it can be observed, the lowest average error (14.7%) is obtained when p = 1 and μ = 0.3. This result shows an extremely small memory space of our

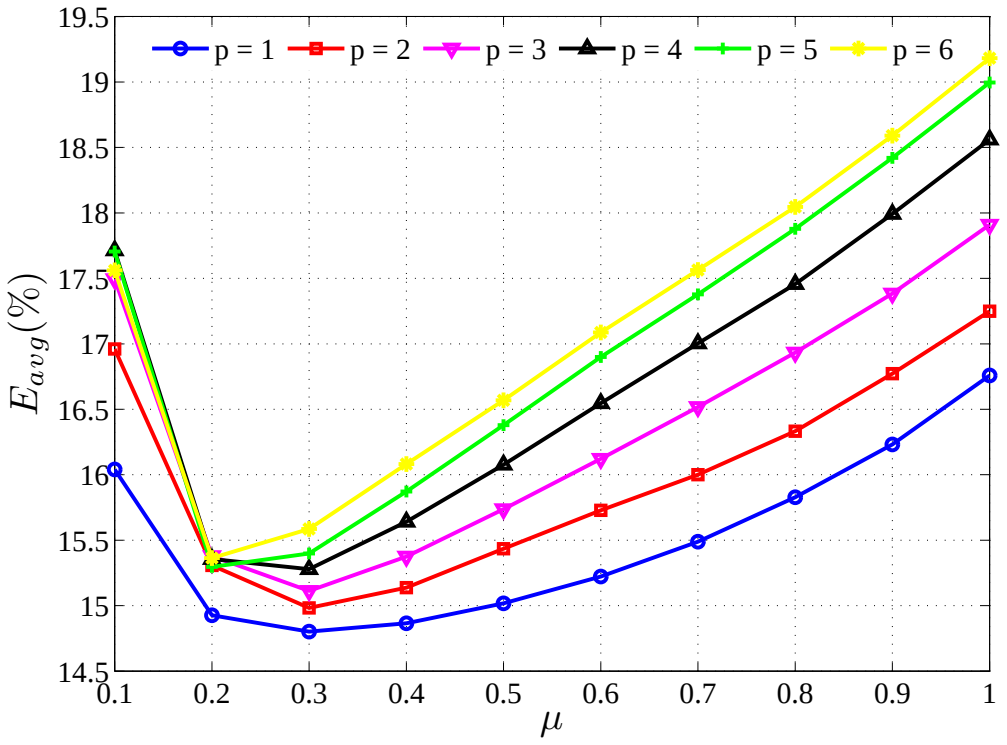

FIGURE 3.8: Average error for solar energy prediction with different combinations of the order (p) and the step size (μ) of the adaptive filter.

TABLE 3.1: Performance of different energy predictors for solar energy

	Mem (words)	Mul	E_{avg} (%)
WCMA	1152	20	12.1
NLMS	1	5	14.7
EWMA	288	3	34.4

AF-EP as only one historical value of harvested energy is used to predict the next one. In this configuration, (3.17) is simplified as follows:

$$W(n+1) = W(n) + \frac{\mu err(n+1)}{\tilde{e}_H(n)} \tag{3.20}$$

since $\tilde{E}_H(n)$ only has one element $\tilde{e}_H(n)$. Therefore, the complexity of the NLMS algorithm is significantly reduced.

The Table 3.1 shows a comparison of our energy predictor using NLMS with WCMA and EWMA. The WCMA presented in [94] requires five days of harvested energy profiles to estimate the current weather condition and therefore, 1152 words are used to store historical values. The WCMA brings the lowest average error but also the highest computations compared to NLMS and WCMA as it needs to compute the GAP factor

which represents the difference between the weather on the current day and five previous days at a given time. The predictor based on WCMA takes into account both the previous harvested energy profiles and the current weather condition to improve the accuracy. Meanwhile, the EWMA predictor presented in [63] only needs 288 words for the historical harvested energy profiles in a day. The prediction of harvested energy in a slot is based on the previous predicted energy and is weighted with the real energy in the historical profiles at the same slot. In this way, EWMA is able to provide a predicted energy profile for all slots in the next day without waiting for the real energy in some previous slots as NLMS or WCMA. However, this is also the drawback of EWMA when the weather condition changes from a sunny day to a cloudy day or vice versa [98]. Predictor based on EWMA has the lowest computation requirement (expressed with the number of multiplications) as the predicted energy is the sum of the previous real energy and the previous predicted energy. In this comparison, the weighting factor for the previous real energy of both WCMA and EWMA is set to 0.5.

In our predictor using NLMS, the next harvested energy is only based on the previous real harvested energy. Therefore, our predictor has the lowest memory space for historical values. However, it is able to provide a low average error (14.7%) with p=1 and $\mu = 0.3$. The improvement of our predictor compared to WCMA and EWMA is the error of each prediction is fed back to adjust the filter coefficients. In this way, the energy predictor is able to faithfully follow the tendency of the incoming harvested energy.

The dynamic adaptation of the filter coefficients in our predictor provides a capability to apply it for different energy sources. In order to demonstrate this dynamic adaptation, we have performed simulation with a wind power profile extracted from an actual output data recorded by NERL from large wind power plants in the Midwest [99]. The average error with different values of the filter order (p) and step size (μ) is shown in Fig. 3.9. When p = 1 and $0.2 < \mu < 1.5$, the predictor achieves a high accuracy with an average error less than 10%.

Another simulation has been performed with a solar harvested power profile extracted from a PowWow [89] wireless sensor node set up near a window in an office. The Fig. 3.10 shows that our energy predictor has precise decisions even if there is a sudden change of the harvested power at around 80 minutes, when the curtain of the window is opened. At the beginning, the predicted power is far from the real one. However, the AF-EP

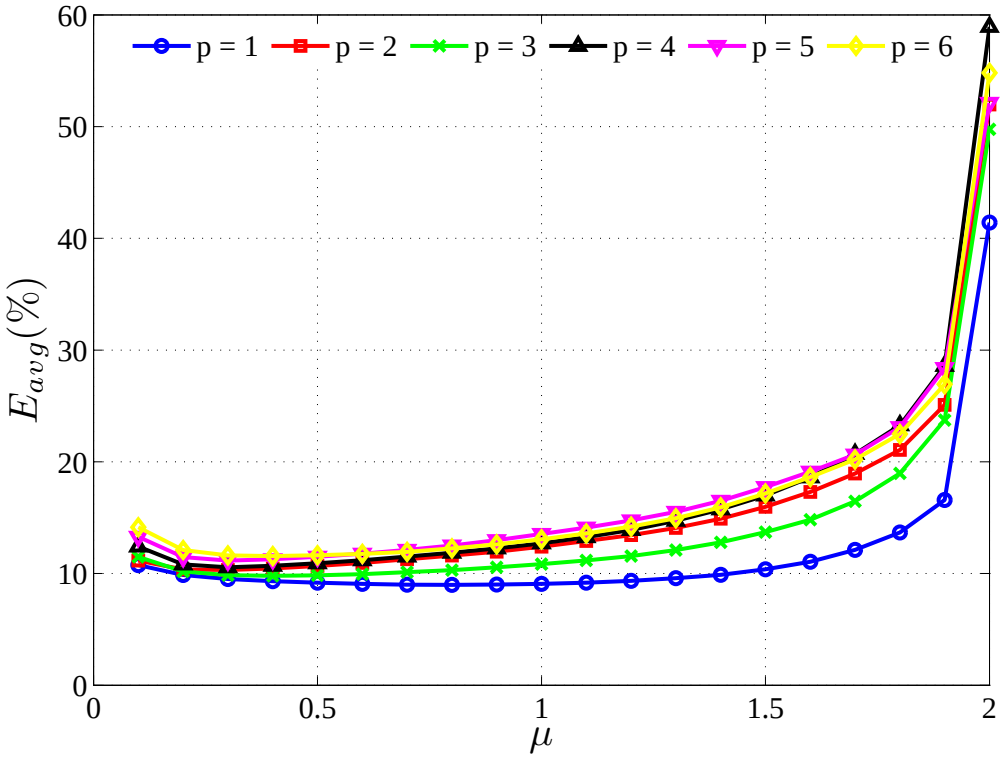

FIGURE 3.9: Average error of the energy predictor when applied to wind energy in seven consecutive days. With the same order and step size as solar prediction (p = 1 and μ = 0.3), the average error is 9.1%.

TABLE 3.2: Average error (%) of different predictor interval

$T_S(n)$ (minutes)	Solar	Wind
5	14.8	9.5
10	27.8	16.0
15	43.7	23.9
20	54.5	27.2

coefficients can be rapidly adjusted as the error is fed back after each prediction. From around 10 minutes, the predicted power follows closely the real power. The average error of the predictor in this case is very low, at 2.5%.

The adaptive filter is analyzed with different predictor interval ($T_S(n)$) for p = 1 and μ = 0.3. The dataset for solar energy in Fig. 3.7 and wind energy in [99] are used for this simulation. Simulation results are summarized in Table 3.2. It can be observed that the average error is proportionally increased with the prediction interval as the previous real value has a lower relevance with the next value when $T_S(n)$ is increased.

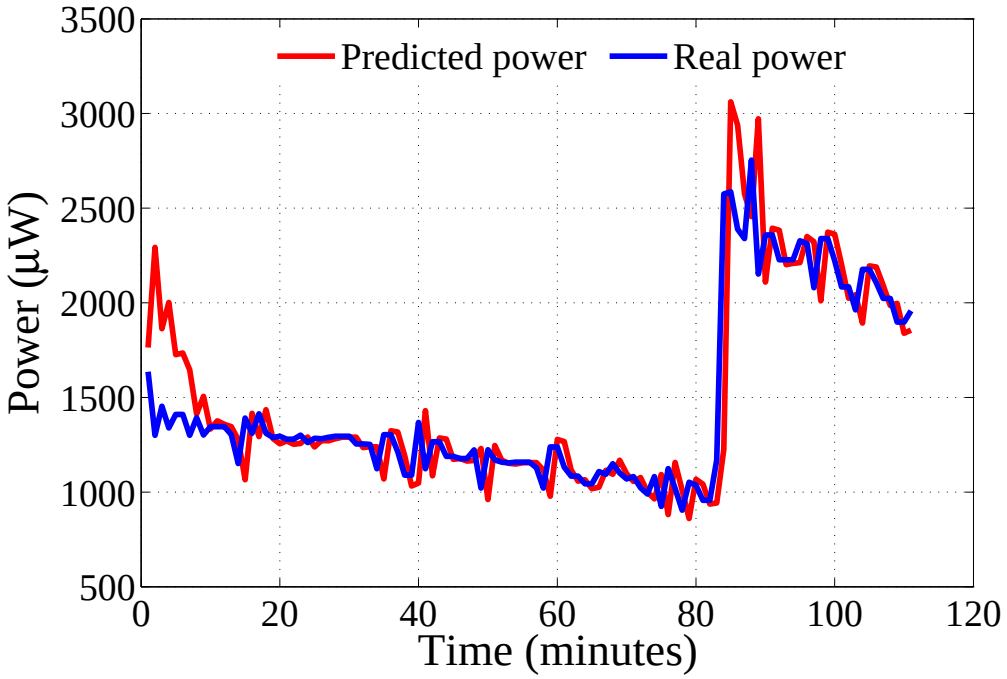

FIGURE 3.10: Energy prediction of harvested energy recorded by a PowWow node near a window in an office with $p = 1$ and $\mu = 0.3$. At around 80 minutes, the curtain is opened and the harvested power suddenly increases.

3.7 Conclusions

The energy monitor is designed to provide the energy aware capability in EH-WSNs. It should be low complexity and low power consumption due to the limited resource of the WSN node. In this chapter, a software-based energy monitor for supercapacitor-based energy storage is proposed. By reading the voltage of the supercapacitor and tracking all activities of the WSN node, the harvested energy, the consumed energy as well as available energy in the supercapacitor are estimated. Therefore, this energy monitor can be easily extended to different energy sources without any change on hardware or software. In the following chapters, the energy monitor is used with the PM to satisfy the ENO condition of an EH-WSN node. However, the PM must have a fault tolerant scheme to overcome the error of the energy monitor due to the noise when reading the voltage of the supercapacitor.

Another contribution in this chapter is an energy predictor using adaptive filter. Compared to state-of-the-art algorithms, the adaptive filter with NLMS algorithm has a low complexity and small memory space. The advantage of our predictor is that the filter coefficients are automatically updated by the error of the predictions. By this way, the energy predictor can be used with different energy sources such as solar energy in outdoor

environments, wind energy or light energy in an office. The energy predictor performs well when the prediction interval is 5 minutes. In this case, the average error is under 15%.

Chapter 4

Duty-Cycle Power Manager for Continuous Energy Sources

4.1 Introduction

This chapter presents a set of novel power managers (PM) for EH-WSNs. Instead of minimizing the consumed energy as in the case of battery-powered systems, it makes the harvesting node converge to Energy Neutral Operation (ENO) by adapting its duty cycle according to the harvested energy. When there is more harvested energy, the wireless node wakes-up frequently (high duty cycle) in order to increase the system Quality of Service (QoS). Otherwise, when there is less harvested energy, the wireless node stays in low power mode longer (low duty cycle) for ensuring perpetual operations without any interruption.

As presented in Section 2.6, energy sources in this work are divided into two categories: continuous and periodic sources. In this chapter, the PM is specifically designed for a continuous energy source. An example of this kind of energy source is fluorescent lights in hospital environment, where indoor lights are switched on all the time. As energy can be scavenged with rare interruption, the wireless node can consume an amount of energy equal to the harvested energy to maximize QoS while still satisfying ENO condition.

Another promising source belonging to this category is the heat energy from industrial machines. Thermoelectric generators (TEG) are used to convert the excess or wasted heat

into electric energy for powering wireless nodes. Thermal-powered WSNs are amenable for monitoring health condition of these machines. By analyzing their temperature, vibration, strain, and pressure in real time, an engine maintenance will not be required until these data show it is necessary, rather than regularly scheduled, and therefore, saving a great deal of cost. Another example concerns the monitoring of patient health in a hospital with the heat from body skin. Some other kinds of energy sources such as wind and vibration energy, even if they are not continuous, can be also classified in this category if monitoring applications using these sources only require tracking data whenever the harvested energy is available. One example involves the tracking of a train, which can exploit the wind energy when it passes through a tunnel. Another example concerns the monitoring pressure in tires of a car with vibration energy.

When following ENO in the context of continuous sources, the energy in the supercapacitor (StoreCap) is kept at a constant level as the consumed energy is always expected to be equal to the harvested energy at a given time. Therefore, two different approaches are proposed in this chapter. Firstly, an adaptive PM using a Proportional Integral Derivative (PID) is proposed and evaluated in this work. The controller estimates the buffered energy by measuring the voltage of the StoreCap (V_S). Then, the controller adapts the QoS of the application to the available energy by determining the next wake-up interval of the node (T_{WI}) to reach stable operations. The main advantage of the PM with a PID controller is that it does not require monitoring either harvested or consumed energy. However, the PID controller requires a long adaptation time to converge the WSN node to ENO state. This problem is overcome in the second PM that utilizes the simple energy monitor proposed in Chapter 3. By exploiting the estimation of the harvested energy as well as the consumed energy, PM with energy monitor takes better decisions to satisfy ENO condition. Both PMs aim to be independent of harvesters and therefore, can be easily extended with different energy sources.

The rest of this chapter is organized as follows. In Section 4.2, the network topology and protocol used in this work are presented. PID controller-based PM (PID-PM) and Energy Monitor-based PM (EM-PM) are proposed in Section 4.3 and 4.4. Experimentations performed on both OMNET++ simulation and real PowWow nodes are presented in Section 4.5. Finally, the chapter ends with some conclusions.

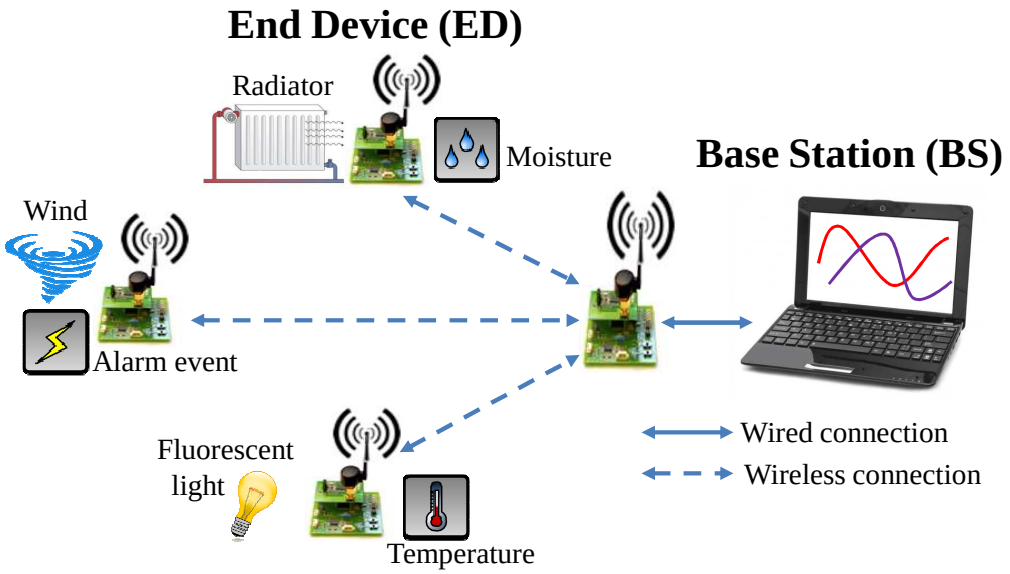

FIGURE 4.1: Single-hop EH-WSN with a base station (BS) and many end device nodes (EDs). All EDs are equipped with a harvested device and a supercapacitor for energy storage. The PM adapts the wake-up interval (T_{WI}) of each ED to respect ENO.

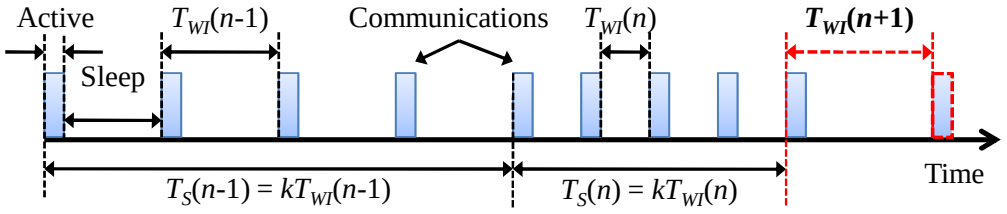

FIGURE 4.2: Power manager with dynamic adaptation period.

4.2 Network Topology and Protocol

A single-hop EH-WSN (see Fig. 4.1), where a base station node (BS) collects data from other end device nodes (ED), is used in this work. Each ED is equipped with a harvester and a supercapacitor. Communications among EDs and BS are based on the RICER MAC protocol [61] shown in Fig. 2.11. However, the ED reads a value from its sensor through an ADC channel (e.g. temprature, pressure,...) (SEN) before waiting for a WUB from the receiver (idle listening). Once a WUB is received, the ED performs CCA, CBT and DT.

The PM is implemented in each ED node to adapt its wake-up interval (T_{WI}) to satisfy the ENO condition. The time domain is divided into slots of duration $T_S(n)$ and the PM is carried out at the end of each slot. After a predefined number of wake-up times (k), the PM is activated to estimate the next wake-up interval T_{WI} as illustrated in Fig.

4.2. Therefore, the adaptation period of the PM is

$$T_S(n) = kT_{WI}(n) \tag{4.1}$$

This dynamic period as shown in [4], provides a way to adapt the reactiveness of the PM according to the current $T_{WI}(n)$. It is obvious that when there is more harvested energy, $T_S(n)$ is decreased with a small value of T_{WI}. It also means that the PM can be activated more frequently and therefore, provides a fast reactivity to the change of harvested energy. Otherwise, when there is less harvested energy, it is reasonable for the PM to have a longer adaptation period as the PM also consumes an amount of energy.

When a ED has converged to ENO, the energy in StoreCap is kept at a constant level. It also means that V_S is kept around a pre-defined desired voltage V_{Ref} as the energy in a supercapacitor is squared proportional to its voltage, which is explained in (3.7) . Therefore, the PM proposed in this chapter estimates the next wake-up interval (T_{WI}) in order to converge V_S to V_{Ref}.

4.3 PID Controller-based Power Manager

In this section, a PID controller, used as a low complex power manager, is applied to energy harvesting ED nodes. PID is a generic control loop feedback mechanism [100]. The PID controller calculates the error as the difference between a measured and a desired value and attempts to minimize this error by adjusting the controlled output. Fig. 4.3 shows the PID structure with three components: Proportional is the error at present time, Integral is the accumulation of past errors, and Derivative is the prediction of future errors. The weighted sum of these components is applied to an adaptation function f to generate the controlled output $T_{WI}(n)$). This wake-up interval is applied to the WSN node and then, a new value of $V_S(n)$ is fed back to the input of the controller.

To apply the PID controller to a supercapacitor-based EH-WSN node, the error $err(n)$, which is evaluated at the end of current slot n, is defined as the change of energy in the StoreCap which acts as the storage device:

$$err(n) = \frac{1}{2}C_S\left(V_S^2(n) - V_{Ref}^2\right) \tag{4.2}$$

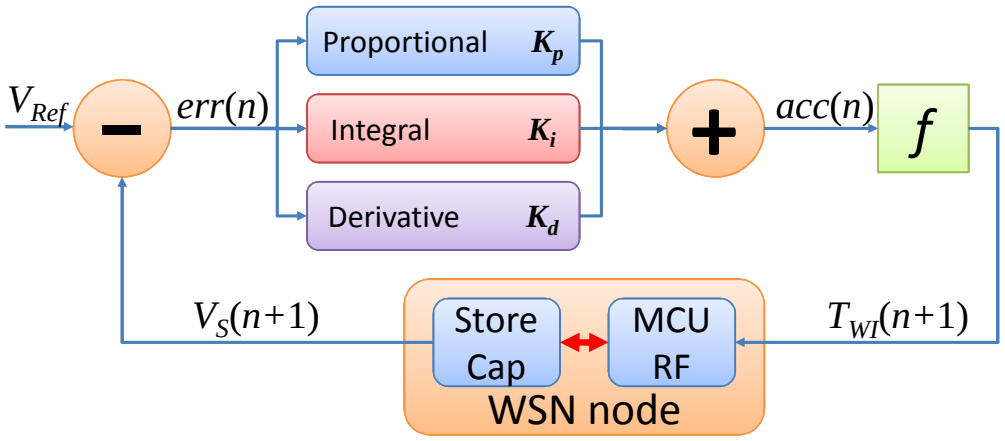

FIGURE 4.3: PID controller-based power manager (PID-PM) with three components: Proportional, Integral and Derivative. Adaptive function f updates the next wake-up interval of the WSN node ($T_{WI}(n+1)$) according to accumulated error $acc(n)$.

The adaptive function f is inversely proportional to the accumulated error $acc(n)$. When $acc(n) > 0$, energy harvesting has a tendency to be higher than energy consumption, the next wake-up interval $T_{WI}(n+1)$ should be reduced. When $acc(n) < 0$, adaptive function will increase $T_{WI}(n+1)$. Therefore, f is gives the next $T_{WI}(n+1)$ through

$$T_{WI}(n+1) = T_{WI}(n) - acc(n)/T_S(n) \tag{4.3}$$

The PID controller-based PM (PID-PM) shows the interest of our approach since monitoring the harvested energy, consumed energy as well as leakage energy is not required. It provides practical adaptations to match harvested and consumed energy of a wireless node when it is powered by a continuous energy source. Based on the principle of ENO, the PID-PM adapts the wake-up interval of a harvesting node according to the voltage level of a supercapacitor, which is used as the energy storage. Moreover, this design is also independent of harvesters and therefore, can be easily extended to different energy sources.

However, this PM suffers from a trial-and-error process before converging to ENO state since it has no awareness of both harvested and consumed energy. The duration of this process is non-deterministic due to variations of the harvested energy in a dynamic environment. This duration directly depends on the three parameters of the PID controller K_p, K_i and K_d. However, it is impractical to find the optimal values for these parameters with different behaviours of harvesting sources. The second approach proposed in Section 4.4 takes advantage of a simple energy monitor to overcome this problem. When

the energy monitor is embedded, the PM is able to estimate both the harvested energy and the consumed energy. In consequence, the PM can quickly converge the harvesting node to ENO state.

4.4 Energy Monitor-based Power Manager

In this section, a PM named Energy Monitor-based Power Manager (EM-PM) is proposed. The aim of this PM is also to determine the next wake-up interval (T_{WI}) to respect the ENO in the next slot and keep V_S around V_{Ref} as PID-PM. The EM-PM also has a dynamic adaptation period as presented in (4.1). Our approach aims to be a low complexity and multi-sources PM.

At the end of slot n, the energy monitor is activated to provide energy profiles, including consumed energy $\tilde{e}_C(n)$ and harvested energy $\tilde{e}_H(n)$. Based on these profiles, the PM predicts the consumed energy $\hat{e}_C(n+1)$ and the harvested energy $\hat{e}_H(n+1)$ for the next slot $(n+1)$. Firstly, $\hat{e}_C(n+1)$ can be predicted as

$$\hat{e}_C(n+1) = \hat{e}_{Active}(n+1) + P_{Sleep}kT_{WI}(n+1) \tag{4.4}$$

where $\hat{e}_{Active}(n+1)$ is the predicted energy during active period and $P_{Sleep}kT_{WI}(n+1)$ stands for sleep energy in slot $(n+1)$.

The harvested energy in the next slot $\hat{e}_H(n+1)$ cannot be predicted from the current harvested energy $\tilde{e}_H(n)$ as two consecutive slots usually have different duration with the dynamic adaptation period of the PM. However, it can be expressed as

$$\hat{e}_H(n+1) = \hat{P}_H(n+1)T_S(n+1) = \hat{P}_H(n+1)kT_{WI}(n+1) \tag{4.5}$$

where $\hat{P}_H(n+1)$ is the prediction of the harvested power in the next slot $(n+1)$, which can be predicted from the harvested power in the previous slot $\tilde{P}_H(n)$.

Moreover, the residual energy at the end of slot n, which is the energy difference between the current state and desired state (when $V_S = V_{Ref}$) can be considered as the additional budget energy for the next slot and is defined as following:

$$\tilde{e}_{Bud}(n+1) = \tilde{e}_S(n) - \frac{1}{2}C_S V_{Ref}^2 = \frac{1}{2}C_S(V_S^2(n) - V_{Ref}^2) \tag{4.6}$$

Therefore, to satisfy the ENO condition in the slot $(n+1)$, the following constraint needs to be respected:

$$\hat{e}_H(n+1) + \tilde{e}_{Bud}(n+1) = \frac{1}{\eta}\hat{e}_C(n+1) + \tilde{e}_{Leak}(n+1) \tag{4.7}$$

where $\tilde{e}_{Leak}(n+1)$ represents the leakage energy in the slot $(n+1)$ and can be estimated from the leakage power (P_{Leak}), which is considered as a constant for a particular supercapacitor, as

$$\tilde{e}_{Leak}(n+1) = P_{Leak}T_S(n+1) = P_{Leak}kT_{WI}(n+1) \tag{4.8}$$

By appling (4.4), (4.5) and (4.8) into (4.7), the next wake-up interval can be determined as follows

$$T_{WI}(n+1) = \frac{[\hat{e}_{Active}(n+1) - \eta\tilde{e}_{Bud}(n+1)]/k}{\eta(\hat{P}_H(n+1) - P_{Leak}) - P_{Sleep}} \tag{4.9}$$

To predict $\hat{e}_{Active}(n+1)$, let's consider how $\tilde{e}_{Active}(n)$ is estimated. Even if two consecutive slots usually have different period, the harvesting node has exactly k wake-up times. For each wake-up, the node reads data from its sensor (SEN), opens an idle listening window for a WUB from the BS and then, performs CCA, CBT and DT. Therefore,

$$\tilde{e}_{Active}(n) = P_{Rx}\sum_{i=1}^{k} t_{idle}(i) + k(E_{SEN} + E_{WUB} + E_{CCA} + E_{CBT} + E_{DT}) + E_{EM} \tag{4.10}$$

where $t_{idle}(i)$ represents the i^{th} idle listening time for the WUB and E_{EM} is related to the computations overhead of the EM-PM. It can be found from (4.10) that variation of $\tilde{e}_{Active}(n)$ is only the $\sum_{i=1}^{k} t_{idle}(i)$ term. It is obvious that $t_{idle}(i)$ is a random number in the range $[0, T_{idle}]$ (see Fig. 2.11). Therefore, the higher value of k is, the closer $\sum_{i=1}^{k} t_{idle}(i)$ converges to $\frac{1}{2}kT_{idle}$. In a consequence, the Exponentially Weighted Moving Average filter (EWMA) [3] is used to predict $\hat{e}_{Active}(n+1)$ as

$$\hat{e}_{Active}(n+1) = \alpha\hat{e}_{Active}(n) + (1-\alpha)\tilde{e}_{Active}(n) \tag{4.11}$$

where $\alpha \in [0,1]$ is a weighted factor. α should be greater than 0.5 to reduce the contribution of the recent value $\tilde{e}_{Active}(n)$ and

$$\hat{e}_{Active}(0) = \frac{1}{2}kT_{idle}P_{Rx} + k(E_{SEN} + E_{WUB} + E_{CCA} + E_{CBT} + E_{DT}) + E_{EM} \tag{4.12}$$

at the beginning (e.g. slot 0). This strategy makes $\hat{e}_{Active}(n+1)$ converge to the average energy for k communications in a slot.

To predict $\hat{P}_H(n+1)$ in (4.9), the energy predictor using adaptive filter presented in Chapter 3 can be used. However, the leakage power P_{Leak} must be characterized when a new supercapacitor is used for the energy storage since leakage power has a capacitance effect. In this section, a new approach to design an EM-PM without characterizing the leakage power is proposed. Let's consider (3.13), by dividing both sides by $T_S(n)$, we have

$$\tilde{P}_H(n) = \frac{\tilde{e}_{Active}(n)}{\eta T_S(n)} + \frac{P_{Sleep}}{\eta} + \frac{\tilde{e}_S(n) - \tilde{e}_S(n-1)}{T_S(n)} + P_{Leak} \tag{4.13}$$

By moving P_{Sleep}/η and P_{Leak} to the left and then, multiplying both sides by η, we achieve

$$\eta(\tilde{P}_H(n) - P_{Leak}) - P_{Sleep} = \eta\left[\tilde{e}_S(n) - \tilde{e}_S(n-1)\right] + \tilde{e}_{Active}(n) \tag{4.14}$$

The only difference between the denominator of (4.9) and (4.14) is $\hat{P}_H(n+1)$ and $\tilde{P}_H(n)$. Therefore, if we assume that the harvested power in the next slot ($\hat{P}_H(n+1)$) is the same as the harvested power in the previous slot ($\tilde{P}_H(n)$), we have:

$$T_{WI}(n+1) = \frac{\left[\hat{e}_{Active}(n+1) - \eta\tilde{e}_{Bud}(n)\right] T_{WI}(n)}{\eta\left[\tilde{e}_S(n) - \tilde{e}_S(n-1)\right] + \tilde{e}_{Active}(n)} \tag{4.15}$$

This result shows the simple implementation of the PM. At the beginning of the next slot, the PM only needs to read the voltage of the StoreCap ($V_S(n)$) and based on the consumed energy in previous slot ($\tilde{e}_{Active}(n)$), the next wake-up interval is computed. The prediction error for both $\hat{e}_C(n+1)$ and $\hat{P}_H(n+1)$ are implicitly included in $\tilde{e}_{Bud}(n+1)$. For instance, the real harvested power $\tilde{P}_H(n+1)$ is the same as $\hat{P}_H(n+1)$ but the consumed energy $\tilde{e}_C(n+1)$ is less than $\hat{e}_C(n+1)$. It means that in the slot $(n+1)$, total consumed energy is less than harvested energy due to the error when prediction $\hat{e}_C(n+1)$. The amount of energy $\hat{e}_C(n+1) - \tilde{e}_C(n+1)$ makes V_S increase ($V_S(n+1) > V_S(n)$). Therefore, from (4.6), the node has a negative budge energy, which is used to increase its QoS in the slot $(n+2)$. Where the error occurs at both $\hat{P}_H(n+1)$ and $\hat{e}_C(n+1)$, the WSN node does not evaluate each error as it is included when considering the budget energy.

Similar to the PID-PM, adaptations mostly based on the voltage of the StoreCap makes the EM-PM independent of harvesters and therefore, can be extended to several kinds of energy sources such as light, heat or wind energy. Another advantage in PID-PM and EM-PM is that the leakage energy for supercapacitor-based energy storage does not need to be characterized. However, both PMs can provide an invalid T_{WI} due to the noise when reading V_S through the ADC channel of the wireless node. To reduce this problem, three samples of V_S are read when the PM is activated and, an average value $\overline{V_S}$ is used to evaluate the next wake-up interval. Therefore, the consumed energy of the PID-PM can be estimated as follows:

$$E_{PID} = 3E_{SEN} + E_{CBT} \tag{4.16}$$

where $3E_{SEN}$ represents the energy for reading $\overline{V_S}$ and E_{CBT} is the overhead computations of the PID-PM. Meanwhile, the consumed energy of EM-PM can be estimated as:

$$E_{EM} = 3E_{SEN} + 2E_{CBT} \tag{4.17}$$

where $3E_{SEN}$ stands for the energy when reading $\overline{V_S}$, which is used as the input to both energy monitor and the PM. The second term in (4.17) is the consumed energy for when executing the energy monitor and the PM.

4.5 Experimental Result

4.5.1 Measurement Setup

Our measurements are performed using PowWow platforms which are based on the MSP430 microcontroller and on the CC2420 RF transceiver. The single-hop network shown in Fig. 4.1 is used to illustrate a monitoring application. Communications among WSN nodes are based on RICER protocol depicted in Fig. 2.11. The BS, connected to a host computer, sends a wake-up beacon each $T_b = 50ms$ and the maximum idle listening time at each ED is set to $T_{idle} = 52$ms to deal with clock drift. The PM is implemented at each ED, which is a harvesting node. A supercapacitor of 0.9F is used for the energy storage and is charged to around 4V before deployment. The resolution of T_{WI} is in second and is set to 1s at the beginning.

Parameters of the PID-PM are determined by a manual tuning method. First, K_i and K_d are set to zero and K_p is chosen to provide fast convergence. Then K_i and K_d are estimated from some trial-and-errors. In this measurement, $K_p = 5750$, $K_i = 5$ and $K_d = 3500$ are used. K_i is small in order to reduce the effect of the integral error when V_S has reached the desired voltage V_{Ref}. Meanwhile, α is set to 0.6 when predicting the consumed energy in EM-PM.

4.5.2 Tuning Reactiveness of PM through OMNET++

The harvested energy profile shown in Fig. 3.5, which is extracted from a real PowWow node, is used as the input of a simulation program on OMNET++ to determine the k parameter in (4.1), which represents the reactiveness of the PM. The single-hop network shown in Fig. 4.1 with two harvesting nodes is used in this simulation. The EM-PM is implemented at the first ED while the PID-PM is implemented at the second one. The voltage of StoreCap (V_S) for different values of k is summarized in Table 4.1. It can be observed that both PMs well adapt the harvesting node as the average value of V_S during the simulation is very close to the desired ENO voltage (V_{Ref}), which is set to 4V. The PID-PM provides a better QoS than EM-PM as it has a lower complexity and therefore, a lower consumed energy as shown in (4.16) and (4.17).

It is also found from Table 4.1 that the variation of V_S is increased proportionally to k. When k = 5, the PM has a fast response to the change of harvested energy and therefore, V_S is more stable compared to higher values of k. Moreover, as there is more occurence of the PM, the total number of transmitted packets is reduced when k = 5. However, this effect is minor as the consumed energy by the PM is negligible compared to the energy for wireless communications during a slot. When k = 10, E_{EM} represents only around 0.9% of $\tilde{e}_C(n)$. Therefore, the choice of k is only required to balance the variation of V_S. If the energy source has a high variation (e.g. outdoor solar energy), k should be low in order to follow the change of harvested energy. Otherwise, higher value of k is suitable for a low variation energy source (e.g. indoor light energy). For the next experiments, k = 10 is used as it presents a good tradeoff between the reactiveness and computations overhead of the PM.

TABLE 4.1: Comparison V_S(mV) with different values of k.

	PID-PM					EM-PM				
k	Min	Max	Mean	Var	Packets	Min	Max	Mean	Var	Packets
5	3993	4008	3999	6.63	1550	3995	4000	3997	0.92	1540
10	3992	4018	3997	20.27	1590	3989	4002	3994	4.00	1582
15	3989	4022	3999	57.87	1605	3984	4032	3991	8.61	1599
20	3980	4030	3998	101.9	1620	3977	4044	3987	21.32	1612

Finally, V_S has a higher variation when using PID-PM instead of EM-PM. The reason is the trial-and-error phase of the PID controller, which is explained in detail in the following subsections.

4.5.3 PID-PM with Light Energy

In this subsection, the PID-PM is implemented on a PowWow platform equipped with two PVs in size of 4x6cm. This node acts as an ED sending a packet to the BS every wake-up. Fig. 4.4 shows the voltage of the StoreCap ($\overline{V_S}$) according to the wake-up interval (T_{WI}) of the node over time. At the beginning of the experiment, the default T_{WI} is 1s, V_{Ref} is set to the initial voltage of the supercapacitor (around 3.86V). The high value of K_p and K_d causes a big step size for the next wake-up interval. After 10s for the first adaptation, T_{WI} = 12s and $\overline{V_S}$ has the tendency to increase. Therefore, the accumulated error is positive and T_{WI} is decreased. In the first half, when the light condition is around 1000lux, T_{WI} stays around 4s. In the second half, the light condition is changed to 450lux. T_{WI} is therefore increased to 19s by the PID controller. $\overline{V_S}$ converges when T_{WI} is around 10s. Even with abrupt changes in light condition, the proposed controller can adapt the wake-up interval to stay in ENO. However, the PID-PM takes time before converging to ENO due to its trial-and-error process. As it can be seen on Fig. 4.4, the PID-PM converges to ENO after around 1500s in the first haft and 2000s in the second one. If the light condition is changed during convergence time, the trial-and-error may be much more longer.

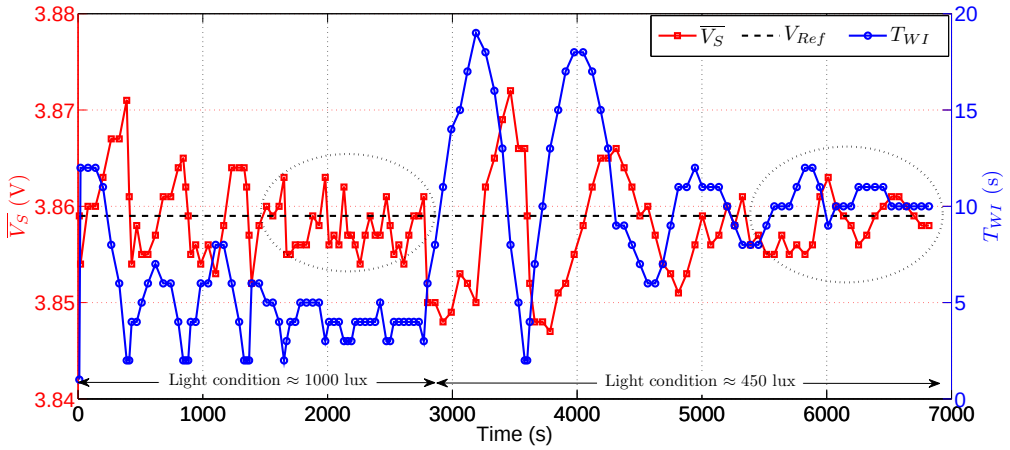

FIGURE 4.4: Voltage of StoreCap when applying PID-PM. In the first half, T_{WI} converges to around $4s$. In the second half, the light condition is changed and T_{WI} converges to around $10s$.

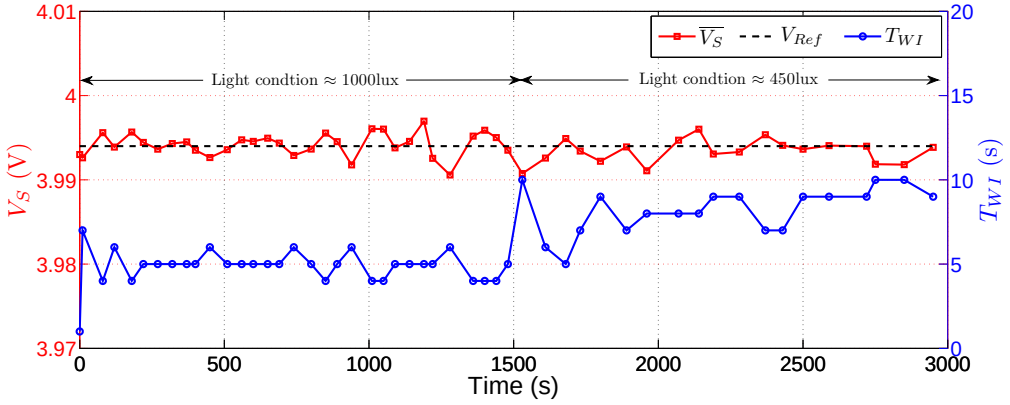

FIGURE 4.5: Voltage of StoreCap when applying EM-PM. $\overline{V_S}$ is fastly converged to V_{Ref} as EM-PM is able to estimate both the harvested and consumed energy.

4.5.4 EM-PM with Short Convergence Time

The same measurement in Section 4.5.3 is repeated with the EM-PM. Results of this measurement are presented in Fig. 4.5. At the beginning, the wake-up interval (T_{WI}) of the wireless node is also set to 1s. After 10s, the EM-PM is executed its first adaptation and the next T_{WI} is increased to 7s as $\overline{V_S}$ is bellow the desired voltage (V_{Ref}). However, PID-PM provides 12s for the first adaptation, which is very far from the ENO state when T_{WI} is around $4s$ as shown in Fig. 4.4. Since EM-PM is able to estimate the harvested energy as well as the consumed energy, it provides better adaptations and therefore, fast converges the wireless node to ENO. It can be observed from Fig. 4.5 that T_{WI} is converged to around $5s$ at the first half when the light condition is around 1000lux after 200s instead of 1500s as in case of PID-PM in Fig. 4.4. At the end of the first half in this measurement, there are some variations of T_{WI} but the $\overline{V_S}$ is closely kept around V_{Ref}.

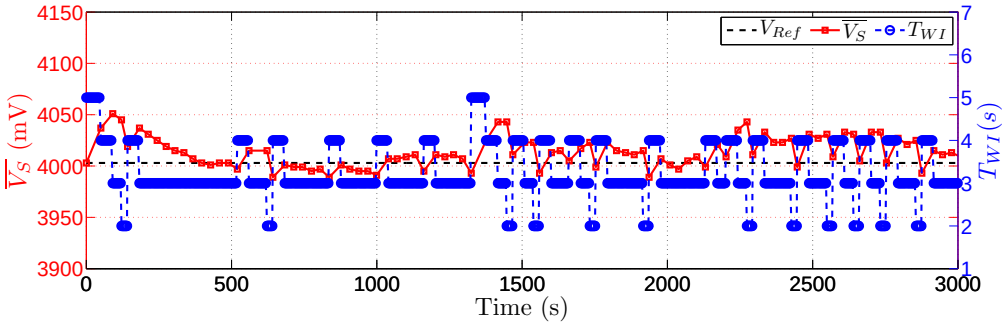

FIGURE 4.6: Power manager performs adaptation on a real PowWow node. V_S is kept almost constant around V_{Ref}, which represents the ENO condition.

In the second half, the light condition is reduced to around 450lux and T_{WI} seems to be converged to $9s$. During the whole measurement, $\overline{V_S}$ is rarely moved far from V_{Ref} as in case of the PID-PM and quickly converges the wireless node to ENO state. Therefore, EM-PM is chosen to extend to the heat energy and is presented in following subsection.

4.5.5 EM-PM with Heat Energy

In this subsection, the EM-PM is extended to heat energy when an ED node is equipped with two TEGs connected in parallel. Their hot surfaces are attached to a laptop charger as the heat source while cold surfaces are chosen to provide the heat spreading effect towards the heat sinks. The temperature gradient between the working PC adapter and the ambient air provides around 50mV output by two TEGs. At the beginning of our measurements, a 0.09F supercapacitor is used for the StoreCap.

Fig. 4.6 presents the adaptation of T_{WI} according to the change of $\overline{V_S}$. At the beginning of the experiment, the default T_{WI} is set to 5s. As k = 10, the PM performs the first adaptation after 50s and T_{WI} is reduced to 4s for the next 40s, T_{WI} = 3s as $\overline{V_S}$ is increasing. In the next 30s, $\overline{V_S}$ slightly decreases, but T_{WI} is reduced to 2s as $\overline{V_S}$ is higher than V_{Ref}. The budget energy now is positive and therefore, the numerator in (4.15) is significantly reduced. After that, T_{WI} is equal to $3s$ as long as the PM detects a considerable drop of $\overline{V}_S$. During the experiment, $\overline{V_S}$ is kept almost constant around V_{Ref}. It means that our PM is able to match the harvested and consumed energy over a long period and to keep the PowWow node running in ENO.

The biggest advantage of our EM-PM is the independence of leakage energy, which is a non-negligible consumed energy in a super capacitor based WSN. As it can be observed

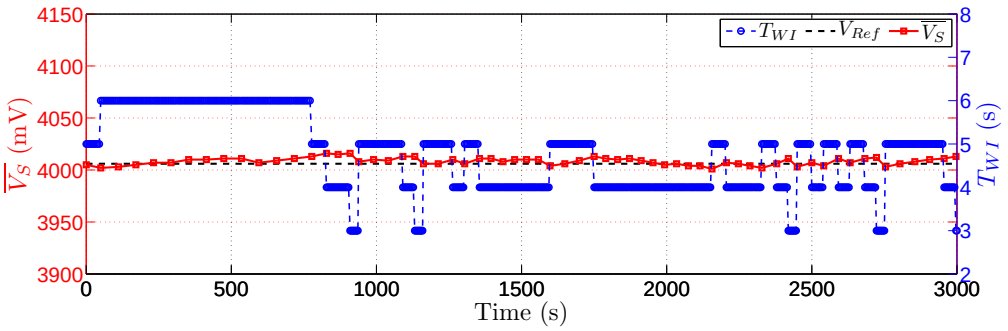

FIGURE 4.7: Votage of the StoreCap and wake-up interval of the PowWow node when a new super capacitor 0.18F is used.

in (4.15), characterization of the leakage energy is not required for adaptations of the EM-PM. Fig. 4.7 presents the voltage of the StoreCap and the wake-up interval of the wireless node when two 0.09F capacitors are connected in parallel (C_S = 0.18F). As the leakage energy increases, the average T_{WI} is also higher than experiment presented in Fig. 4.6. During the first 750s, T_{WI} converges to 6s. However, in the next 2000s, there seems to be more heat from TEG and T_{WI} is around 4s in average. Moreover, due to bigger capacitance, $\overline{V_S}$ is more stable than in case of Fig. 4.6. This behavior can be amenable for monitoring the health of industrial engines by exploiting the wasted heat when they are running. Real time detection and diagnosis of patient disease is also a promising application for our EM-PM.

4.6 Conclusions

The power manager is the heart of energy harvesting WSNs. Its main goal is to adapt the system to ENO. In this chapter, PID controller-based PM (PID-PM) and Energy Monitor-based PM (EM-PM) provide practical adaptations to match harvested and consumed energy in a dynamic environment. It is amenable to monitoring applications with solar cells in industrial or hospital environments where indoor lights are switched on all the time. While the PID-PM only considers the available energy in the supercapacitor used as the storage device (StoreCap), the EM-PM exploits from a simple energy monitor to provide a short convergence time. Our measurements show that the controller can achieve stable voltage to power the PowWow node for a long period of time. Both PID-PM and EM-PM can moreover be extended to other energy sources because their adaptations are mostly based on the voltage of the StoreCap.

Chapter 5

Power Manager for Periodic Energy Sources

5.1 Introduction

In this chapter, a set of novel power managers (PMs) is designed for EH-WSN node when it is powered by a periodic energy source such as: outdoor solar energy or indoor light energy. In these kinds of energy sources, harvested energy is only available during energy harvesting interval (T_{EI}) and there is no more harvested energy in the next non-energy harvesting interval (T_{NEI}). This behavior is repeated every cycle $T_C = T_{EI} + T_{NEI}$ as presented in Section 2.6. In order to operate continuously during a whole cycle T_C, the PM must have a strategy to save energy during T_{EI} and then, uses it in the next T_{NEI}. Therefore, the voltage of a supercapacitor which is used for the secondary storage (StoreCap) is increased during T_{EI} and decreased during T_{NEI}. In order to satisfy the ENO condition, which is the primary goal of the PM for EH-WSNs, its voltage at the end of T_{NEI} has to be equal to the value at the beginning of a cycle.

Not only satisfying the ENO condition, the secondary goal of PMs proposed in this chapter is to balance the Quality of Service (QoS) of an EH node during the whole cycle T_C. This feature is really useful for EH-WSNs based monitoring applications, which usually require regular data tracking. This is the improvement of our PMs compared to state-of-the-art PMs proposed in [33] or [4]. These PMs only satisfy ENO but do not take into account the QoS between T_{EI} and T_{NEI}. Therefore, these PMs usually

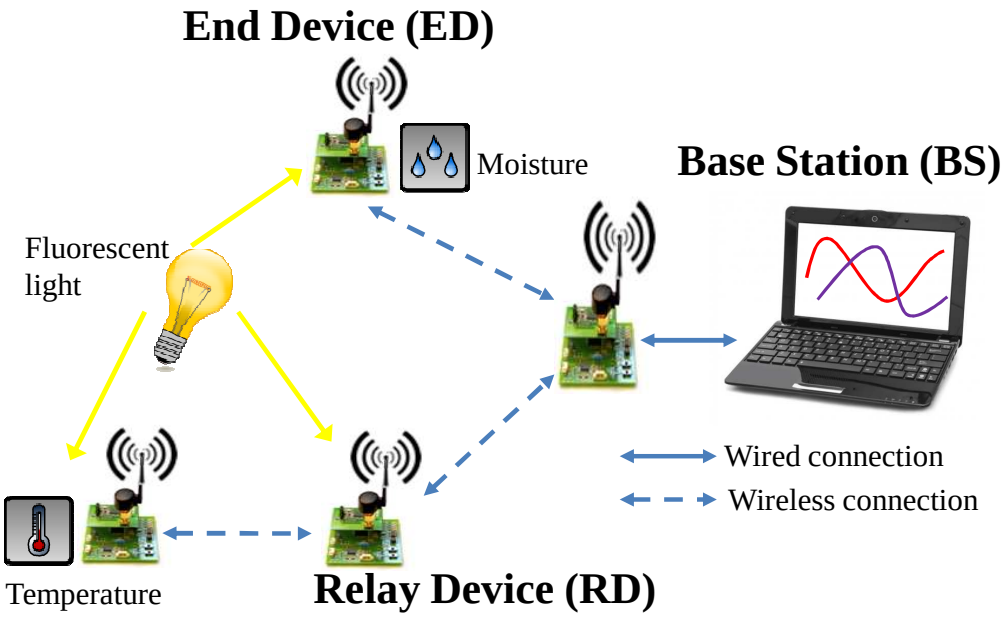

FIGURE 5.1: Multi-hop energy harvesting wireless sensor network.

provide very high QoS when the harvested energy is available but very low QoS when there is no more environmental energy. By predicting the duration of T_{EI} and T_{NEI}, our proposed PM, named PEriOdic Power Manager (PEO-PM) is able to balance the QoS during the whole cycle while still satisfying the ENO condition. PEO-PM is composed of two sub-PMs: a Positive Energy Power Manager (PE-PM) applied during T_{EI} and a Negative Energy Power Manager (NE-PM) applied during T_{NEI}.

The PEO-PM is firstly deployed in a single-hop EH WSN shown in Fig. 4.1 to compare with state-of-the-art PMs. All the EDs are EH nodes powered by light energy extracted by two small PVs. With a base station powered by a permanent power supply, the WUB can be sent frequently (e.g. $T_b = 50$ms) when RICER protocol (see Fig. 2.11) is used to ensure that whenever an ED wakes-up, it receives an appropriate WUB and then, sends a data packet to the BS. However, in a multi-hop EH WSN depicted in Fig. 5.1, it is impractical for a relay device (RD) to send its WUB every 50ms. Due to the limitation of radio range, an ED must forward its packet to a RD and then, the RD sends this packet to the BS. To increase the data rate between the ED and RD, a partial synchronous protocol is required instead of an asynchronous protocol as RICER. The wake-up interval of the ED must have a low variation in order to keep the synchronization with the RD. For instance, when the wake-up intervals of the ED and RD are 10s and 5s, respectively and they are synchronized each other. Therefore, whenever the ED wakes-up, it can meet the RD to forward its packet. Unfortunately, the harvested energy of ED can be reduced

and its wake-up interval must be increased to 12s for instance. However the wake-up interval of the RD can be still 5s. In this case, the synchronization between them is lost for at least 60s (five wake-up times of the ED). If there is clock-drift, this period can be longer and therefore, reduces the overall data rate between ED and RD. A better solution is to keep a 10s wake-up interval of the ED or increase it up to 15s, which is a multiple of 5s. This strategy will keep the synchronization among many EH nodes by reducing the variation of their wake-up period. Following this goal, a new PM, named Wake-up Variation Reduction Power Manager (WVR-PM), is proposed. Its main core is the PEO-PM and some simple components (such as an Exponentially Weighted Moving Average filter (EWMA) and a uniform quantizer) are added to reduce the variation of the wake-up interval. Moreover, a new Synchronized Wake-up Interval MAC protocol (SyWiM) is also proposed to take advantage of the fact that the wake-up interval of the node is a multiple of a quantization step size (e.g. 5s). The protocol stack of SyWiM is similar to RICER shown in Fig. 2.11. However, after receiving a data packet, the transmitter responses an acknowledgement (ACK) which includes the synchronization time as proposed in WiseMAC [62]. Based on this information, the transmitter can wake-up at the right time to receive a WUB from the receiver.

The rest of this chapter is organized as follows. In Section 5.2, an overview of state-of-the-art PMs is presented. The PEO-PM and WVR-PM are proposed in Section 5.3. Then, the SyWiM protocol is presented in Section 5.4. Experimentations performed on OMNET++ simulator are presented in Section 5.5. Finally, the chapter ends with conclusions.

5.2 State-of-the-Art Power Managers

Kansal et al. [3] proposed a low complexity PM (KAN-PM) for dynamically adapting the duty cycle of a wireless node by considering the predicted harvested energy. Their approach takes advantage of the periodic energy source when photovoltaics (PVs) are used in an outdoor environment. Indeed, the harvested energy can be predicted based on previous samples. A cycle lasting for a day is divided into slots of the same duration (e.g. 30 minutes) and adaptation calculations are performed at the end of each slot. To ensure ENO condition, the residual energy (the difference between predicted energy and real harvested energy) of previous slot is used to adapt the duty cycle of future slots.

However, the initial duty cycle of slots are determined at the beginning of a day and are only based on the harvested energy of a previous day. Therefore, when there is a change from a sunny to a cloudy day, or vice versa, it has been demonstrated in [98] that the PM performs poorly. Moreover, the objective of KAN-PM is only to maximize instead of balancing the QoS during a whole day. As a consequence, the EH-WSN node usually has a high QoS during day-time, when there is plenty of harvested energy, but very low QoS during night-time, when there is no more harvested energy. Another disadvantage of KAN-PM is that its adaptations do not take into account the State-of-Charge (SoC) of the storage device. Therefore, if the node is deployed with a minimum SoC and the energy predictor using an Exponential Weighted Moving Average (EWMA) filter produces a negative error, the SoC can be less than the minimum level after a day and the node operations must be interrupted. To overcome this problem, EH-WSN nodes using KAN-PM are usually charged to a high level before their deployment. The ENO concept is extended in [65] by using a class of linear programs to model various constraints in energy harvesting WSNs such as the duty cycle, the sensing rate or the local memory access. In this approach, the PM is able to maximize the minimum duty cycle of the node, which presenst an idea to balance QoS during a day. However, solving the optimization problem in their approach requires high complexity in terms of running time and energy consumption [65]. Therefore, most of the computation overhead is moved to an offline computer before a real sensor node implementation.

Castagnetti et al. [4] presented two PMs, the Open-Loop (OL-PM) and Close-Loop (CL-PM) which improve the throughput of a WSN node up to 50% compared to [3]. Simulation results are based on the TI EZ430, a real solar energy harvesting WSN platform with a solar cell in size of 2.25in x 2.25in. The harvested energy is approximated by a function of the light intensity using an illuminance sensor (expressed in lux). Meanwhile, the consumed energy is the average current delivered from the battery during a period and is computed independently for each activity of the WSN node (e.g. sensing, RF transmission). Their approach takes advantage of a dynamic adaptation period (instead of a fixed one as KAN-PM) to trade-off between the computation overhead and the reactivity of the PM. Moreover, the battery SoC is considered in CL-PM to increase the QoS during the night-time while still ensuring the SoC is always greater than a minimum value. However, the next wake-up interval T_{WI} of positive energy PM in CL-PM is computed by a ceil function of T_{WI} produced by an energy neutral PM. As this function

always returns a higher wake-up interval than the real neutral value, there is always a small part of harvested energy that is used to charge the battery. Therefore, CL-PM provides very high QoS during day-time but very low QoS during the night-time, especially when the node is deployed with a low initial SoC. In this case, the voltage of the battery is lightly increased during the day and to satisfy ENO, QoS during the night must be reduced. This problem is more crucial when considering the supercapacitor-based EH-WSN, where leakage energy is much higher than battery and can therefore, degrade QoS. Moreover, the harvested energy is estimated from a function of the value from the illuminance sensor. Therefore, this function needs to be characterized again when the solar cells are changed.

In this chapter, our periodic power manager (PEO-PM) not only satisfies the ENO condition but also balances the QoS during a whole cycle of a periodic energy source (e.g. light energy in an office). The concept of dynamic adaptation period [4] is also used in our approaches in order to adapt the reactiveness of the PM according to the current harvested energy. PEO-PM is able to monitor the SoC of a supercapacitor used for the energy storage by reading its voltage and therefore, ensures it always greater than the minimum value. Finally, a wake-up variation reduction power manager (WVR-PM) is proposed to reduce the variation of the wake-up interval. This WVR-PM copes with the problem of PEO-PM when EH-WSN nodes are deployed in a multi-hop EH-WSN.

5.3 Periodic Power Manager Architecture

The architecture of our periodic power manager (PEO-PM) is depicted in Fig. 5.2. The PEO-PM is composed of two main components: a Positive Energy Power Manager (PE-PM) and a Negative Energy Power Manager (NE-PM). The PE-PM is activated during the energy harvesting interval (T_{EI}), when the environmental energy is available, while the NE-PM is applied during the non-energy harvesting interval (T_{NEI}), when there is no more environmental energy. The energy monitor proposed in Chapter 3 is embedded to provide the harvested energy ($\tilde{e}_H(n)$), the consumed energy ($\tilde{e}_C(n)$) as well as the available energy in a supercapacitor (StoreCap) ($\tilde{e}_S(n)$). In order to adapt the wake-up interval in the next slot ($T_{WI}(n+1)$), an energy predictor using adaptive filter (AF-EP) proposed in Chapter 3 and an Exponentially Weighted Moving Average filter (EWMA) are used to predict the harvested power ($\hat{P}_H(n+1)$) and the consumed energy ($\hat{e}_C(n+1)$)

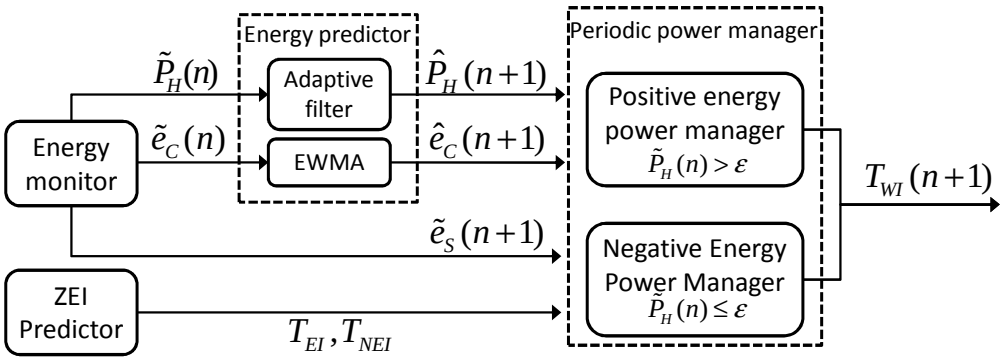

FIGURE 5.2: Periodic power manager (PEO-PM) architecture with two main components: positive and negative energy power manager.

in the next slot. Unfortunately, AF-EP is proposed for fixed-slots but PEO-PM has a dynamic adaptation period where two consecutive slots usually have different durations. Therefore, instead of predicting the harvested energy, the harvested power is predicted in our PEO-PM.

According to the amount of harvested energy, either PE-PM or NE-PM is chosen. When $\tilde{P}_H(n)$ is greater than a pre-defined value ε, PEO-PM considers that the node is staying in T_{EI} and therefore, PE-PM is activated. Not only adapting the wake-up interval according to the harvested energy, PE-PM also needs to buffer energy for the non-energy harvesting interval (T_{NEI}), which begins when $\tilde{P}_H(n) \leq \varepsilon$. Then, NE-PM regularly monitors the available energy of the StoreCap as well as the remaining time of the non-harvesting period to ensure continuous operations until the next cycle of the periodic energy source, when harvested energy is available again. Moreover, in order to balance the QoS during a whole cycle, a zero energy interval (ZEI) predictor is activated to estimate T_{EI} and T_{NEI}. The ratio between T_{EI} and T_{NEI} directly impacts the next wake-up interval during energy-harvesting interval. The longer T_{NEI} requires higher T_{WI} during T_{EI} to respect the same QoS during both T_{EI} and T_{NEI}. In this context, more harvested energy is saved during T_{EI} for operations during T_{NEI}. Following subsections will explain in details how PE-PM and NE-PM adapt the wake-up interval of the node powered by a periodic energy source.

5.3.1 Positive Energy Power Manager

A cycle of a periodic energy source lasting for T_C is divided into two sub-intervals, the harvesting energy (T_{EI}) and non-energy harvesting interval (T_{NEI}) as shown in Fig. 5.3.

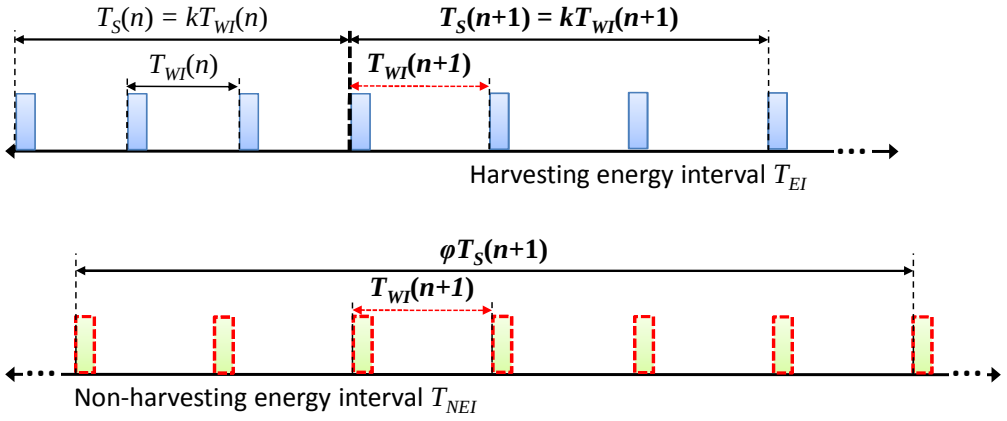

FIGURE 5.3: Positive Energy Power manager. The harvested energy is not only used for the next slot, but also for φ slots during T_{NEI}.

The PE-PM is applied during the first interval (T_{EI}) while NE-PM is used during the second one (T_{NEI}). This subsection explains how PE-PM adapts the wake-up interval in the next slot while still saving energy for the non-energy harvesting interval.

At the end of the slot n, the energy monitor is activated to provide energy profiles, including the consumed energy $\tilde{e}_C(n)$ and the harvested power $\tilde{P}_H(n)$, which is obtained by dividing the harvested energy ($\tilde{e}_H(n)$) by the slot duration $T_S(n)$. Then, the prediction of both harvested energy ($\hat{e}_H(n+1)$) and consumed energy ($\hat{e}_C(n+1)$) for slot $(n+1)$ is performed. Similar to the energy monitor-based power manager (EM-PM) proposed in Chapter 4, $\hat{e}_C(n+1)$ is divided into two parts:

$$\hat{e}_C(n+1) = \hat{e}_{Active}(n+1) + P_{Sleep}kT_{WI}(n+1) \tag{5.1}$$

where $\hat{e}_{Active}(n+1)$ is the consumed energy for active mode and $P_{Sleep}kT_S(n+1)$ stands for the energy consumed in sleep mode during slot $(n+1)$. Since the node has the same k wake-up times in every slot, $\hat{e}_{Active}(n+1)$ can be predicted from the consumed energy for active mode in the previous slot ($\tilde{e}_{Active}(n)$) by using EWMA:

$$\hat{e}_{Active}(n+1) = \alpha_C \hat{e}_{Active}(n) + (1-\alpha_C)\tilde{e}_{Active}(n) \tag{5.2}$$

where $\alpha_C \in [0,1]$ is a weighting factor, which will be determined later in this chapter. Meanwhile the harvested power ($\hat{P}_H(n+1)$) is predicted by using the AF-EP. As a consequence, the harvested energy in slot $(n+1)$ is predicted as follows:

$$\hat{e}_H(n+1) = \hat{P}_H(n+1)kT_{WI}(n+1) \tag{5.3}$$

In order to respect the ENO condition after a cycle of the periodic energy source, this predicted energy is not only used for the next slot $(n+1)$, but also for a period $\varphi T_S(n+1)$ in non-energy harvesting interval, with $\varphi = T_{NEI}/T_{EI}$. By this way, harvested energy during T_{EI} is buffered for T_{NEI}. Moreover, we expect the same QoS during the whole cycle of the periodic energy source. Therefore, the wake-up interval during $\varphi T_S(n+1)$ (see Fig. 5.3) is assumed to be $T_{WI}(n+1)$, which is the same wake-up interval during slot $(n+1)$. Total consumed energy in $\varphi T_S(n+1)$ can be predicted as $\varphi \hat{e}_C(n+1)$ since this period is φ times longer than slot $(n+1)$. Finally, the following constraint needs to be satisfied:

$$\hat{e}_H(n+1) = \frac{1+\varphi}{\eta}\hat{e}_C(n+1) + (1+\varphi)P_{Leak}T_S(n+1) \tag{5.4}$$

where η is the converter efficiency of the harvesting circuit, which has been characterized in Chapter 2. The left hand side in (5.4) is the prediction of total harvested energy in slot $(n+1)$. The first term of the right hand side is the prediction of consumed energy of the wireless node, while the second term is the total leakage energy during slot $(n+1)$ and φ slots during T_{NEI}. By appling (5.1), (5.3) and $T_S(n+1) = kT_{WI}(n+1)$ into (5.4), the next wake-up interval during T_{EI} is achieved as:

$$T_{WI}(n+1) = \frac{(1+\varphi)\,\hat{e}_{Active}(n+1)/k}{\eta\hat{P}_H(n+1) - (1+\varphi)(\eta P_{Leak} + P_{Sleep})} \tag{5.5}$$

This result shows a simple implementation of the PE-PM, which is applied during the harvesting-energy interval (T_{EI}) of a periodic energy source. By tracking all activities of the wireless node during slot n, $\tilde{e}_{Active}(n)$ is estimated and then, $\hat{e}_{Active}(n+1)$ is predicted by using the EWMA filter defined in (5.2). Moreover, $\hat{P}_H(n+1)$ is also predicted from $\tilde{P}_H(n) = \tilde{e}_H(n)/T_S(n)$ by the AF-EP proposed in Chapter 3. Since η, P_{Leak} and P_{Sleep} are characterized in Chapter 2, $T_{WI}(n+1)$ can be easily estimated using (5.5). Moreover, φ directly impacts the computation of the next wake-up interval $T_{WI}(n+1)$. A longer non-energy harvesting interval produces a higher value of φ and therefore, $T_{WI}(n+1)$ is increased. This feature helps our periodic power manager (PEO-PM) to respect the same average wake-up interval between T_{EI} and T_{NEI}.

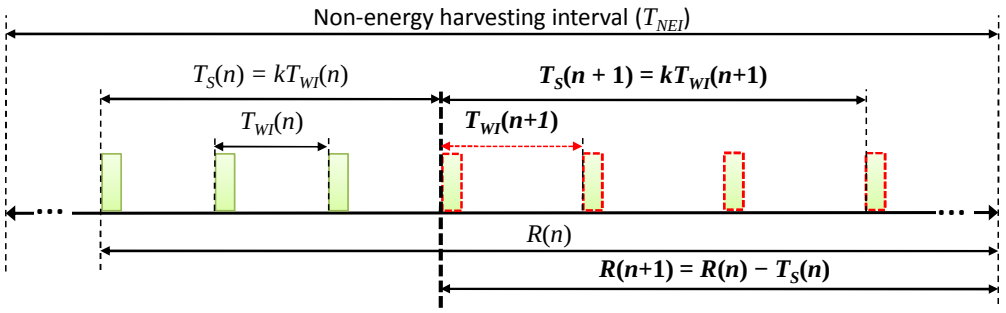

FIGURE 5.4: Negative energy power manager (NE-PM) for non energy harvesting interval (T_{NEI}). The next wake-up interval ($T_{WI}(n+1)$) is estimated from the remaining duration of non energy harvesting and current energy in StoreCap.

5.3.2 Negative Energy Power Manager

The negative energy power manager (NE-PM) shown in Fig. 5.4 is the second component of the periodic power manager (PEO-PM), which is activated during the non-energy harvesting interval (T_{NEI}) when $\tilde{P}_H(n)$ is less than a pre-defined threshold ε. Since there is no more harvested energy, node operations are only based on the available energy in the StoreCap, which is used for the energy storage. The voltage of StoreCap (V_S) therefore, keeps decreasing during T_{NEI}. However, V_S is expected to be equal to V_0 at the end of non-energy harvesting interval, which is the voltage of the StoreCap at the beginning of the energy harvesting interval. This constraint is required to satisfy the ENO condition after each cycle of the energy source.

First, NE-PM estimates the remaining time of the non-harvesting energy duration ($R(n+1)$), which is set to T_{NEI} at the end of energy-harvesting interval, as follows:

$$R(n+1) = R(n) - T_S(n) = R(n) - kT_{WI}(n) \tag{5.6}$$

Then, the available energy for sending packets during $R(n+1)$ is computed from the voltage of StoreCap at the end of slot n ($V_S(n)$) as:

$$E_R(n+1) = \frac{1}{2}C_S(V_S^2(n) - V_0^2) - (P_{Sleep} + \eta P_{Leak})R(n+1) \tag{5.7}$$

Based on the prediction of the consumed energy for sending k packets ($\hat{e}_{Active}(n+1)$) in (5.2), the total number of packets ($Pkt(n+1)$) allowed during $R(n+1)$ is:

$$Pkt(n+1) = \frac{kE_R(n+1)}{\hat{e}_{Active}(n+1)} \tag{5.8}$$

Therefore, the next wake-up interval can be determined as follows:

$$T_{WI}(n+1) = \frac{R(n+1)}{Pkt(n+1)} = \frac{R(n+1)\hat{e}_{Active}(n+1)}{kE_R(n+1)} \tag{5.9}$$

The NE-PM is activated again after $T_S(n+1) = kT_{WI}(n+1)$ to converge V_S to V_0 during non-energy harvesting interval (T_{NEI}). At the beginning of a new cycle, V_S is expected to recover to V_0 that satisfies the ENO condition after each cycle T_C. However, NE-PM does not try to balance the wake-up interval between T_{EI} and T_{NEI}. The main goal of NE-PM is to satisfy the ENO condition after the non-energy harvesting interval (V_S is expected to be equal to V_0). In fact, the average T_{WI} during T_{NEI} depends on V_S at the beginning of the non-energy harvesting interval. Therefore, the same QoS during the whole cycle is achieved when these conditions are met:

1. ZEI predictor provides precise values of T_{EI} and T_{NEI}.
2. StoreCap is sufficient to buffer harvested energy during energy harvesting interval.

When the first condition is false for example, if the real non-harvesting interval is greater than the predicted value, T_{WI} should be increased to satisfy ENO. Otherwise, if the real non-harvesting interval is less than the predicted value, T_{WI} can be increased to maximize the QoS. Moreover, when the second condition is not satisfied, a part of harvested energy is discarded as there is not enough free space in the StoreCap. T_{WI} is therefore, reduced in order to respect the ENO condition. The size of StoreCap must be meticulously chosen in the design phase, which is proposed in Chapter 2. Impacts of the ZEI and the size of StoreCap on the T_{WI} during T_{NEI} are explained in more details in the simulation results.

5.3.3 Wake-up Variation Reduction Power Manager

As explained in Section 5.1, regular change of wake-up interval can degrade the global QoS in a multi-hop EH-WSNs. In this subsection, efficient solutions are proposed to reduce the wake-up interval variations produced by the PEO-PM. A new power manager, named Wake-up Variation Reduction Power Manager (WVR-PM), is presented.

The first component causing the wake-up interval variations is $\hat{e}_{Active}(n+1)$. This component occurs in both PE-PM and NE-PM when it is required to determine the next

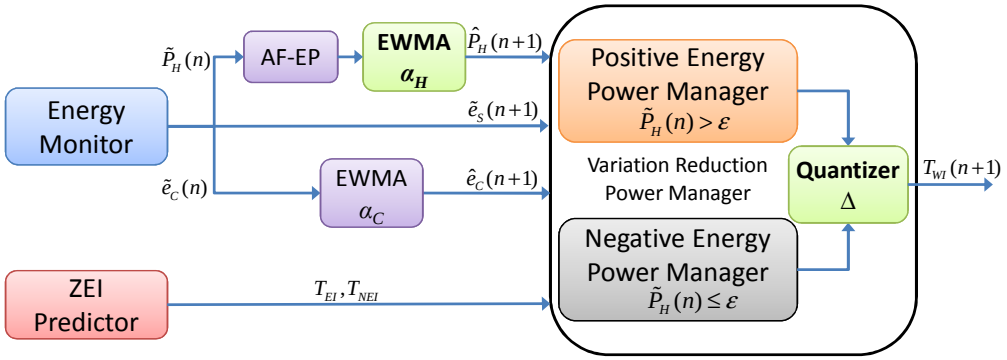

FIGURE 5.5: Wake-up variation reduction power manager (WVR-PM) architecture. Its main core is the periodic power manager (PEO-PM). An EWMA filter and a uniform quantizer are added in order to reduce the variation of the wake-up interval.

wake-up interval $T_{WI}(n+1)$ (see (5.5) and (5.9)). Therefore, reducing the variation of $\hat{e}_{Active}(n+1)$ will also reduce the variation of $T_{WI}(n+1)$. As $\hat{e}_{Active}(n+1)$ is predicted by using an EWMA filter (5.2), its variation is reduced when α_C is close to 1. This solution is also applied to $\hat{P}_H(n+1)$, which affects the variation of $T_{WI}(n+1)$ in (5.5). In consequence, another EWMA filter, whose weighted factor is α_H, is added after the adaptive filter-base energy predictor (AF-EP). However, the value of α_H must be trade-off as the variation of $T_{WI}(n+1)$ also presents the adaptations of the wireless node according to the harvested energy. When α_H is close to 1, the variation of $T_{WI}(n+1)$ is reduced but then, the wireless node has a low response to the change of the real harvested energy.

Finally, a uniform quantizer with a quantization step size Δ is embedded to normalize the output $T_{WI}(n+1)$ as shown in Fig. 5.5, and can be expressed as:

$$Q(T_{WI}(n+1)) = \Delta \left\lfloor \frac{T_{WI}(n+1)}{\Delta} \right\rceil \tag{5.10}$$

where $\left\lfloor \frac{T_{WI}(n+1)}{\Delta} \right\rceil$ returns the nearest integer number when dividing $T_{WI}(n+1)$ by Δ. The new wake-up interval is therefore, always a multiple of Δ. A MAC protocol can take the advantage of WVR-PM to reduce the global consumed energy.

With a quantization step size Δ, any variation of T_{WI} lower than $\Delta/2$ is discarded. Therefore, the choice of Δ is also a trade-off between the variation of T_{WI} and the adaptation of the wireless node. When Δ is high, T_{WI} is rarely changed even if the harvested energy has a big variation. Otherwise, when Δ is low, T_{WI} is frequently updated, which causes many variations on T_{WI}. Moreover, it is noticed that the minimum wake-up interval is Δ as zero is an invalid value.

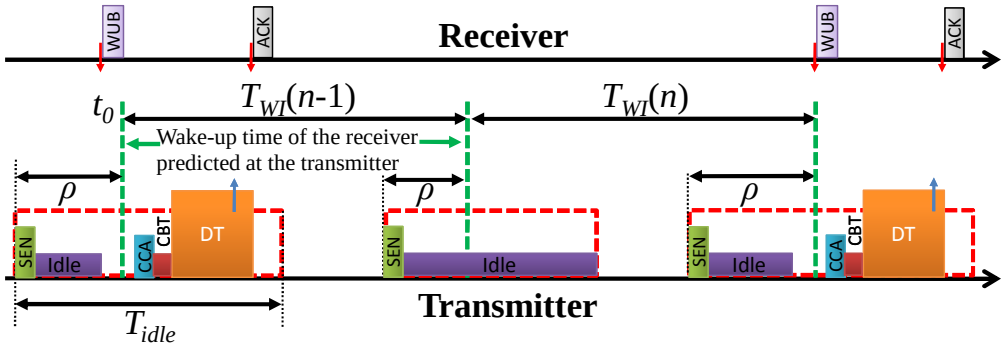

FIGURE 5.6: Synchronized wake-up interval MAC protocol for low wake-up variations multi-hop EH-WSNs (SyWiM).

5.4 Synchronized Wake-Up Interval MAC Protocol

In this section, a new protocol designed for EH-WSN node using WVR-PM, named Synchronized Wake-up Interval MAC (SyWiM), is proposed. SyWiM takes advantage of the fact that a node wake-up interval is always a multiple of Δ. The basic idea of SyWiM is that after synchronizing the timer of the transmitter with the receiver, the time domain from this point is divided in blocks of Δ. Whenever the transmitter wakes-up, the receiver is also expected to wake-up around this point. SyWiM uses the theory proposed in WiseMAC to overcome the clock-drift problem so that the transmitter can receive the WUB from the receiver with a short idle listening time.

The first communication between two nodes when they are not synchronized is done with a long idle listening time (e.g. Δ). Once there is a successful communication at time t_0, this idle listening time can be reduced as the ACK packet contains the remaining time until the next $t_0 + \Delta$, as this moment is a potential wake-up time of the receiver. To deal with clock drift between the transmitter and the receiver, the transmitter must wake-up sooner than the potential wake-up timer of the receiver an interval ρ. Let θ be the frequency tolerance of the clock source used in EH-WSN nodes, according to WiseMAC [62], we have:

$$\rho = min(2\theta L, T_{WI}(n)) \tag{5.11}$$

where L is the interval from the last successful communication and current wake-up time of the transmitter, $T_{WI}(n)$ is the current wake-up interval of the transmitter. The result in 5.11 is explained as follows: assume that two nodes have a first communication at t_0 and they have the same wake-up interval $T_{WI}(n)$. However, the receiver has a real frequency $f(1+\theta)$ instead of f. Therefore, it will wake-up $\theta T_{WI}(n)$ sooner than

$t_0 + T_{WI}(n)$. If the transmitter has a precise frequency f, it has to wake up at $t_0 + \Delta - \theta T_{WI}(n)$ to cover the clock drift at the receiver. However, the clock source of the transmitter can be late if its real frequency is $f(1-\theta)$. Therefore, the transmitter must wake-up $2\theta T_{WI}(n)$ in advance. In this example, $L = T_{WI}(n)$. In the case L is very large (e.g. lost synchronization or the wake-up interval of the receiver is increased due to bad harvested energy), $2\theta L$ can be greater than $T_{WI}(n)$ and therefore, $\rho = T_{WI}(n)$. After waking-up, the transmitter opens an idle listening window which is able to take into account the clock-drift when the clock source of the receiver and transmitter is $f(1-\theta)$ and $f(1+\theta)$, respectively. In this case, the receiver wakes up $2\theta L$ later than the transmitter. As the transmitter needs to wake-up $2\theta L$ sooner for the first scenarios, its maximum idle listening (T_{idle}) must be at least $4\theta L$. Similarly to ρ, a min function is used to avoid having the case $4\theta L$ is greater than $T_{WI}(n)$:

$$T_{idle} = min(4\theta L, T_{WI}(n)) \tag{5.12}$$

Not only considering the frequency tolerance of hardware components (e.g. oscillators), the fault tolerance of software components is also included in this work (e.g. software timers). For instance, the real-time clock source 32,768kHz used for timers in PowWow platform has a frequency tolerance ±20 ppm (parts per million), or the peak frequence variation (δ_f) is

$$\delta_f = \frac{20(ppm)f(Hz)}{10^6} \tag{5.13}$$

Therefore, the maximum error of this clock source after 1s is $err_H = f\delta_f \approx 0.02$ms.

This clock source is used as the input for a software timer, which causes an interrupt every 10ms. Therefore, the value 328 is loaded to the timer counter register (TCR). However, 328 clocks is approximated to 10.0098ms or the error is 0.0098 for each 10ms. Finally, the error due to software timer after each second is $err_S = 0.98$ms. By considering both errors of hardware and software components, θ can be set to $err_H + err_S = 0.1$. If all EH-WSNs are consistent with the same clock source and software timer configuration, err_S can be removed. However, ρ and T_{idle} must be quantized with a step size 10ms, which is the resolution of the software timer. For instance, if $\theta = err_H$, L = 20, from (5.11), $\rho = 0.8$ms. Unfortunately, the software timer cannot indicate this period. In this case, the node will wake up 10ms in advance instead of 0.8ms. It is noticed that $T_{WI}(n)$ is in order of second and therefore, much more longer than ρ and T_{idle}, which are in

order of ms. Based on ρ and T_{idle}, the transmitter is able to wake up at the right time in order to receive a WUB from its receiver.

The detail of SyWiM is depicted in Fig. 5.6. After the first successful communication at t_0, the transmitter resets its timer and waits until its next wake-up time ($t_0+T_{WI}(n-1)$). As the wake-up interval at each node is a multiple of step size Δ, the receiver can also wakes-up at $t_0+T_{WI}(n-1)$. Therefore, the transmitter wakes-up at $t_0+T_{WI}(n-1)-\rho$, where $\rho = 2\theta T_{WI}(n-1)$, and opens a short idle listening window for $T_{idle} = 4\theta T_{WI}(n-1)$ (ρ and T_{idle} now are much less than $T_{WI}(n-1)$ in (5.11) and (5.12)). If there is no WUB, the transmitter immediately turns into sleep mode until its next wake-up time ($t_0 + T_{WI}(n-1) + T_{WI}(n)$). It wakes-up again with greater ρ and T_{idle} than previous wake-up since L at this time is $T_{WI}(n-1) + T_{WI}(n)$ instead of $T_{WI}(n-1)$.

The first difference between WiseMAC and SyWiM is that WiseMAC is proposed based on TICER protocol (Transmitted Initiated Cycled Receiver) where the transmitter starts the communication by sending its WUB to the receiver. Meanwhile, SyWiM is relied on RICER protocol (Receiver Initiated Cycled Receiver) where the communication initialization is performed by the receiver. The second difference is WiseMAC is designed for battery-based system which the aims to minimize the consumed energy of the MAC protocol by reducing the idle listening time. In WiseMAC, the wake-up interval of the transmitter can be updated according to the wake-up interval of the receiver to achieve an energy efficiency communication. In contrast, the wake-up interval of the transmitter in SyWiM cannot be updated as the node has to satisfy ENO condition in EH-WSNs. Each node has its own wake-up interval produced by the WVR-PM, which is a multiple of the step size Δ. The SyWiM takes advantage of this feature and tries to synchronize the wake-up time of the transimtter node. Whenever the transmiter wakes-up, it only needs to open a short idle listening window to communicate with the receiver.

5.5 Simulations on OMNET++

5.5.1 Simulation Setup

The single-hop network shown in Fig. 4.1 with three EDs and one BS is used to validate our periodic power manager (PEO-PM). The resolution of T_{WI} is set to second by applying a rounding function to (5.5) and (5.9) in order to produce the nearest integer number. Therefore, SyWiM can be applied in this simulation with a step size $\Delta = 1$. $\theta = 0.02$ms as explained in Section 5.4. The value of k in (4.1) when determining the adataption period of the PM is set to 10. This value is the trade-off between the reactiveness and computations overhead of the PM which can be found in Section 4.5.2 or [4]. In order to predict $\hat{e}_{Active}(n+1)$ by using EWMA filter in (5.2), α_C is commonly set to 0.5 due to its minimum prediction error [33]. All EDs are equipped with the same harvested power profile, which is extracted from a real PowWow node powered by two PVs of size 4x6cm and setup in our office. The threshold ε used to switch between PE-PM and NE-PM is set to 200μW. Table 2.1 is used to evaluate the consumed energy of EDs.

The first condition to achieve a balanced QoS using PEO-PM is that the size of StoreCap must be sufficient to buffer harvested energy during the energy interval (T_{EI}). According to the measurements of the design framework presented in Section 2.7.4, the harvested power from two PVs is estimated in range of $[800-1000](\mu W)$, two capacitors 0.9F can be used to provide C_S = 1.8F for the StoreCap. The minimum and maximum voltage of StoreCap is V_{Min} = 1.8V and V_{Max} = 5.2V, respectively. The StoreCap is charged to V_0 = 2V before deployment. Total leakage power (P_{Leak}) is estimated to 73μW which includes 30μW for each 0.9F supercapacitor and 13μW for remaining components of the harvesting circuit (see more details in Section 2.4).

Following metrics are used to evaluate different PMs:

- W_{EI} (s): Average wake-up interval during T_{EI}.
- W_{NEI} (s): Average wake-up interval during T_{NEI}.
- W_C (s): Average wake-up interval during $T_C = T_{EI} + T_{NEI}$.
- Mem (16-bit words): the memory footprint for the PM.

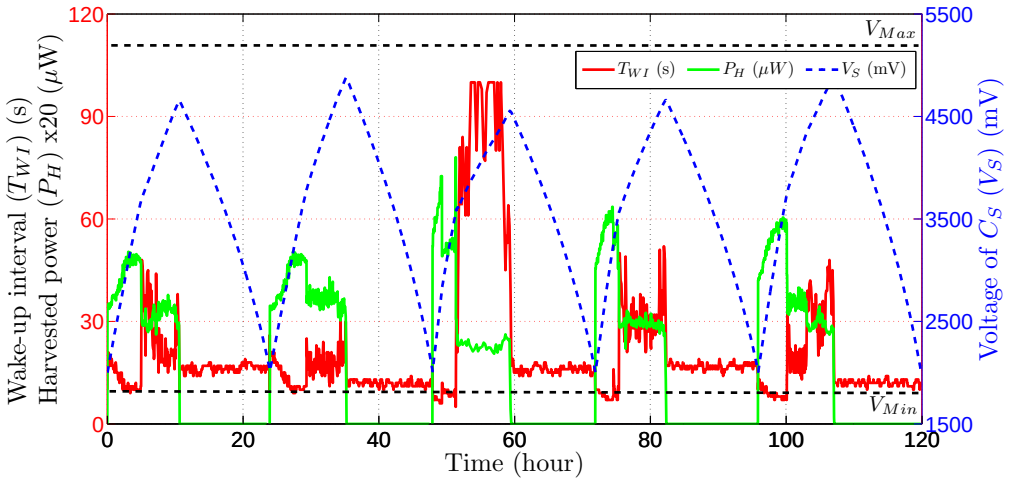

FIGURE 5.7: Adaptations of an EH ED node using PEO-PM. The voltage of the StoreCap (V_S) is recovered to around $V_0 = 2$V after a day to respect the ENO condition.

- Mul: the number of multiplications required for PM computations.
- B_f (minute): the battery failure duration.
- Gap: the difference of W_{EI} and W_{NEI} compared W_C, which is defined as:

$$Gap = \frac{|W_{EI} - W_C| + |W_{NEI} - W_C|}{W_C} \tag{5.14}$$

In order to balance W_{EI} and W_{NEI}, Gap is expected as small as possible.

5.5.2 PEO-PM Simulation Results

As the role of all three EDs is the same in the single-hop network shown in Fig. 4.1, the first ED is chosen to analyse its adaptations. Fig. 5.7 presents its wake-up interval (T_{WI}) and voltage of StoreCap (V_S) according to the harvested power (P_H). At the beginning of the first day, T_{WI} is around 20s and PE-PM is activated. Then, T_{WI} is reduced to 10s by the PEO-PM as the harvested power keeps increasing during five hours. After that, the harvested energy is lower and therefore, T_{WI} must be increased up to 45s. After around ten hours, the NE-PM is activated as P_H is less than ε. As the PE-PM can save a big amount of harvested energy during T_{EI}, the ED can have a high QoS during T_{NEI}. In this simulation, the average T_{WI} is around 15s during T_{NEI} of the first day. It can be observed that the wake-up interval during T_{NEI} has a lower variation compared to T_{EI} as its variation depends on $\hat{e}_{Active}(n+1)$ (see (5.9)). Fortunately, ED has the same

TABLE 5.1: Performance of PEO-PM with different C_S.

	C_S = 0.9F			C_S = 1.8F			C_S = 2.7F		
Day	W_{EI}	W_{NEI}	W_C	W_{EI}	W_{NEI}	W_C	W_{EI}	W_{NEI}	W_C
1	13.82	35.56	20.93	16.70	16.28	16.45	20.76	20.33	20.52
2	12.35	31.22	18.12	14.99	11.86	13.16	17.92	13.43	15.25
3	17.78	30.32	22.66	20.16	16.93	18.09	24.14	21.42	22.69
4	13.75	38.29	21.50	16.20	16.79	16.53	20.26	20.79	20.55
5	12.75	32.23	18.78	14.58	11.99	13.08	17.59	13.70	15.32
Average	14.09	33.52	20.40	16.53	14.77	15.46	20.13	17.93	18.87

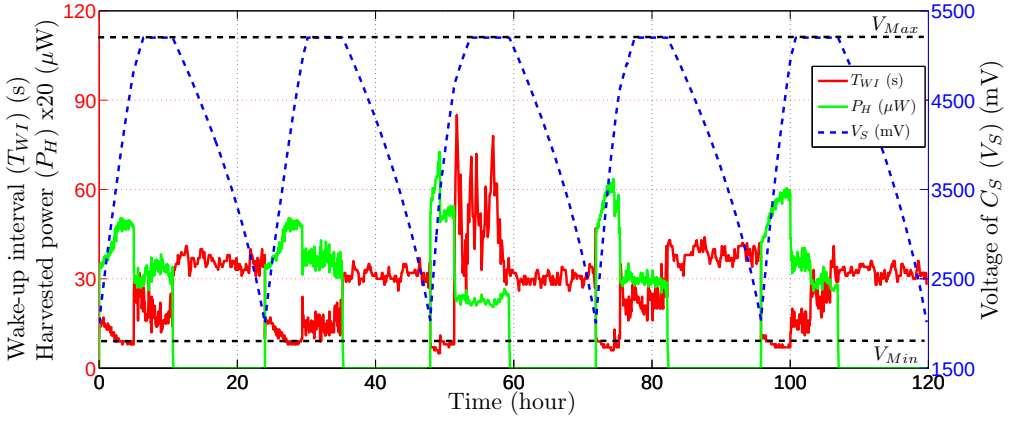

FIGURE 5.8: Adaptations of ED when C_S = 0.9F. As a part of harvested energy is discarded once $V_S = V_{Max}$, T_{WI} has to be increased in order to satisfy ENO condition.

k = 10 wake-up times every slot, $\hat{e}_{Active}(n+1)$ easily converges to the average consumed energy during active period of the node, which results a low variation of $T_{WI}(n+1)$.

Behaviors of the node during the first day are repeated on the next four days. During T_{EI}, the wake-up interval of the node (T_{WI}) presents an inverse shape with the harvested power (P_H), which shows fast adaptations of PE-PM according to P_H. Meanwhile, during T_{NEI}, T_{WI} is adapted by monitoring the voltage of StoreCap (V_S). Therefore, after a day, which is the cycle of the energy source, V_S is recovered closely to $V_0 = 2V$, which is the voltage of StoreCap at the beginning of the cycle. PEO-PM ensures continuous operations of the ED during five days without any interruptions ($B_f = 0$). However, to balance the average T_{WI}, which actually represents the average QoS, the size of StoreCap (C_S) must be sufficient to buffer all reservation energy when NE-PM is activated. This simulation is restarted with different values of C_S and the results are gathered in Table 5.1.

When C_S = 0.9F, the average wake-up interval during T_{EI} (W_{EI}) is reduced compared to

C_S = 1.8F and C_S = 2.7F as the leakage is reduced (P_{Leak} = 43μW). However, when V_S reaches V_{Max}, all harvested energy is discarded. Therefore, the average wake-up interval during T_{NEI} (W_{NEI}) is increased by NE-PM to ensure V_S around V_0 after a cycle. This is the reason why there is a big difference data rate between T_{EI} and T_{NEI} when C_S = 0.9F as shown in Table 5.1. Adaptations of the node in this case is presented in Fig. 5.8. When C_S is increased to 1.8F or 2.7F, there is enough space for the harvested energy during T_{EI} and therefore, W_{NEI} is very close to W_{EI}. However, the average wake-up period during a whole cycle (W_C) when C_S = 2.7F is reduced compared to C_S = 1.8F as the leakage power is increased to 103μW. Therefore, the value of C_S must be meticulously determined at the design phase as presented in Section 2.7.4. Only the smallest value of C_S that buffers enough harvested energy can not only satisfy the ENO, balance the QoS during a cycle, but also maximize the global QoS. In following simulations, C_S is set to 1.8F as the maximum V_S during five days is 4.86V, which is closed to V_{Max}. The small gap between W_{EI} and W_{NEI} when C_S = 1.8F and C_S = 2.7F comes from the prediction error of the ZEI predictor. The biggest difference can be found from Table 5.1 is the last day, when the real T_{EI} (11 hours) is longer than usual (10 hours). The PE-PM can buffer more energy but the non-energy harvesting interval (T_{NEI}) is shorter. Therefore, there is a slight decrease of the wake-up interval during T_{NEI} on the last day.

5.5.3 Performance Comparison

This section presents the comparison of our periodic power manager (PEO-PM) with two state-of-the-art PMs: KAN-PM [3] and CL-PM [4]. Beside the ENO condition of a PM for EH-WSN, we focus on the gap between W_{EI} and W_{NEI}, which is required as small as possible for a monitoring application with regular data tracking. Firstly, adaptations of KAN-PM and CL-PM are presented with the same simulation setup as PEO-PM. Finally, performance comparisons with PEO-PM are summarized. The OL-PM [4] is not implemented in this work as its adaptations are the same as CL-PM except that the wake-up interval is set to a maximum value during T_{NEI}.

5.5.3.1 Kansal Power Manager (KAN-PM)

There are two processes in KAN-PM: duty cycle initialization and duty cycle adaptation. The first process is only performed at the beginning of a new cycle (e.g. a new day

with light energy in this simulation) while the second one is carried out at the end of each slot to deal with the prediction error of harvested power using EWMA filter. The initialization process uses a full profile of harvested power on previous day to predict the harvested power for the next 48 slots (each slot is 30 minutes and a cycle T_C = 24 hours). Then, it assigns the minimum duty cycle (or maximum wake-up interval) to slots during T_{NEI} and maximum duty cycle (or minimum wake-up interval) to slots during T_{EI}. Total consumed energy for this assignment is estimated and then, compared with total predicted harvested energy. As we focus on indoor monitoring applications in this thesis, this consumed energy is usually greater than predicted harvested energy. Therefore, the duty cycle during T_{EI} must be reduced by increasing T_{WI} to balance total consumed and predicted harvested energy.

The duty cycle adaptation process is activated at the end of a slot in running time to cover the error of EWMA filter, which is the difference between the predicted and the real harvested power ($\hat{P}_H(n)$ and $\tilde{P}_H(n)$, respectively). When $\tilde{P}_H(n) < \hat{P}_H(n)$, the wake-up interval of future slots has to increase to compensate the negative energy error. In KAN-PM, the slot which has the maximum predicted harvested power is firstly chosen to reduce its wake-up interval to decrease the amount of consumed energy in this slot, which is expected to be equal to the negative energy error. However, if the wake-up interval reaches the maximum value (or minimum duty cycle), the wake-up interval of the second maximum predicted harvested power slot is also reduced, and so on. This loop is only stopped when total reduced consumed energy is equal to the negative energy or all of future slots are assigned with maximum wake-up interval. On the other hand, the positive energy error occurs when $\tilde{P}_H(n) > \hat{P}_H(n)$, meaning that more energy has been harvested than predicted. In this case, KAN-PM will reduce the wake-up interval (or increase the duty cycle). A future slot which has the lowest energy is firstly decreased its wake-up interval in order to maximize the total throughput.

To apply KAN-PM in our simulation, the consumed energy P_C, which is a constant value in KAN-PM, is defined as

$$P_C = \bar{e}_{Active} + P_{Sleep} + \frac{P_{Leak}}{\eta} \tag{5.15}$$

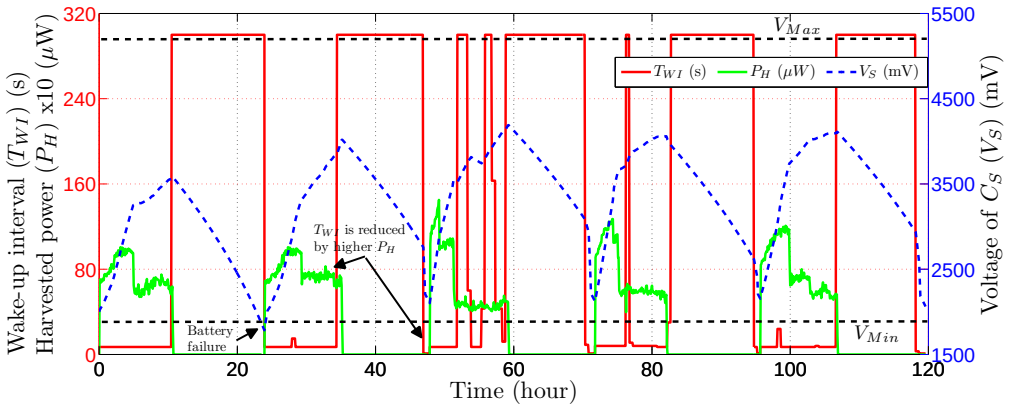

FIGURE 5.9: Adaptations of ED using PM proposed in [3] (KAN-PM). As KAN-PM does not take into account SoC, there is a short battery failure, $B_f = 15$ (minutes).

where $\bar{e}_{Active}$ is the average consumed energy for one communication. When SyWiM is used for the MAC protocol, $\bar{e}_{Active}$ can be evaluated as

$$\bar{e}_{Active} = \bar{T}_{idle} P_{Rx} + E_{SEN} + E_{CCA} + E_{CBT} + E_{DT} + E_{ACK} \tag{5.16}$$

where $\bar{T}_{idle}$ is the average idle listening and is set to 28ms. This value is obtained from the simulation performed with PEO-PM. The minimum and maximum wake-up intervals are set to 1s and 300s, respectively. Moreover, the harvested energy profile of the first day is considered as historical values, which is required by the duty cycle initialization. With this assumption, the duty cycle adaptation during the first day is not activated as there is no error of the prediction method. The wake-up interval of the node on this day is used to explain the duty cycle initialization of KAN-PM.

Duty cycle adaptations of KAN-PM are presented in Fig. 5.9. It can be observed that after the wake-up interval during T_{NEI} is assigned by 300s, the wake-up interval during T_{EI} is reduced to 7s. Unfortunately, high wake-up intervals during T_{NEI} also requires longer idle listening window as expressed in (5.12) with $L = 300$. Therefore, the real consumed energy of the node is greater than the average P_C in (5.15). As the SoC of StoreCap is not considered in KAN-PM, the V_S is not only less than V_0 (the deployed voltage of StoreCap) but also lower than V_{Min}, causing a battery failure of 15 minutes at the end of the first day. As it can be observed from Fig. 5.9, the node is completely turned off for around $B_f = 15$ minutes and turned on again on the second day when harvested energy is available. The first 5 hours of the second day provide a harvested power similar to the first day. There is a small amount of negative energy, which requires

TABLE 5.2: Performance of KAN-PM over five days.

	Day 1	Day 2	Day 3	Day 4	Day 5
W_{EI}	7.00	8.01	13.11	8.34	7.38
W_{NEI}	300.00	54.46	43.77	58.46	32.32
W_C	15.54	14.64	20.72	16.30	12.62
B_f	15	0	0	0	0

to increase T_{WI} from 7s to 15s. After that, the harvested power is higher but KAN-PM keeps T_{WI} =7s as on the first day. Instead of immediately reducing T_{WI}, positive energy is used to increase the QoS of slots which have the lowest harvested power. Therefore, T_{WI} of a slot at the end of the second day is reduced to 1s. In fact, the consumed energy of the node during this slot is much more lower than P_C due to the shortest idle listening as L =1 in (5.12). Therefore, at the end of the second day V_S is much more higher than V_0 = 2.0V. Finally, there are three conclusions when applying KAN-PM in indoor EH-WSNs:

1. KAN-PM has a low response to the change of harvested energy as the energy error is used to update T_{WI} of future slots, which can be very far from current slot. This is the main drawback of KAN-PM when there is a change from a cloudy day to a sunny day. As it can be observed from Fig. 5.9, even if the harvested energy at the beginning of the third day is much more higher than the second one, KAN-PM performs QoS poorly as the second day.

2. KAN-PM does not well satisfy ENO condition after a cycle of a periodic energy source. First, the total consumed energy of the node, which mostly depends on the scenarios of MAC protocol, is considered as a constant. Moreover, the SoC of StoreCap, which is used for the energy storage, is not taken into account in the duty cycle adaptation process.

3. KAN-PM provides a big wake-up interval difference between T_{EI} and T_{NEI}. It only focuses on minimizing instead of balancing the wake-up interval during a whole cycle. As it can be observed from Table 5.2, the performance during T_{NEI} is very poor compared to T_{EI}.

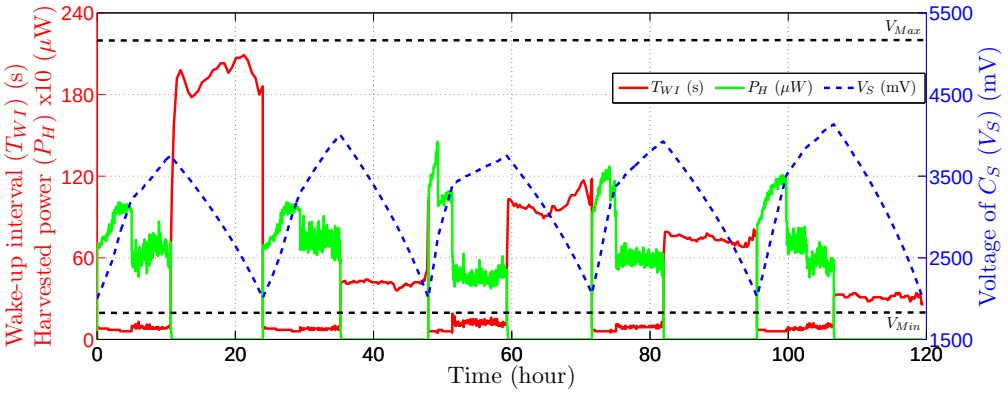

FIGURE 5.10: Adaptations of ED using PM proposed in [4] (CL-PM). Taking into account SoC of StoreCap, ENO condition is respected without any battery failure.

TABLE 5.3: Performance of CL-PM over five days.

	Day 1	Day 2	Day 3	Day 4	Day 5
W_{EI}	7.84	7.53	9.49	8.07	7.61
W_{NEI}	189.38	42.10	99.53	73.86	31.29
W_C	16.88	13.36	17.86	16.25	12.78

5.5.3.2 Close Loop Power Manager (CL-PM)

In contrast to KAN-PM, CL-PM has a fast response to the changes of the harvested energy. The positive energy power manager, which is a combination of a energy neutral power manager and a ceil function for the wake-up interval (T_{WI}), provides a higher QoS with lower T_{WI} during T_{EI} compared to our PEO-PM. As it can be observed from Fig. 5.10 and Table 5.2, the average wake-up interval during T_{EI} (W_{EI}) of the first day is 7.8s, which is 53% better than PEO-PM (16.70s). Therefore, even if there is no energy predictor, CL-PM still performs well as with a shorter adaptation period T_S, harvested power in the next slot is very close to the current harvested energy. It also means that the predicted harvested power in the next slot is the same as the real harvested power in the current slot ($\hat{P}_H(n+1) = \tilde{P}_H(n)$). This simplest energy predictor is also applied in the thermal-powered EH-WSNs proposed in Chapter 4. When the PM has a low T_{WI}, it is able to follow the tendency of harvested energy based on the current harvested power. However, CL-PM uses a ceil function for its positive energy power manager. Therefore, only a small part of harvested energy is saved for T_{NEI}, leading to a lower QoS when there is no harvested energy.

An important improvement in CL-PM compared to KAN-PM is the SoC of the energy

TABLE 5.4: Peformance comparison of different power managers.

	PEO-PM	KAN-PM	Gain (%)	CL-PM	Gain (%)
W_{EI}	16.53	8.77	-46.93	8.11	-50.92
W_{NEI}	14.77	97.80	84.89	87.23	83.07
W_C	15.46	15.96	3.13	15.42	-0.26
Gap	0.11	5.58	98.03	5.13	97.86
Mem	11	48	77.08	10	-10.00
Mul	16	28	42.86	9	-77.78
B_f	0	15	-	0	-

storage (supercapacitor StoreCap in this simulation) is considered in its adaptations during T_{NEI}. Therefore, the voltage of StoreCap (V_S) is returned to V_0 after a day lasting for $T_C = T_{EI} + T_{NEI}$. Similar to PEO-PM, CL-PM tightly satisfies ENO condition without any battery failure. However, as it can be found on Table 5.3, the average wake-up interval is really different between T_{EI} and T_{NEI}, which is also similar to KAN-PM.

Finally, a comparison of our proposed PEO-PM with KAN-PM and CL-PM is summarized in Table 5.4. As PEO-PM is able to balance the QoS, average wake-up interval is extremely reduced during T_{NEI}. The QoS during T_{NEI}, when there is no harvested energy is improved 84.89% and 83.07% compared to KAN-PM and CL-PM, respectively. The difference of average wake-up interval during five days (Gap) is reduced 98.03% with KAN-PM and 97.86% with CL-PM. However, PEO-PM does not improve the global QoS compared to KAN-PM and CL-PM as after five days, the voltage of V_S is very close to V_0 which means that most of the harvested energy is consumed by the wireless node to maximize the throughput. While PEO-PM balances the total of packets during a whole cycle T_C, KAN-PM and CL-PM send plenty of packets during T_{EI} but very limited packets during T_{NEI}. However, the overall packets during five consecutive days is the same, which results the same average wake-up interval W_C.

When considering the memory footprint, 11 words are required for PEO-PM, including 10 words for a LUT in the energy monitor and 1 word for the energy predictor using adaptive filter. Meanwhile, KAN-PM needs 48 words for saving historical values used by the duty cycle initialization. Without the energy predictor, CL-PM only uses 10 words for the LUT to estimate the consumed energy of the wireless node. Among these PMs, KAN-PM has the highest number of multiplications (Mul = 28) due to the complexity of the duty cycle adaptation process. With a simple positive energy power manager

(the combination of an energy neutral power manager and a ceil function), CL-PM only requires 9 multiplications. Meanwhile, the positive energy power manager in PEO-PM is more complex than CL-PM as it requires 16 multiplications. Finally, both PEO-PM and CL-PM ensure continuous operations of the node during five days without any battery failure as the SoC of StoreCap (V_S) is considered in their adaptation. In the contrast, there is around 15 minutes interruption when using KAN-PM as this PM does not aware of V_S.

5.5.4 WVR-PM Simulation Results

In this section, the multi-hop EH WSN depicted in Fig. 5.1 is implemented in OMNET++ for our simulation. More following metrics are defined to evaluate the performance of WVR-PM:

- Nb_Var : Number of variations, increased by 1 whenever the wake-up interval is changed.
- Sum_Var : Summation of variations, which is the absolute summation of the difference between current and previous wake-up interval.

$$Sum\_Var = \sum_{i=1}^{N} |T_{WI}(i) - T_{WI}(i-1)| \tag{5.17}$$

- R_d : Average data rate, which is defined as the ratio between the size of the data packet (16 bytes) and the wake-up interval.
- Idl : Average idle listening time for one successful packet, which is considered at both receiver and transmitter.
- E_C : Average consumed energy for one successful packet, which is considered at both receiver and transmitter.

In order to reduce variations of the wake-up interval for EH-WSN nodes, both Nb_Var and Sum_Var are required to be as small as possible. Firstly, the single-hop connection between the ED(0) and the BS is used for tuning three important parameters of WVR-PM, which are α_C, α_H and Δ. The improvement of WVR-PM in terms of average wake-up interval (W_C), data rate (R_D) and energy for one successful communication (E_C) using SyWiM is analysed on communications between ED(1) and the RD.

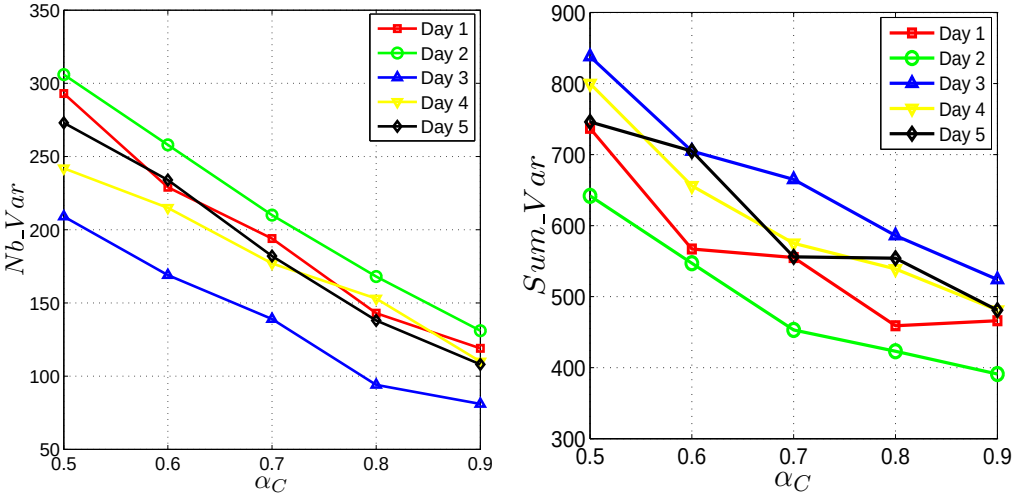

FIGURE 5.11: Nb_Var and Sum_Var with different values of α_C ($\alpha_H = 0$, $\Delta = 1$).

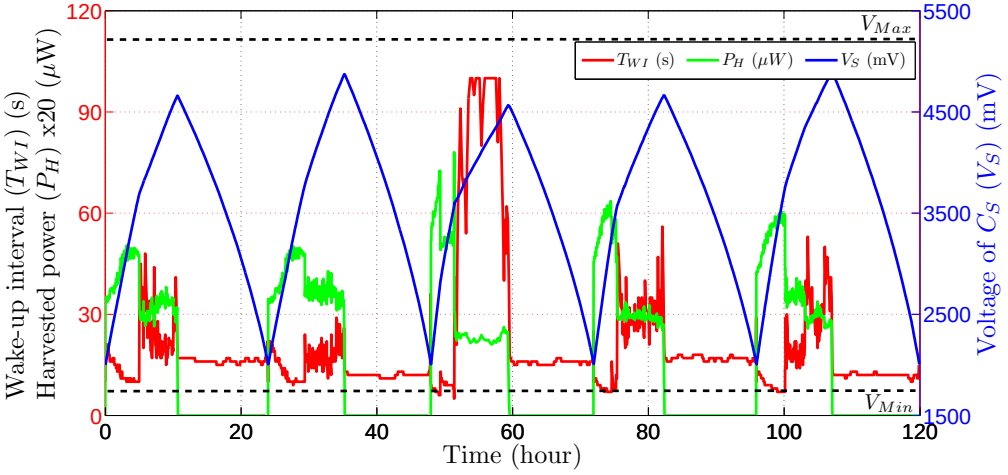

FIGURE 5.12: Adaptations of ED(1) using WVR-PM with $\alpha_C = 0.9$, $\alpha_H = 0$ and $\Delta = 1$. The variation of T_{WI} is significantly reduced during T_{NEI} as $\hat{e}_{Active}(n+1)$ is very close to $\hat{e}_{Active}(n)$ when $\alpha_C = 0.9$. Over five days, the variation is reduced down to 60% in average.

TABLE 5.5: Average Nb_Var and Sum_Var and their gain compared to PEO-PM ($\alpha_C = 0.5$) over five days ($\alpha_H = 0$, $\Delta = 1$).

α_C	Nb_Var	Gain (%)	Sum_Var	Gain (%)
0.5	264.6	-	752.6	-
0.6	221.0	16.48	633.6	15.81
0.7	180.4	31.82	563.2	25.17
0.8	139.2	47.39	512.2	31.94
0.9	109.8	58.50	468.6	37.74

TABLE 5.6: Average Nb_Var and Sum_Var and their gain when EWMA is applied to $\hat{P}_H$.

α_H	Nb_Var	Gain (%)	Sum_Var	Gain (%)
0.5	90.6	17.49	265.6	43.32
0.6	83.8	23.68	226.8	51.60
0.7	75.6	31.15	196.4	58.09
0.8	72.6	33.88	175.2	62.61
0.9	69.6	36.61	160.0	65.86

5.5.4.1 Tuning α_C, α_H and Δ

Firstly, α_H is set to zero and Δ is set to 1 for tuning α_C. Fig. 5.11 presents Nb_Var and Sum_Var over five days simulation with α_C starting from 0.5, which is the common value for EWMA filter, and ending with 0.9. It can be observed that Nb_Var is linearly decreased when α_C is increased. In average (see Table 5.5), the variation of T_{WI} is reduced by 58.50% when α_C = 0.9 (Nb_Var = 264.6) compared to α_C = 0.5 (Nb_Var = 109.8). Meanwhile, Sum_Var presenting the amplitude of variations is reduced by 37.74%. Adaptations of ED(0) when α_C = 0.9 are presented in Fig. 5.12. When α_C = 0.9, $\hat{e}_{Active}(n+1)$, which is used for evaluating $T_{WI}(n+1)$, is very close to $\hat{e}_{Active}(n)$, which is used for evaluating $T_{WI}(n)$. Therefore, the variation of T_{WI} is rapidly reduced, especially in T_{NEI}, when T_{WI} mostly depends on $\hat{e}_{Active}(n+1)$ (see (5.9)).

Although the error of predicting $\hat{e}_{Active}(n+1)$ can be different with α_C = 0.9, the NE-PM still provides a good fault tolerance. By monitoring V_S, NE-PM ensures that V_S is always close to V_0 = 2.0V to satisfy ENO condition after a cycle of the energy source, which is a day (24 hours) in our simulation. Therefore, α_C is set to 0.9 for the rest of our simulations.

Another EWMA filter is applied to $\hat{P}_H(n+1)$, which impacts on the variation of T_{WI} during energy harvesting interval (see (5.5)). Simulation results are presented in Fig. 5.13 when α_H is varied from 0.5 to 0.9. Moreover, the average of Nb_Var, Sum_Var and their gains over five days compared to WVR-PM when there is no EWMA filter for $\hat{P}_H(n+1)$ are summarized in Table 5.6. It can be observed that the improvement of Nb_Var when increasing α_H is not so efficient as in case of α_C. The reason is $\tilde{P}_H(n)$ has a higher variation than $\tilde{e}_{Active}(n)$. While the node always has k wake-up times during a slot that results a low variation of $\tilde{e}_{Active}(n)$ (which is used to predict $\hat{e}_{Active}(n+1)$),

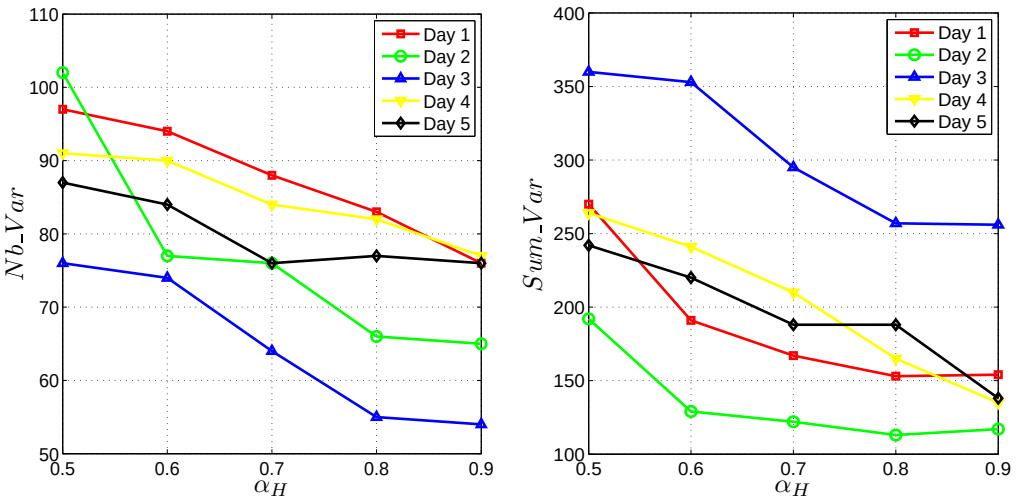

FIGURE 5.13: Nb_Var and Sum_Var with different values of α_H ($\alpha_C = 0.9$, $\Delta = 1$).

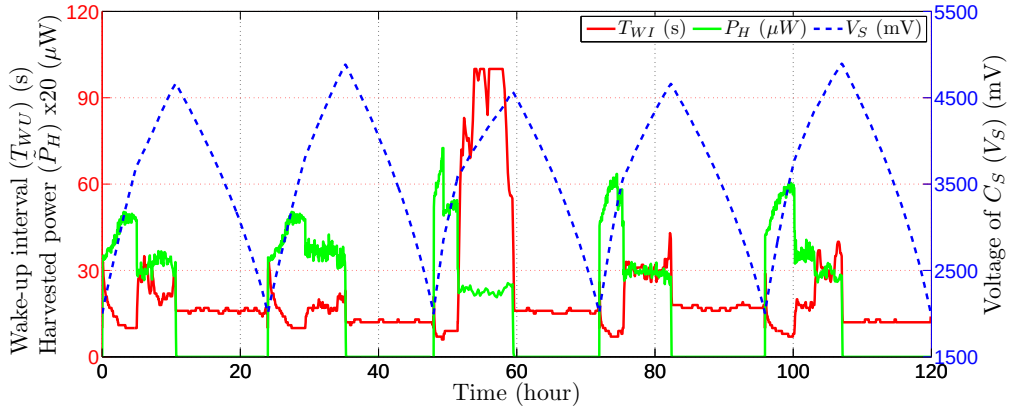

FIGURE 5.14: Adaptations of ED(1) using WVR-PM with $\alpha_H = 0.7$.

$\tilde{P}_H(n)$ is influenced by various light conditions that brings a high variation. Therefore, increasing α_H does not rapidly reduce the variation of T_{WI}.

However, the choice of α_H is a trade-off as higher value does not rapidly reduce the variation of T_{WI}, but will reduce the adaptability of the node according to the change of $\tilde{P}_H$. When there is a drop on $\tilde{P}_H$, T_{WI} must be increased. While a high value of α_H only increases T_{WI} with a small step size, a small value makes T_{WI} fastly increasing, which represents the adaptability of the node. Therefore, from Table 5.6, $\alpha_H = 0.7$ and adaptations of ED[1] in this case are presented in Fig. 5.13. In average, there are 75.6 variations of T_{WI} over five days simulation, which is improved by 31.13% compared to a solution without EWMA for $\hat{P}_H(n+1)$, which has 109.8 variations.

Finally, measurements with three different values of step size (Δ = 5, 10 and 15) are performed. Simulation results of Nb_Var and Sum_Var for each day are presented

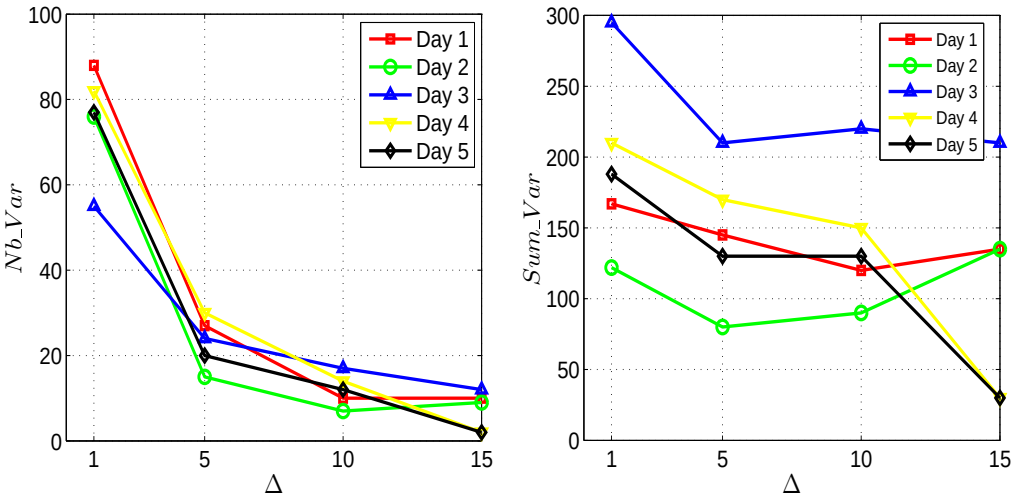

FIGURE 5.15: Nb_Var and Sum_Var with different values of Δ ($\alpha_C = 0.9$, $\alpha_H = 0.7$).

TABLE 5.7: Average values of Nb_Var, Sum_Var and W_C over five days. The gains are compared to WVR-PM without quantizer (or $\Delta = 1$).

Δ	Nb_Var	Gain (%)	Sum_Var	Gain (%)	W_C	Gain (%)
1	75.6		196.4		14.99	
5	23.2	69.31	147	25.15	15.07	-0.53
10	12	84.13	142	27.70	16.12	-7.01
15	7	90.74	108	45.01	18.31	-18.31

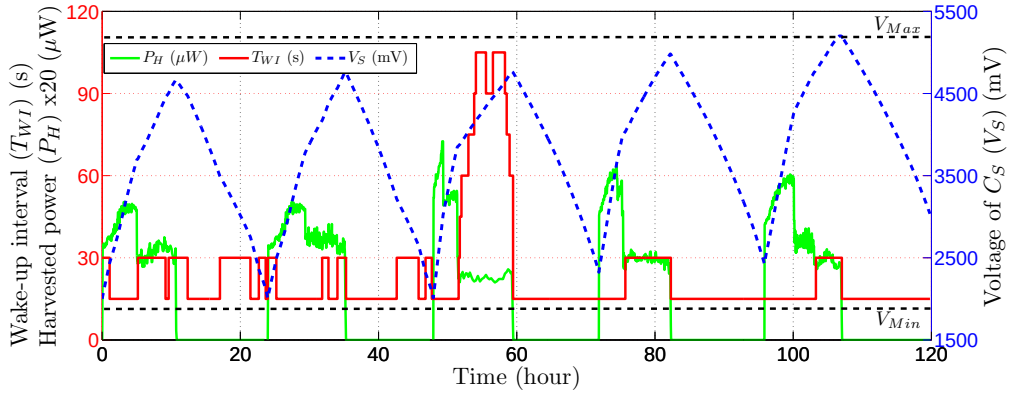

FIGURE 5.16: Adaptations of ED(1) using WVR-PM with $\Delta = 15$.

in Fig. 5.15 while their average values over five days are summarized in Table 5.7. As it can be observed from these results, the quantizer provides a breakthrough to reduce the variations of T_{WI} (Nb_Var). However, Sum_Var is not improved so efficiently as Nb_Var as the quantizer only removes the variation less than $\Delta/2$ but still keeps big moves of T_{WI}. This feature allows WVR with a quantizer to adapt T_{WI} only when there is a considerable variation of harvested energy.

TABLE 5.8: Comparison of different power manager in a multi-hop EH-WSN.

	WVR-PM	PEO-PM	Gain (%)	CL-PM	Gain (%)	KAN-PM	Gain (%)
R_d	7.42	4.75	36.04	5.36	27.76	3.01	59.56
Idl	31.44	47.70	35.08	44.15	28.79	65.24	51.80
E_C	3111.40	4361.62	28.66	4088.81	23.90	5709.70	45.51
B_f	0	0		37		63	

Although increasing the step size can reduce the variation of T_{WI}, the performance of the node (QoS) can be reduced. As shown in Table 5.7, the average wake-up interval when Δ = 15, which represents the QoS, is increased by 18.31% compared to Δ = 1 (or without the quantizer). As the minimum output of the quantizer in WVR-PM is Δ, T_{WI} cannot be less than Δ even if there is plenty of harvested energy. In our simulation, this problem occurs at the beginning of the last three days, as shown in Fig. 5.16 when Δ is set to 15. Without the quantizer, T_{WI} at the beginning of the third day can be reduced to 7s as shown in Fig. 5.13 instead of 15s in Fig. 5.16. This behavior is repeated on the next two days and therefore, degrades the global QoS. When the harvested energy is not available, the negative energy power manager (NE-PM) is activated to converge the voltage of StoreCap (V_S) to V_0 = 2.0V. Unfortunately, whenever T_{WI} is less than Δ = 15, the next wake-up interval is set to Δ. Therefore, to trade-off between the variation of T_{WI} and the decrease of QoS, Δ is set to 10 for the quantizer.

5.5.4.2 Performance between end device (ED(0)) and relay device (RD)

In this section, the WVR-PM with α_C = 0.9, α_H = 0.7 and Δ = 10 is implemented on a multi-hop EH WSN presented in Fig. 5.1. The performance between the ED(0) and RD is used to show the improvement of WVR-PM compared to other power managers such as PEO-PM, CL-PM and KAN-PM. Their average metrics over five days are summarized in Table 5.8.

It is noticed that RD is also an EH-WSN node and therefore, cannot send the WUB as frequently as the BS (e.g. 1s). The period of this WUB depends on the wake-up interval of RD, which is adapted to satisfy ENO. Therefore, with random change of T_{WI} provided by PEO-PM, CL-PM and KAN-PM, ED(0) cannot receive a WUB from RD. WVR-PM overcomes this problem by forcing the change of T_{WI} to a multiple of the step size Δ. This solution increases the probability to receive a WUB whenever ED(0) wakes up. As shown in Table 5.8, the average data rate (R_d) is improved by 36.04%,

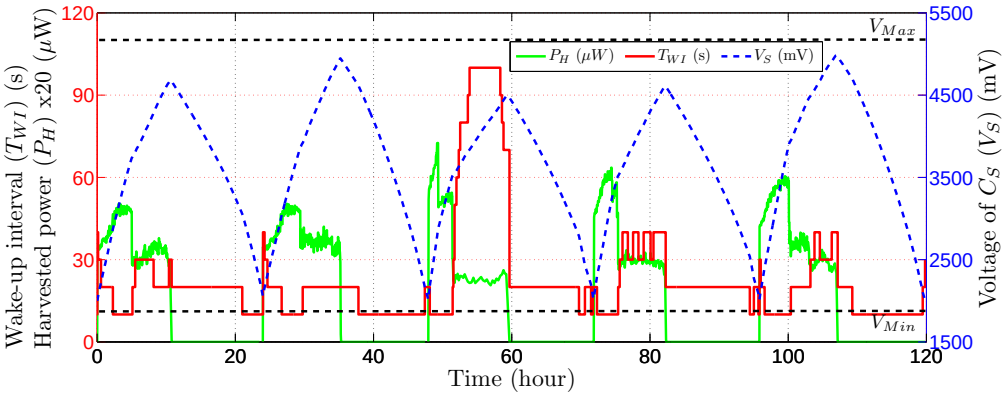

FIGURE 5.17: Adaptations of ED(0) using WVR-PM with $\Delta = 10$.

27.76% and 59.56% using our WVR-PM compared to PEO-PM, CL-PM and KAN-PM, respectively.

It is noticed that not only the throughput (R_d) is improved, the average idle listening considered at both ED(0) and RD, is also significantly reduced. The reason is that ED(0) has to perform a maximum idle listening window when it wakes-up if the RD does not wake-up at this time. Until the next wake-up time, the idle listening windows is increased due to the increase of L in (5.12). With WVR-PM, the ED(0) easily receives a WUB whenever it wakes-up. Finally, the average ilde listening (Idl) when using WVR-PM is reduced by 47.70%, 34.08% and 51.80% compared to PEO-PM, CL-PM and KAN-PM, respectively. As idle listening is the dominant energy consumption for communication, the average energy for one successful communication is also reduced by 28.66%, 23.90% and 45.51%.

As the main core of WVR-PM is the PEO-PM, both WVR-PM and PEO-PM are able to ensure that there is no battery failure over five days. Although CL-PM considers the voltage of StoreCap when determining T_{WI}, there is a battery failure duration lasting for B_f =37 minutes. As the average energy for communication (E_C) is increased, the light increasing of V_S during energy harvesting interval in CL-PM cannot buffer enough energy for the next non-energy harvesting interval even if T_{WI} is set to maximum value (300s). The battery failure when using KAN-PM is much longer as it does not consider V_S when performing adaptations (B_f =63 minutes).

Finally, adaptations of ED[0] are presented in Fig. 5.17. Not only satisfying ENO condition after each day, WVR-PM provides a low variation of T_{WI} but is still able to adapt T_{WI} according to the change of harvested power.

5.6 Conclusions

In this chapter, a periodic power manager (PEO-PM) is proposed for EH-WSNs powered by a periodic energy source (e.g light energy in an office). As the harvested energy is only available during an interval T_{EI}, PEO-PM provides a simple strategy for saving energy, which is used afterwards in the next interval T_{NEI}, when there is no more harvested energy. The first improvement of PEO-PM is that the ratio between T_{NEI} and T_{EI} is considered for wake-up interval adaptations during T_{EI}. This solution provide a balanced QoS during a whole cycle of energy source and is useful for monitoring applications which require regular data tracking. Although the QoS is reduced by 46.93% and 50.92% during T_{EI}, PEO-PM improves the QoS during T_{NEI} up to 84.89% and 83.07% compared to KAN-PM and CL-PM, respectively. The second improvement of PEO-PM comes from CL-PM. By considering the SoC of StoreCap (V_S), PEO-PM ensures continuous operations of the EH WSN node without any interruption (no battery failure, $B_f = 0$). Finally, PEO-PM has a low complexity with a small memory footprint. For all these reasons, PEO-PM can be easily implemented on a real sensor node.

However, PEO-PM performance is reduced when applied in a multi-hop EH-WSN. As the relay device (RD) cannot send its beacon (WUB) as frequently as the base station (BS), there are some over idle listenings when the end device (ED) wakes-up. This problem not only reduces the global QoS but also increases the consumed energy of the ED. Therefore, a wake-up variation reduction power manager (WVR-PM) has been proposed in order to reduce the variation of the wake-up interval (T_{WI}). Moreover, T_{WI} is quantized and therefore, is always a multiple of a step size (Δ). Considering this feature, a synchronized wake-up interval MAC protocol (SyWiM) is proposed as a partial synchronous MAC protocol to increase the global QoS when WVR-PM is applied. Simulation results show that WVR-PM with SyWiM can increase by 36.04%, 27.76% and 59.56% the average data rate compared to PEO-PM, CL-PM and KAN-PM, respectively.

Chapter 6

Conclusions and Perspectives

6.1 Conclusions

The limited energy and recharged cycle of batteries are crippled the design of autonomous Wireless Sensor Networks (WSNs). To overcome this issue, everlasting harvested energy and supercapacitor-based energy storage are considered the potential solution to achieve a theoretically infinite lifetime. However, to achieve a theoretically infinite lifetime, a Power Manager (PM) needs to be embedded in each WSN node to respect Energy Neutral Operation (ENO), which means harvested energy is equal to consumed energy for a long period. In this thesis, global approaches for PMs embedded in supercapacitor-based energy harvesting wireless sensor networks (EH-WSN) are presented. PMs are designed independently of harvested energy sources and therefore, can be applied for light, heat or air-flow energy. In addition, proposed PMs are low complexity and memory footprint and therefore, can be implemented in real EH-WSN nodes. Based on predictions of both harvested and consumed energy for the next slot, the wake-up interval (T_{WI}) of the node is adapted to respect the energy neutral operation (ENO) condition. When ENO has been satisfied, total harvested energy is equal consumed energy, providing an infinite lifetime of the EH-WSN node.

Environmental energy sources are classified into two categories in this thesis, the continuous and the periodic sources. In the first one, energy can be scavenged continuously without any interruption. These energy sources can be found from fluorescent lights

hospitals or heat emitted by industrial machines. The Duty-Cycle PM (DC-PM) proposed for this kind of energy sources allows the EH-WSN node to consume energy as much as it can harvest. The voltage of the supercapacitor used for the energy storage (V_S) is kept almost constant when ENO has been satisfied as all harvested energy is used for maximizing the system QoS. There is no more energy for charging the supercapacitor (StoreCap) in this context. This behavior is also useful for applications which only require tracking data when the harvested energy is available such as tire pressure monitoring using vibration energy [101] or velocity monitoring using air flow energy passing through a tunnel [102]. Taking advantage of a simple energy monitor, our DC-PM provides a fast convergence to ENO compared to adaptive controllers such as PID-PM presented as well in this thesis.

Meanwhile, ambient energy is only available during energy harvesting (T_{EI}) interval instead of non-energy harvesting interval (T_{NEI}) when considering periodic energy sources. Therefore, the proposed periodic PM (PEO-PM) is able to reserve harvested energy during T_{EI} for perpetual operations during T_{NEI}. The ENO condition in periodic energy sources is respected after a cycle $T_C = T_{EI} + T_{NEI}$. Moreover, our PEO-PM aims to balance the QoS during a whole cycle T_C instead of a high QoS during T_{EI} but a low QoS during T_{NEI} as state-of-the-art PMs. The *Gap* defined in (5.14) which represents the difference of QoS between T_{EI} and T_{NEI} is reduced up to 98% when using PEO-PM. This improvement is amenable for monitoring applications which require regularly tracking data such as temperature monitoring in offices.

Not only satisfy ENO, maximizing QoS in a multi-hop EH-WSN is finally addressed in this thesis. Regularly updating T_{WI} can decrease the global QoS due to synchronizations among EH nodes. Therefore, a new approach, named Wake-up Variation Reduction PM (WVR-PM), is presented. The main core of WVR-PM is PEO-PM. However, two Exponential Weighted Moving Average filters and a quantizer are used to reduce variations of T_{WI}. By this way, T_{WI} is kept the same for a long period, guaranteeing successful wireless communications. Moreover, a new MAC protocol, named synchronized wake-up interval MAC (SyWiM), taking advantage of low wake-up interval variations is also proposed. Our simulations show that WVR-PM and SyWiM can improve the QoS up to 36.04% while reduce 28.66% of average energy for one successful communication compared to PEO-PM.

6.2 Perspectives

Based on results in this thesis, several interesting topics can be investigated. This section provides a short discussion of future works.

Multi-Energy Sources Power Manager

Although power managers presented in this thesis are independent of energy sources, there is only one energy source is connected for powering the wireless node in our measurements or simulations. To the best of our knowledge, there is no PM designed for multi-energy sources WSNs. The combination of different energy sources at the same time (e.g. light and air-flow energy) can bring more advantages, but also new challenges in EH-WSNs. The basic advantage of multi-energy sources WSNs is that more energy can be scavenged to increase the system QoS. Moreover, there seems to be a mutual complement between these sources: strong winds usually occur when the weather is bad rather than in sunny days, or during the night-time where solar energy is not available [84]. However, the PM for this system must deal with the variations of total harvested energy, which can be very different compared to each source.

Adaptive Quantizer in Wake-Up Variation Reduction Power Manager

In the simulations with wake-up variation reduction power manager (WVR-PM), the main component to reduce the variation of wake-up interval is the quantizer. So far, the quantizer step size (Δ) is a fixed value before deploying EH-WSN nodes. When harvested energy is extracted from two PVs in our office, the optimized Δ seems to be 10. However, if the node is setup in another condition (e.g. monitoring in a supermarket) with higher harvested energy (e.g. better light condition), the best value of Δ can be changed. Therefore, future works can provide an adaptive algorithm to determine Δ when the network is deployed. This algorithm may have a high consumed energy due to its complexity and therefore, should be implemented at the base station node, which usually has a permanent energy supply. By learning the average harvested power during a period (e.g. a day), an optimized Δ can be computed and then, broadcasted to the whole EH-WSN. This information is used by the SyWiM protocol at each node.

Wake-Up Radio-based MAC Protocols

When the node has satisfied the ENO, optimizing the consumed energy of MAC protocols is the key to increase global QoS of the system. Idle listening is the most wasted energy in asynchronous MAC protocols as the node does not know when it is allowed to transmit. Most of the time the radio is consuming while idle listening, just waiting to awake to be reactive. A nano-watt wake-up radio receiver (WUR) in [103] can be embedded in an EH-WSN node in order to drastically reduce the energy due to idle listening, which is the most significant source of energy consumption in MAC protocols, especially with asynchronous protocols [22]. Our works in [104] show that average energy consumption for one successful communication using TICER protocol can be reduced up to 53% when applying the WUR. However, the WUR is only simulated in a single-hop EH-WSN with a continuous energy source. Future works can extend this simulation in a multi-hop network and then, validate results on real WUR-based platforms when considering a periodic energy source. Another advantage can be achieved is the network latency, especially in a multi-hop network. As WUR is able to continuously listen to a wireless channel, the relay device (RD) can immediately forward a packet by sending a trigger signal (e.g. a wake-up beacon) to the WUR of the base station (BS) (see Fig. 5.1). With SyWiM protocol presented in this thesis, after receiving a packet from an ED, the RD must wait for a WUB from the BS. If there is no WUB, the RD will turn into sleep mode and wait until its next wake-up to forward this packet. Therefore, the network latency is increased in this scenario.

Reconfigurable Antennas in Mobility Energy Harvesting WSNs

Another approach to optimize the consumed energy is the use of reconfigurable antennas for WSN nodes [105]. Indeed, most of the current WSN systems use omni-directional antennas [106]. As the output RF signals are emitted in all directions in this case, it is inefficient in terms of power, range and interferences. Reconfigurable antennas (or directive antennas), that are able to focus the output signal beam in a reduced direction, provide a solution to overcome these issues. They can provide lower power consumption, longer range and reduce interferences, especially in a dense network. However, using reconfigurable antennas impacts the way WSN nodes will communicate. As a consequence, the physical, MAC [107] and network (routing) protocol layers [108] need to be reconsidered. Moreover, the PM must be able to configure the antenna and the RF chip of the EH-WSN node according to its position or its distance from the base station. The combination of the PM and reconfigurable antennas opens opportunities to design efficient

mobile multi-hop EH-WSNs. In that case, the node will have to dynamically control its antenna and its RF circuit according to its position as well as to the fluctuating channel conditions.

Personal Publications

- A. Castagnetti, A. Pegatoquet, **T. N. Le**, and M. Auguin. A joint duty-cycle and transmission power management for energy harvesting WSN. *IEEE Transactions on Industrial Informatics*, pages 1–9, 2014.
- **T. N. Le**, M. Magno, A. Pegatoquet, O. Berder, O. Sentieys, and E. Popovici. Ultra low power asynchronous MAC protocol using wake-up radio for energy neutral WSN. *International ACM Workshop on Energy Neutral Sensing Systems (ENSSys)*, pages 1–6, 2013.
- **T. N. Le**, A. Pegatoquet, O. Berder, and O. Sentieys. Demo abstract: Multi-source power manager for super-capacitor based energy harvesting wireless sensor networks. *International ACM Workshop on Energy Neutral Sensing Systems (ENSSys)*, pages 1–2, 2013.
- **T. N. Le**, A. Pegatoquet, O. Sentieys, O. Berder, and C. Belleudy. Duty-cycle power manager for thermal-powered wireless sensor networks. *IEEE International Symposium on Personal, Indoor and Mobile Radio Communications (PIMRC)*, pages 1645–1649, 2013.
- **T. N. Le**, O. Sentieys, O. Berder, A. Pegatoquet, and C. Belleudy. Adaptive filter for energy predictor in energy harvesting wireless sensor networks. *IEEE International Conference on Architecture of Computing Systems (ARCS)*, pages 1–4, 2013.
- **T. N. Le**, O. Sentieys, O. Berder, A. Pegatoquet, and C. Belleudy. Power manager with PID controller in energy harvesting wireless sensor networks. *IEEE International Conference on Green Computing and Communications (GreenCom)*, pages 668–670, 2012.

Bibliography

[1] A. Didioui, C. Bernier, D. Morche, and O. Sentieys. Harvwsnet: A co-simulation framework for energy harvesting wireless sensor networks. In *International Conference on Computing, Networking and Communications (ICNC)*, pages 808–812, 2013.

[2] S. Bandyopadhyay and A.P. Chandrakasan. Platform architecture for solar, thermal, and vibration energy combining with mppt and single inductor. *IEEE Journal of Solid-State Circuits*, 47(9):2199–2215, 2012.

[3] J. Hsu, S. Zahedi, A. Kansal, M. Srivastava, and V. Raghunathan. Adaptive duty cycling for energy harvesting systems. In *Proceedings of the International Symposium on Low Power Electronics and Design (ISLPED)*, pages 180–185, 2006.

[4] A. Castagnetti, A. Pegatoquet, C. Belleudy, and M. Auguin. A framework for modeling and simulating energy harvesting wsn nodes with efficient power management policies. *EURASIP Journal on Embedded Systems*, pages 1–16, 2012.

[5] M. K. Stojcev, M. R. Kosanovic, and L. R. Golubovic. Power management and energy harvesting techniques for wireless sensor nodes. In *Telecommunication in Modern Satellite, Cable, and Broadcasting Services (TELSIKS)*, pages 65–72, 2009.

[6] M.M. Alam, O. Berder, D. Menard, T. Anger, and O. Sentieys. A hybrid model for accurate energy analysis of wsn nodes. *Journal on Embedded Systems (EURASIP)*, pages 1–16, 2011.

[7] L. Atzori, A. Iera, and G. Morabito. The internet of things: A survey. *Computer Networks*, 54(15):2787 – 2805, 2010.

[8] L. Mainetti, L. Patrono, and A. Vilei. Evolution of wireless sensor networks towards the internet of things: A survey. In *International Conference on Software, Telecommunications and Computer Networks (SoftCOM)*, pages 1–6, 2011.

[9] D. Christin, A. Reinhardt, P. S. Mogre, and R. Steinmetz. Wireless sensor networks and the internet of things: selected challenges. *Proceedings of GI/ITG KuVS Fachgespräch Drahtlose Sensornetze*, pages 31–33, 2009.

[10] V. Potdar, A. Sharif, and E. Chang. Wireless sensor networks: A survey. In *International Conference on Advanced Information Networking and Applications Workshops (WAINA)*, pages 636–641, 2009.

[11] M. A. Pasha, S. Derrien, and O. Sentieys. Toward ultra low-power hardware specialization of a wireless sensor network node. In *International Multitopic Conference (INMIC)*, pages 1–6, 2009.

[12] D. Puccinelli and M. Haenggi. Wireless sensor networks: applications and challenges of ubiquitous sensing. *IEEE Circuits and Systems Magazine*, 5(3):19 – 31, 2005.

[13] P.H. Chou and C. Park. Energy-efficient platform designs for real-world wireless sensing applications. In *International Conference on Computer-Aided Design (ICCAD)*, pages 913–920, 2005.

[14] M. Y. I. Idris, E. M. Tamil, N. M. Noor, Z. Razak, and K. W. Fong. Parking guidance system utilizing wireless sensor network and ultrasonic sensor. *Journal on Information Technology*, 8(2):138–146, 2009.

[15] F.J. Rincon, M. Paselli, J. Recas, Q. Zhao, M. Sanchez-Elez, D. Atienza, J. Penders, and G. D. Micheli. Os-based sensor node platform and energy estimation model for health-care wireless sensor networks. In *Design, Automation and Test in Europe (DATE)*, pages 1027–1032, 2008.

[16] T. He, S. Krishnamurthy, L. Luo, T. Yan, L. Gu, R. Stoleru, G. Zhou, Q. Cao, P. Vicaire, J. A. Stankovic, T. F. Abdelzaher, J. Hui, and B. Krogh. Vigilnet: An integrated sensor network system for energy-efficient surveillance. *ACM Transactions on Sensor Networks*, 2(1):1–38, 2006.

[17] Jason Hill, Mike Horton, Ralph Kling, and Lakshman Krishnamurthy. The platforms enabling wireless sensor networks. *Communications of the ACM journal*, 47 (6):41–46, 2004. ISSN 0001-0782.

[18] Jan Beutel, Matthias Dyer, Martin Hinz, Lennart Meier, and Matthias Ringwald. Next-generation prototyping of sensor networks. In *International Conference on Embedded Networked Sensor Systems (SenSys)*, pages 291–292, 2004.

[19] L. Nachman, R. Kling, R. Adler, J. Huang, and V. Hummel. The intel mote platform: A bluetooth-based sensor network for industrial monitoring. In *International Symposium on Information Processing in Sensor Networks (IPSN)*, pages 61–67, 2005. ISBN 0-7803-9202-7.

[20] Olivier Berder and Olivier Sentieys. Powwow : Power optimized hardware/software framework for wireless motes. In *International Conference on Architecture of Computing Systems (ARCS)*, pages 1–5, Feb 2010.

[21] I. Demirkol, C. Ersoy, and E. Onur. Wake-up receivers for wireless sensor networks: benefits and challenges. *IEEE Wireless Communications*, 16(4):88–96, 2009. ISSN 1536-1284.

[22] A. Bachir, M. Dohler, T. Watteyne, and K.K. Leung. Mac essentials for wireless sensor networks. *IEEE Communications Surveys Tutorials*, 12(2):222–248, 2010.

[23] G. Anastasi, M. Conti, and M. Di Francesco. Extending the lifetime of wireless sensor networks through adaptive sleep. *IEEE Transactions on Industrial Informatics*, 5(3):351–365, 2009.

[24] P. Karumbu and A. Kumar. Optimum sleep-wake scheduling of sensors for quickest event detection in small extent wireless sensor networks. *Journal on Computing Research Repository (CoRR)*, abs/1105.6024, 2011.

[25] D. Carli, D. Brunelli, D. Bertozzi, and L. Benini. A high-efficiency wind-flow energy harvester using micro turbine. In *International Symposium on Power Electronics Electrical Drives Automation and Motion (SPEEDAM)*, pages 778–783, 2010.

[26] V. Raghunathan, A. Kansal, J. Hsu, J. Friedman, and M. Srivastava. Design considerations for solar energy harvesting wireless embedded systems. In *International*

Symposium on Information Processing in Sensor Networks (IPSN), pages 463–468, 2005.

[27] M. Stordeur and I. Stark. Low power thermoelectric generator-self-sufficient energy supply for micro systems. In *International Conference on Thermoelectrics (ICT)*, pages 575–577, 1997.

[28] A. S. Weddell, M. Magno, G. V. Merrett, D. Brunelli, B. M. Al-Hashimi, and L. Benini. A survey of multi-source energy harvesting systems. In *Conference on Design, Automation and Test in Europe (DATE)*, pages 905–908, 2013.

[29] A. Sinha and A. Chandrakasan. Dynamic power management in wireless sensor networks. *IEEE Design Test of Computers*, 18(2):62–74, 2001.

[30] R. A. F. Mini, B. Nath, and A. A. F. Loureiro. A probabilistic approach to predict the energy consumption in wireless sensor networks. In *IV Workshop de Comunicao sem Fio e Computao Mvel*, pages 23–25, 2002.

[31] M. Younis, M. Youssef, and K. Arisha. Energy-aware routing in cluster-based sensor networks. In *IEEE International Symposium on Modeling, Analysis and Simulation of Computer and Telecommunications Systems (MASCOTS)*, pages 129–136, 2002.

[32] R. C. Shah and J. M. Rabaey. Energy aware routing for low energy ad hoc sensor networks. In *IEEE Wireless Communications and Networking Conference (WCNC)*, volume 1, pages 350–355, 2002.

[33] A. Kansal, J. Hsu, S. Zahedi, and M.B. Srivastava. Power management in energy harvesting sensor networks. *ACM Transactions on Embedded Computing Systems (TECS)*, 6(4):32, 2007.

[34] Luca Benini, Robin Hodgson, and Polly Siegel. System-level power estimation and optimization. In *Proceedings of the 1998 international symposium on Low power electronics and design*, ISLPED '98, pages 173–178, New York, NY, USA, 1998. ACM. ISBN 1-58113-059-7. doi: http://doi.acm.org/10.1145/280756.280881. URL http://doi.acm.org/10.1145/280756.280881.

[35] M.B. Srivastava, A.P. Chandrakasan, and R.W. Brodersen. Predictive system shutdown and other architectural techniques for energy efficient programmable

computation. *Very Large Scale Integration (VLSI) Systems, IEEE Transactions on*, 4(1):42 –55, march 1996. ISSN 1063-8210. doi: 10.1109/92.486080.

[36] T. Šimunic. *Energy efficient system design and utilization.* PhD thesis, Citeseer, 2001.

[37] L.C. Weng, X.J. Wang, and B. Liu. A survey of dynamic power optimization techniques. In *IEEE International Workshop on System-on-Chip for Real-Time Applications*, pages 48–52, 2003.

[38] Yung-Hsiang Lu and G. De Micheli. Comparing system level power management policies. *Design Test of Computers, IEEE*, 18(2):10 –19, mar/apr 2001. ISSN 0740-7475. doi: 10.1109/54.914592.

[39] D. Ramanathan and R. Gupta. System level online power management algorithms. In *Design, Automation and Test in Europe Conference and Exhibition 2000. Proceedings*, pages 606 –611, 2000. doi: 10.1109/DATE.2000.840847.

[40] L. Benini, A. Bogliolo, and G. De Micheli. A survey of design techniques for system-level dynamic power management. *Very Large Scale Integration (VLSI) Systems, IEEE Transactions on*, 8(3):299 –316, june 2000. ISSN 1063-8210. doi: 10.1109/92.845896.

[41] Chi-Hong Hwang and Allen C.-H. Wu. A predictive system shutdown method for energy saving of event-driven computation. *ACM Trans. Des. Autom. Electron. Syst.*, 5:226–241, April 2000. ISSN 1084-4309. doi: http://doi.acm.org/10.1145/335043.335046. URL http://doi.acm.org/10.1145/335043.335046.

[42] S. Irani, S. Shukla, and R. Gupta. Competitive analysis of dynamic power management strategies for systems with multiple power saving states. In *Design, Automation and Test in Europe Conference and Exhibition, 2002. Proceedings*, pages 117 –123, 2002. doi: 10.1109/DATE.2002.998258.

[43] Eui-Young Chung, L. Benini, A. Bogliolo, Yung-Hsiang Lu, and G. De Micheli. Dynamic power management for nonstationary service requests. *Computers, IEEE Transactions on*, 51(11):1345 – 1361, nov 2002. ISSN 0018-9340. doi: 10.1109/TC.2002.1047758.

[44] Qinru Qiu and Massoud Pedram. Dynamic power management based on continuous-time markov decision processes. In *Proceedings of the 36th annual ACM/IEEE Design Automation Conference*, DAC '99, pages 555–561, New York, NY, USA, 1999. ACM. ISBN 1-58113-109-7. doi: http://doi.acm.org/10.1145/309847.309997. URL http://doi.acm.org/10.1145/309847.309997.

[45] S.K. Shukla and R.K. Gupta. A model checking approach to evaluating system level dynamic power management policies for embedded systems. In *High-Level Design Validation and Test Workshop, 2001. Proceedings. Sixth IEEE International*, pages 53 –57, 2001. doi: 10.1109/HLDVT.2001.972807.

[46] L. Benini, A. Bogliolo, G.A. Paleologo, and G. De Micheli. Policy optimization for dynamic power management. *Computer-Aided Design of Integrated Circuits and Systems, IEEE Transactions on*, 18(6):813 –833, jun 1999. ISSN 0278-0070. doi: 10.1109/43.766730.

[47] P. Pillai and K. G. Shin. Real-time dynamic voltage scaling for low-power embedded operating systems. In *ACM Symposium on Operating Systems Principles (SOSP)*, pages 89–102, 2001. ISBN 1-58113-389-8.

[48] A. P. Chandrakasan, S. Sheng, and R. W. Brodersen. Low-power cmos digital design. *IEEE Journal of Solid-State Circuits*, 27(4):473–484, 1992. ISSN 0018-9200.

[49] A. Qadi, S. Goddard, and S. Farritor. A dynamic voltage scaling algorithm for sporadic tasks. In *IEEE Real-Time Systems Symposium (RTSS)*, pages 52–62, 2003. doi: 10.1109/REAL.2003.1253253.

[50] J. Zhuo and C. Chakrabarti. Energy-efficient dynamic task scheduling algorithms for dvs systems. *Acm Transactions on Embedded Computing Systems (TECS)*, 7: 1–25, 2008. ISSN 1539-9087.

[51] W. Tuming, Y. Sijia, and W. Hailong. A dynamic voltage scaling algorithm for wireless sensor networks. In *International Conference on Advanced Computer Theory and Engineering (ICACTE)*, pages 554–557, 2010.

[52] T. Hamachiyo, Y. Yokota, and E. Okubo. A cooperative power-saving technique using dvs and dms based on load prediction in sensor networks. In *International*

Conference on Sensor Technologies and Applications (SENSORCOMM), pages 7–12, 2010.

[53] C. Schurgers, O. Aberthorne, and M. B. Srivastava. Modulation scaling for energy aware communication systems. In *International Symposium on Low Power Electronics and Design (ISLPED)*, pages 96 –99, 2001.

[54] Y. Sun, O. Gurewitz, and D. B. Johnson. Ri-mac: a receiver-initiated asynchronous duty cycle mac protocol for dynamic traffic loads in wireless sensor networks. In *ACM conference on Embedded network sensor systems (Sensys)*, pages 1–14, 2008.

[55] W. Ye, J. Heidemann, and D. Estrin. An energy-efficient mac protocol for wireless sensor networks. In *IEEE Conference of the Computer and Communications Societies (INFOCOM)*, pages 1567–1576, 2002.

[56] T. V. Dam and K. Langendoen. An adaptive energy-efficient mac protocol for wireless sensor networks. In *ACM Conference on Embedded networked sensor systems (Sensys)*, pages 171–180, 2003.

[57] S. Du, A. K. Saha, and D. B. Johnson. Rmac: A routing-enhanced duty-cycle mac protocol for wireless sensor networks. In *IEEE International Conference on Computer Communications (INFOCOM)*, pages 1478 –1486, 2007.

[58] Y. Sun, S. Du, O. Gurewitz, and D. B. Johnson. Dw-mac: a low latency, energy efficient demand-wakeup mac protocol for wireless sensor networks. In *Proceedings of the 9th ACM international symposium on Mobile ad hoc networking and computing*, pages 53–62. ACM, 2008.

[59] J. Polastre, J. Hill, and D. Culler. Versatile low power media access for wireless sensor networks. In *Proceedings of the 2nd international conference on Embedded networked sensor systems*, pages 95–107. ACM, 2004.

[60] M. Buettner, G. V. Yee, E. Anderson, and R. Han. X-mac: a short preamble mac protocol for duty-cycled wireless sensor networks. In *Proceedings of the 4th international conference on Embedded networked sensor systems*, pages 307–320. ACM, 2006.

[61] E. Y. A. Lin, J. M. Rabaey, and A. Wolisz. Power-efficient rendez-vous schemes for dense wireless sensor networks. In *IEEE International Conference on Communications*, pages 3769 – 3776, 2004.

[62] A. El-Hoiydi and J. D. Decotignie. Wisemac: An ultra low power mac protocol for multi-hop wireless sensor networks. *Algorithmic Aspects of Wireless Sensor Networks*, pages 18–31, 2004.

[63] A. Kansal, J. Hsu, M. Srivastava, and V. Raqhunathan. Harvesting aware power management for sensor networks. In *ACM/IEEE Design Automation Conference (DAC)*, pages 651–656, 2006.

[64] C.M. Vigorito, D. Ganesan, and A.G. Barto. Adaptive control of duty cycling in energy-harvesting wireless sensor networks. In *IEEE Communications Society Conference on Sensor, Mesh and Ad Hoc Communications and Networks (SECON)*, pages 21–30, 2007. doi: 10.1109/SAHCN.2007.4292814.

[65] C. Moser, L. Thiele, D. Brunelli, and L. Benini. Adaptive power management in energy harvesting systems. In *Design, Automation Test in Europe (DATE)*, pages 1–6, 2007.

[66] S. Roundy, D. Steingart, L. Frechette, P. Wright, and J. Rabaey. Power sources for wireless sensor networks. *Wireless Sensor Networks*, pages 1–17, 2004.

[67] C. Park and P. H. Chou. Ambimax: Autonomous energy harvesting platform for multi-supply wireless sensor nodes. In *IEEE Communications Society on Sensor and Ad Hoc Communications and Networks (SECON)*, pages 168–177, 2006.

[68] T. Esram and P. L. Chapman. Comparison of photovoltaic array maximum power point tracking techniques. *IEEE Transactions on Energy Conversion*, 22(2):439–449, 2007.

[69] L. Mateu, C. Codrea, N. Lucas, M. Pollak, and P. Spies. Energy harvesting for wireless communication systems using thermogenerators. In *Conference on Design of Circuits and Integrated Systems (DCIS)*, 2006.

[70] S. Roundy, P. K. Wright, and J. Rabaey. A study of low level vibrations as a power source for wireless sensor nodes. *Computer Communications*, 26(11):1131 – 1144, 2003.

[71] G. K. Ottman, H. F. Hofmann, and G. A. Lesieutre. Optimized piezoelectric energy harvesting circuit using step-down converter in discontinuous conduction mode. *IEEE Transactions on Power Electronics*, 18(2):696–703, 2003.

[72] S. Meninger, J. O. Mur-Miranda, R. Amirtharajah, A. P. Chandrakasan, and J. H. Lang. Vibration-to-electric energy conversion. *IEEE Transactions on Very Large Scale Integration Systems (VLSI)*, 9(1):64–76, 2001.

[73] K. Vijayaraghavan and R. Rajamani. Active control based energy harvesting for battery-lesswireless traffic sensors: Theory and experiments. In *American Control Conference*, pages 4579–4584, 2008.

[74] Y. K. Tan, K. Y. Hoe, and S. K. Panda. Energy harvesting using piezoelectric igniter for self-powered radio frequency (rf) wireless sensors. In *International Conference on Industrial Technology (ICIT)*, pages 1711–1716, 2006.

[75] F. Chraim and S. Karaki. Fuel cell applications in wireless sensor networks. In *Instrumentation and Measurement Technology Conference (I2MTC)*, pages 1320–1325, 2010.

[76] M. Magno, S. Marinkovic, D. Brunelli, E. Popovici, B. O'Flynn, and L. Benini. Smart power unit with ultra low power radio trigger capabilities for wireless sensor networks. In *Proceedings of the Conference on Design, Automation and Test in Europe (DATE)*, pages 75–80, 2012.

[77] C. Y. Chen and P. H. Chou. Duracap: A supercapacitor-based, power-bootstrapping, maximum power point tracking energy-harvesting system. In *International Symposium on Low Power Electronics and Design (ISLPED)*, pages 313–318, 2010.

[78] F.I. Simjee and P.H. Chou. Efficient charging of supercapacitors for extended lifetime of wireless sensor nodes. *IEEE Transactions on Power Electronics*, 23(3): 1526–1536, 2008.

[79] X. Jiang, J. Polastre, and D. Culler. Perpetual environmentally powered sensor networks. In *International Symposium on Information Processing in Sensor Networks (IPSN)*, pages 463–468, 2005.

[80] T. Zhu, Z. Zhong, Y. Gu, T. He, and Z. L. Zhang. Leakage-aware energy synchronization for wireless sensor networks. In *International Conference on Mobile systems, applications, and services*, pages 319–332, 2009.

[81] G.W. Allen, L. Konrad, J. Johnson, J. Lees, and M. Welsh. Fidelity and yield in a volcano monitoring sensor network. In *Symposium on Operating Systems Design and Implementation (OSDI)*, pages 381–396, 2006.

[82] K. Martinez, R. Ong, and J. Hart. Glacsweb: a sensor network for hostile environments. In *Conference on Sensor and Ad Hoc Communications and Networks (SECON)*, pages 81–87, 2004.

[83] S. Kim and P.H. Chou. Energy harvesting by sweeping voltage-escalated charging of a reconfigurable supercapacitor array. In *International Symposium on Low-power Electronics and Design (ISLPED)*, pages 235–240, 2011.

[84] C. Liu, K.T. Chau, and X. Zhang. An efficient wind-photovoltaic hybrid generation system using doubly excited permanent-magnet brushless machine. *IEEE Transactions on Industrial Electronics*, 57(3):831–839, 2010.

[85] N. Ferry, S. Ducloyer, N. Julien, and D. Jutel. Power and energy aware design of an autonomous wireless sensor node. *Journal on Advances in Computer Science*, 2(4):11–36, 2013.

[86] D. Carli, D. Brunelli, L. Benini, and M. Ruggeri. An effective multi-source energy harvester for low power applications. In *Design, Automation Test in Europe Conference Exhibition (DATE)*, pages 1–6, 2011.

[87] E. J. Carlson, K. Strunz, and B. P. Otis. A 20 mv input boost converter with efficient digital control for thermoelectric energy harvesting. *IEEE Journal of Solid-State Circuits*, 45(4):741–750, 2010.

[88] URL http://cap-xx.com.

[89] URL http://powwow.gforge.inria.fr.

[90] M. M. Alam, O. Berder, D. Menard, and O. Sentieys. Tad-mac: Traffic-aware dynamic mac protocol for wireless body area sensor networks. *IEEE Journal on Emerging and Selected Topics in Circuits and Systems*, (99):1, 2012.

[91] T.N. Le, A. Pegatoquet, O. Sentieys, O. Berder, and C. Belleudy. Duty-Cycle power manager for Thermal-Powered wireless sensor networks. In *IEEE Symposium on Personal, Indoor and Mobile Radio Communications (PIMRC)*, pages 1655–1659, 2013.

[92] X. Jiang, P. Dutta, D. Culler, and I. Stoica. Micro power meter for energy monitoring of wireless sensor networks at scale. In *International Symposium on Information Processing in Sensor Networks (IPSN)*, pages 186–195, 2007.

[93] T. Olivo. Analysis of ultra capacitors as ups energy storage devices. In *IEEE SoutheastCon*, pages 398 –401, 2010.

[94] C. Bergonzini, D. Brunelli, and L. Benini. Algorithms for harvested energy prediction in batteryless wireless sensor networks. In *International Workshop on Advances in sensors and Interfaces (IWASI)*, pages 144–149, 2009.

[95] R.C. Hsu, C.T. Liu, and W.M. Lee. Reinforcement learning-based dynamic power management for energy harvesting wireless sensor network. *Next-Generation Applied Intelligence*, pages 399–408, 2009.

[96] N. Karunanithi, D. Whitley, and Y.K. Malaiya. Using neural networks in reliability prediction. *IEEE Software*, pages 53–59, 1992.

[97] URL http://www.nrel.gov.

[98] J.R. Piorno, C. Bergonzini, D. Atienza, and T.S. Rosing. Prediction and management in energy harvested wireless sensor nodes. In *Wireless Communication, Vehicular Technology, Information Theory and Aerospace Electronic Systems Technology (VITAE)*, pages 6–10, 2009.

[99] M. Milligan, M. Schwartz, and Y. Wan. Statistical wind power forecasting models: results for us wind farms. *National Renewable Energy Laboratory, Golden, CO*, 2003.

[100] K. H. Ang, G. Chong, and Y. Li. Pid control system analysis, design, and technology. *IEEE Transactions on Control Systems Technology*, 13(4):559–576, 2005.

[101] I. Roufa, R. Millerb, H. Mustafaa, S. O. T. Taylora, W. Xua, M. Gruteserb, W. Trappeb, and I. Seskarb. Security and privacy vulnerabilities of in-car wireless networks: A tire pressure monitoring system case study. In *USENIX Security Symposium, Washington DC*, pages 11–13, 2010.

[102] E. Sardini and M. Serpelloni. Self-powered wireless sensor for air temperature and velocity measurements with energy harvesting capability. *IEEE Transactions on Instrumentation and Measurement*, 60(5):1838–1844, 2011.

[103] M. Magno, S. Marinkovic, D. Brunelli, E. Popovici, B. O'Flynn, and L. Benini. Smart power unit with ultra low power radio trigger capabilities for wireless sensor networks. In *Design, Automation and Test in Europe (DATE)*, pages 75–80, 2012.

[104] T. N. Le, M. Magno, A. Pegatoquet, O. Berder, O. Sentieys, and E. Popovici. Ultra low power asynchronous mac protocol using wake-up radio for energy neutral wsn. In *ACM Workshop on Energy Neutral Sensing Systems (ENSSys)*, pages 1–6, 2013.

[105] G. Giorgetti, A. Cidronali, S. K. S. Gupta, and G. Manes. Exploiting low-cost directional antennas in 2.4 ghz ieee 802.15.4 wireless sensor networks. In *European Conference on Wireless Technologies*, pages 217–220, 2007.

[106] T. Wu, R. L. Li Li, and M. M. Tentzeris. A scalable solar antenna for autonomous integrated wireless sensor nodes. *IEEE Antennas and Wireless Propagation Letters*, 10:510–513, 2011.

[107] R. R. Choudhury, X. Yang, R. Ramanathan, and N. H. Vaidya. Using directional antennas for medium access control in ad hoc networks. In *ACM Conference on Mobile Computing and Networking (MobiCom)*, pages 59–70, 2002.

[108] X. Huang, J. Wang, and Y. Fang. Achieving maximum flow in interference-aware wireless sensor networks with smart antennas. *Ad Hoc Networks*, 5(6):885 – 896, 2007.